

Table of Contents

Table of contents	i
Acknowledgements	iii
Chapter 1: Colloidal nanocrystals and NMR	1
1.1 Nanocrystals.....	2
1.2 Colloidal synthesis of NCs.....	5
1.3 Colloidal synthesis of NCs.....	5
1.4 NMR in comparison to other characterization techniques.....	7
1.5 Outline of this thesis.....	8
1.6 References	11
Chapter 2: NMR toolbox for nanocrystals	15
2.1 Different types of colloidal quantumdot systems.....	16
2.2 Effects of exchange on resonance appearance.....	18
2.3 1D ¹ H NMR	21
2.4 Nuclear Overhauser effect spectroscopy (NOESY)	23
2.5 Rotating frame Overhauser Spectroscopy (ROESY)	30
2.6 Diffusion Ordered Spectroscopy (DOSY).....	31
2.7 References	36
Chapter 3: Aluminium-Zinc-Oxide nanocrystals	39
3.1 Introduction.....	40
3.2 Basic characterization	43
3.3 Distinguishing OLAc and OLAm.....	47
3.4 Dynamic behavior of OLAc on the AZO NC surface.....	50
3.5 Conclusion	55
3.6 References	56
Chapter 4: Hafnium-Oxide nanocrystals	57
4.1 Introduction.....	58

4.2 Characterization of the nanocrystal surface	59
4.3 Binding mode of the carboxylic acid	63
4.4 Role of the amine	69
4.5 Conclusion	73
4.6 References	74
Chapter 5: Copper-Indium-Sulfide nanocrystals	77
5.1 Introduction.....	78
5.2 OLAm capped CIS – basic characterization	79
5.3 OLAm capped CIS – Ligand behavior	84
5.3.1 Technical considerations for high temperature measurements.....	85
5.3.2 High temperature measurements of OLAm capped CIS NCs.....	86
5.4 ODPAc capped CdSe – Ligand behavior.....	91
5.5 OLAm capped CIS – Ligand exchange	93
5.6 ODAm capped CIS – Ligand behavior.....	98
5.7 Conclusion	102
5.8 References	103
Chapter 6: Hydroxyapatite microparticles	105
6.1 Introduction.....	106
6.2 Materials	107
6.3 NMR study of L-lysine with hydroxyapatite in suspension.....	108
6.4 high resolution- Magic Angle Spinning (hr-MAS).....	112
6.5 Saturation Transfer Difference (STD) NMR spectroscopy	115
6.6 Conclusions.....	118
6.7 References	119
General conclusions	121
Nederlandstalige samenvatting	129
List of publications	135
Appendix A	137

Acknowledgements

First of all I would like to thank my promotor Prof. dr. José Martins and co-promotor Prof. dr. Zeger Hens for the great opportunity to start and finish my PhD under their excellent guidance.

Also, I would like to thank the SIM Flanders for the funding.

Finally I want to thank all my research partners, colleagues, friends, family and loved ones for their scientific and moral support.

Thank you!

No one who achieves success does so without the help of others. The wise and confident acknowledge this help with gratitude.

- *Alfred North Whitehead*

1

COLLOIDAL NANOCRYSTALS and NMR

In this chapter, nanocrystals are introduced and their very wide range of applications are given. NMR is compared to different characterization techniques used in nanoscience. Finally, the outline of this thesis is given.

1.1 Nanocrystals

First of all, let us think about the nano-dimension. The prefix ‘nano’ is derived from the greek word for dwarf. One nanometre is equal to 10^{-9} m. In order to give you an idea, a human hair is about 80.000 nm wide. Figure 1.2 depicts a length scale to illustrate this nanometre size.¹ Nanocrystals are on the nanoscale in all three dimensions.

But why are materials on the nanoscale so interesting? There are two main reasons for this.¹⁻³ First, the increased relative surface area means that more of their atoms are found at the surface compared to bulk materials. This changes their properties, including reactivity, with respect to bulk materials. Second, quantum effects start to govern the behavior and properties of the particles. As a result, the properties of the nanocrystal become dependent on the size of the particle. These properties can be for example fluorescence, opto-electronic properties, magnetic permeability or chemical reactivity.

Quantumdots

If a nanocrystal is constructed from a semiconductor material and the bound state of an electron and an electron hole or exciton are confined in all three dimensions, it is referred to as a quantumdot (QD).⁴ Interestingly, the confinement of size to the nm level introduces quantization, most notably in the distribution of energy states available to the electrons as compared to a bulk material. This quantum confinement principle is illustrated in figure 1.1.⁵⁻⁷ Considering a bulk material, their macroscopic size leads to a conductance and valence band characterized by a continuum of energy levels accessible for the electrons. When the size of the material is confined to nm size in three dimensions, the band structure is reduced to a set of discrete energy levels, similar to that of the quantized atom. Quantumdots,

therefore are sometimes described as superatoms.⁸ The presence of these discrete energy levels and the size-dependent energy differences causes them to exhibit size-tunable properties, making them highly interesting.

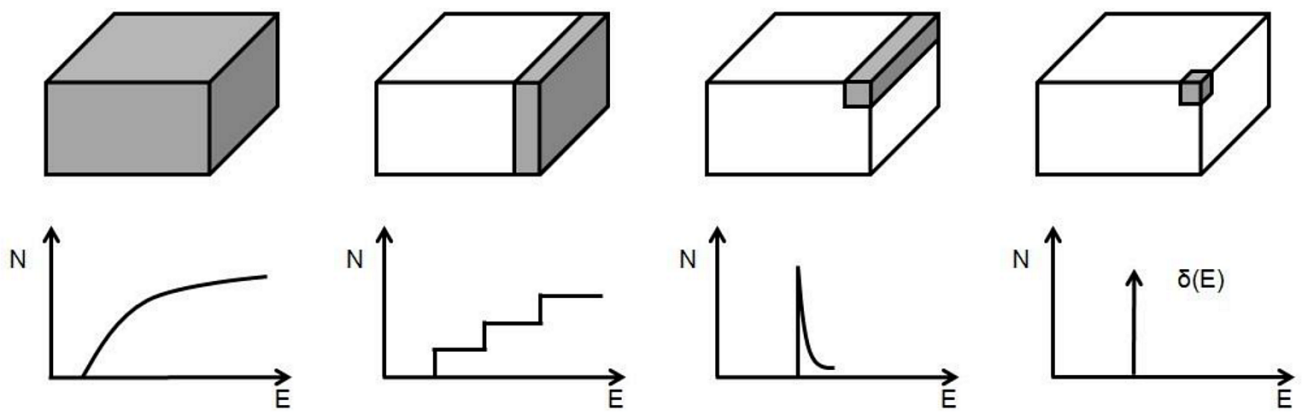


Figure 1.1. Density and distribution of energy levels (states) in bulk, quantum confined and molecular states of matter (from ref 7).

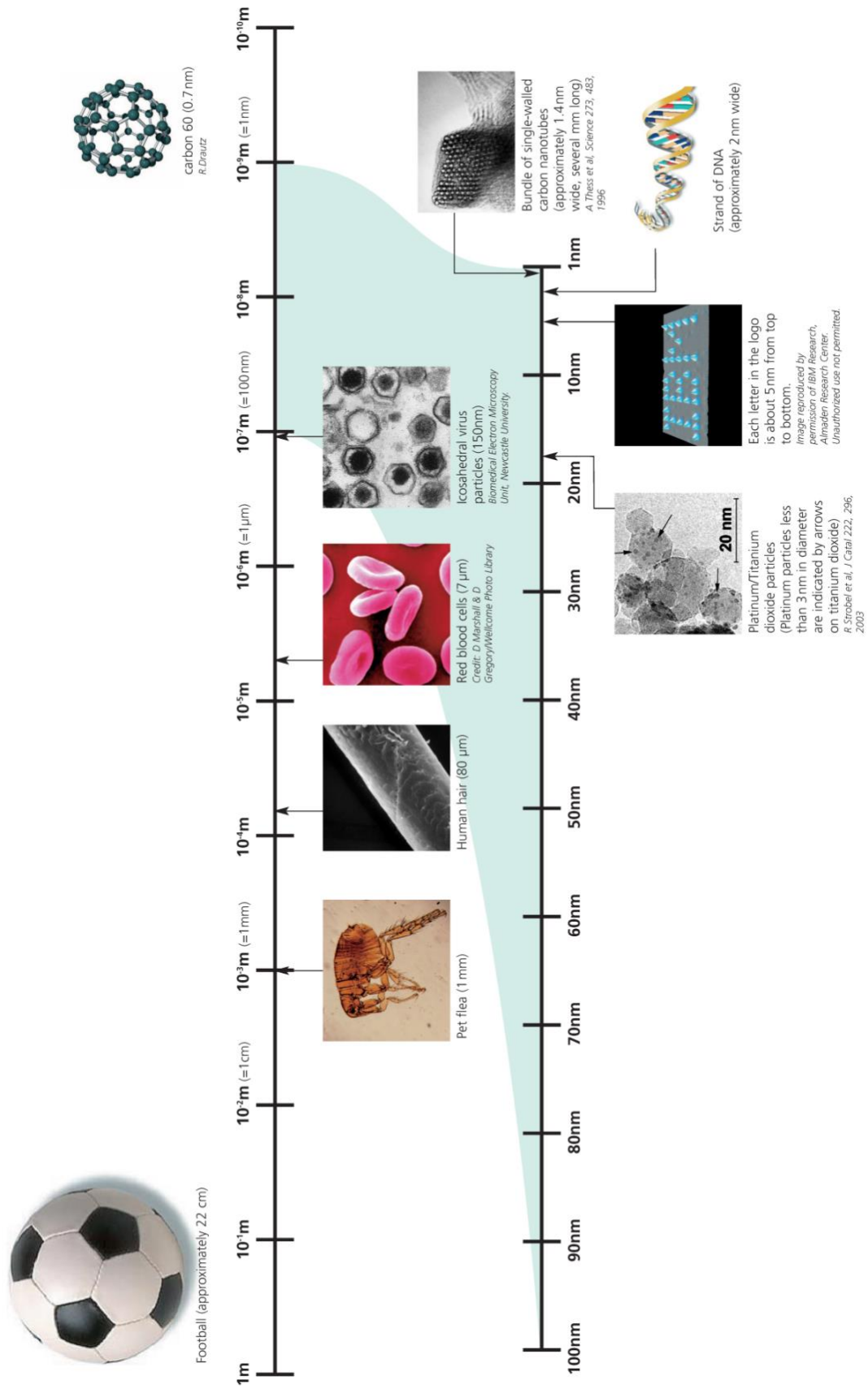


Figure 1.2. Length scale illustrating the nanometre dimension (from ref 1).

1.2 Colloidal synthesis of NCs

Solution-processed nanocrystals (NCs) are very attractive due to their low-cost fabrication and easy customization to different shapes and sizes.⁹⁻¹⁴ The research in this field took a leap forward following the paper of Murray *et al.* in 1993 in which they introduced the “hot injection method” that allows facile production of high quantities of QDs.¹⁵ This bottom-up approach is based on the rapid injection of organometallic reagents into a hot coordinating organic solvent. The slow growth and annealing in the coordinating solvent results in uniform surface derivatization and regularity in core structure. Also, size selective precipitation allows production of highly monodisperse nanocrystallites.

Colloidal nanocrystals have been developed towards different applications in photovoltaics¹⁶⁻¹⁸, photodetection¹⁹, photodiodes²⁰, light-emitting diodes (LEDs)²¹, bioimaging²²⁻²⁴ and biosensing^{25,26}.

1.3 Surface chemistry

Even though the inorganic core determines the physical properties of the nanocrystals, the ligand shell that surrounds this core also plays an important role in the nanocrystal's properties. Used during synthesis to control nucleation and crystal growth⁹, organic moieties end up as a monolayer covering the NC surface and providing colloidal stability. Depending on the type of ligand, nanocrystal solubility will be affected, making the nanocrystal either hydrophobic or hydrophilic.²⁷ Other important properties that are affected by the ligand shell are the photoluminescence efficiency²⁸⁻³¹ and chemical reactivity. In view of processing possibilities, it should also be noted that the ligand shell influences the formation of aggregates and attachment to surfaces. Often, it

is also necessary or preferable to exchange the original capping ligands by others to improve the above mentioned properties for certain applications.³²

In literature, the various types of ligands binding to NC surfaces have been divided into three categories: X-, L- and Z-types.^{33,34} A depiction of X-type and L-type binding on an NC surface is given in figure 4.5. As can be seen in this picture, they bind in a different way to the NC surface. An X-type ligand balances the net formal charge on the NC surface. Typically these NCs' charge is caused by the excess of metal cations, stabilized by ligands with a formally negative charge. But also the opposite situation could be possible. Some examples of X-type ligands are carboxylates, thiolates and phosphonates. Their ligand behavior has already been studied as reported in literature.^{31,35,36} An L-type ligand on the other hand brings in 2 electrons when binding. It passivates the NCs surface of which the formal charge is already balanced by the cations and anions of the NC itself.

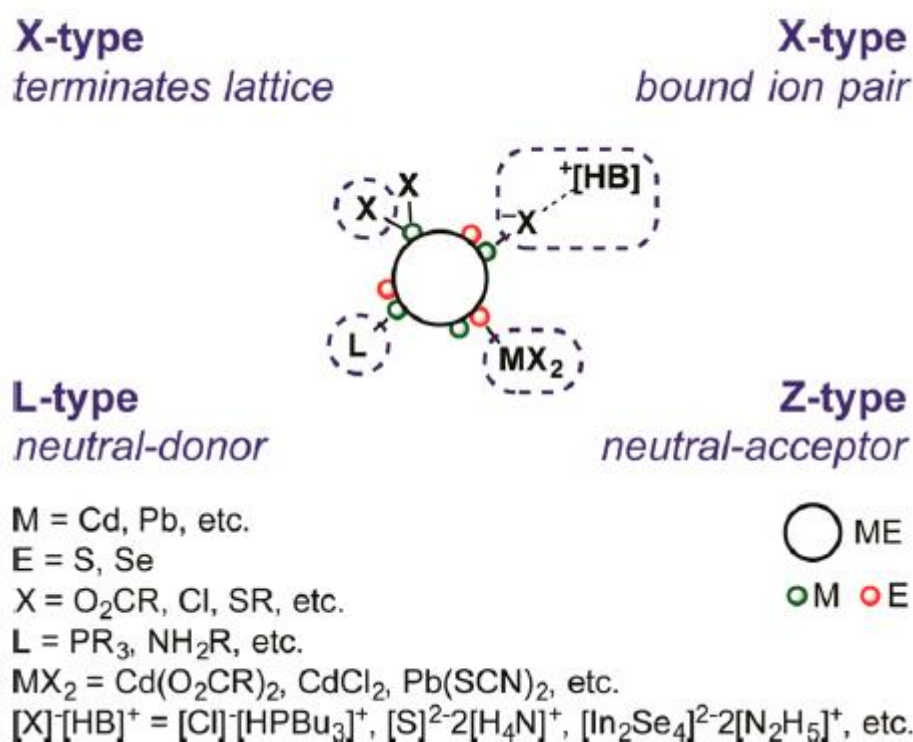


Figure 1.3. A schematic illustration of the different types of ligand binding possible on NCs (from ref. 31)

Typically, these ligands exhibit a dynamic adsorption/desorption behavior.^{37,38} Since L-type ligands reclaim the 2 electrons of the NC-ligand bond upon desorption, while X-type ligands only take 1, both ligands are incompatible for mutual ligand exchange reactions, provided that the NC composition is to be preserved. The information above allows the design of a useful exchange procedure, since only X-by-X and L-by-L exchange is possible.³⁴ However, first, knowledge of the type of ligands stabilizing the as-synthesized NC surface is crucial for this ligand exchange design.

All the points above illustrate how important it is to fully characterize the ligand shell and the dynamic behavior of the ligands at the surface for a complete understanding and efficient processing of QDs.

1.4 NMR in comparison to other characterization techniques

Many characterization techniques exist and are being used in nanoresearch, some of the most important ones are listed here with their main advantages and limitations. With X-Ray diffraction spectroscopy (XRD) and transmission electron microscopy (TEM), information can be obtained on the size, shape, crystallinity and dispersity of the nanocrystals. However, these techniques give no information on the capping ligands. An indirect method that is often used to measure the binding and exchange of ligands is photoluminescence³⁹⁻⁴¹. Although this technique is very important for the validation of quantumdots, it does not provide any information on the binding mode and exchange mechanisms of the ligand shell. Direct observation of ligands with characteristic functionalities and ligand exchange is often performed with infrared spectroscopy^{34,42}. While this is a valuable technique for distinction of different types of ligands it does not provide any information on the dynamic binding of the ligands. X-ray photoelectron spectroscopy⁴³ (XPS) is used to determine the different atoms

in the nanocrystal and especially the different binding types between surface atoms and capping ligands. These measurements are however not performed in the colloid but this is first deposited on a substrate, thus, no information can be given on the dynamic behavior in the colloid.

Nuclear Magnetic Resonance (NMR) spectroscopy is different from the techniques described above as it provides direct information on the binding and dynamic behavior of different capping ligands on the nanocrystal's surface. Other advantages of this technique are the fact that information is obtained from the colloids *in situ* without perturbing the sample. In view of these advantages, the use of NMR methodology in nanoresearch has been developed over the last decade. Pioneering work in this field was carried out in our research groups, PCN and NMRSTR.^{35-38,44-47} Other research groups have implemented NMR studies in their work and contributed to the dissemination of NMR as investigative method.^{30,34,48-50} However, still a lot of effort is necessary when studying colloidal NCs since every new system provides new challenges and the interpretation of NMR data that make a full dynamic picture of the system is not unequivocal. Often, new strategies and experiments have to be elaborated.

1.5 Outline of this thesis

The multidisciplinary work presented in this thesis is organized in various chapters and is the result of collaborations involving the NMR and structure analysis unit with different other research groups: PCN (Prof. Hens, UGent), IMO (Prof. Van Bael, Prof. Hardy, UHasselt), Scripts (Prof. Van Driessche, Ugent) and VITO (Dr. Mullens). The research of NMRSTR with PCN and IMO occurred within the context of the research project SOPPOM within the Strategic Initiative Flanders (SIM), aiming at the development of improved performance materials for photovoltaic

applications. All collaborative research groups focus on the study of the dynamic behavior and surface chemistry of nanocrystals and their ligands. In these collaborations, I was responsible for the design and implementation of the NMR strategy for elucidation of the systems' behavior. I performed all NMR measurements and analysis and reported and discussed the results with the collaborators, after which alterations on the synthesis or exchange strategies could be implemented, and validated by NMR. As a result, the published papers have several contributing authors, including me. In this thesis, emphasis will be placed on the contribution of NMR for the understanding of surface chemistry, rather than on synthesis or other characterization methods, which will be referred to via the available literature.

In chapter 2, the Nuclear Magnetic Resonance (NMR) Spectroscopy techniques are overviewed that are typically applied in nanocrystal research in our groups. Their use is demonstrated using oleic acid capped CdSe NCs which constitute a well-studied nanocrystal-ligand system will be used. These NMR techniques, commonly referred to as the 'NMR toolbox', formed the basis for further development and expansion into new investigative strategies that can be used in different nano- and microparticle suspensions as detailed in further chapters.

In chapter 3, a first application of the NMR toolbox in a new research study is given. Aluminium doped Zinc Oxide is explored as a new Transparent Conductive Oxide (TCO) material. Synthesized via a heat initiated thermal decomposition route, the combination of oleic acid and oleylamine is used to stabilize the obtained NCs. In order to verify the reaction mechanism that is needed for the stabilization and the actual

interactions of the surfactants with the NC surface, an in depth NMR study was performed.⁵¹

In chapter 4, Hafnium Oxide (HfO_2) NCs are studied (in collaboration with Scripts, Prof. Van Driessche, UGent) as an example of the more general group of Metal Oxide NanoCrystals (MONCs). The microwave assisted non-aqueous surfactant-free synthesis is followed by a post-synthetic stabilization with small amount of surfactant. However, surprisingly, it appears that two types of surfactants are needed to provide stability. In order to gain an in-depth understanding of the surface chemistry during all stages of synthesis and functionalization an in depth NMR study was performed.⁵²

In chapter 5, the elucidation of the complex surface chemistry of amine capped Copper Indium Sulfide NCs required the development and implementation of new NMR strategies. CuInS_2 NCs are explored for the application in different optical and electronic applications. They are synthesized typically by using a long-chain amine surfactant in a hot-injection procedure. With respect to applications it is important however that these long-chain ligands are replaced by shorter ones. This exchange of ligands requires a detailed understanding of the surface chemistry because a choice of appropriate reaction conditions and exchanging ligand is crucial. To achieve this understanding, the NMR toolbox was further expanded, including *in situ* high temperature measurements.⁵³

In chapter 6, the NMR toolbox is tested and expanded for use in micro-sized particles. Hydroxyapatite powder is used as an inorganic carrier for antigen delivery in the human body. Besides the many advantages of this approach, the disadvantage is the low loading capacity of the

hydroxyapatite surface. In this respect, the hydroxyapatite surface is functionalized first with an amino acid molecule. This approach provides a 60% increase in loading capacity for Bovine Serum Albumin. However, to gain insight in the mechanism behind this approach, the amino acid functionalized powders have to be characterized. In this chapter, we show how known NMR experiments can be used or have to be adjusted for the characterization of these functionalized micro-sized powder. Also, high-resolution Magic Angle Spinning (hr-MAS) and Saturation Transfer Difference (STD) experiments that were so far not used in this type of research are implemented for the first time and used to obtain even more insight in these micro-sized particles.⁵⁴

1.6 References

- (1) *Nanoscience and nanotechnologies: opportunities and uncertainties*, The Royal Society & The Royal Academy of Engineering, 2004.
- (2) Alivisatos, A. P. *Endeavour* **1997**, *21*, 56.
- (3) El-Sayed, M. A. *Accounts of Chemical Research* **2004**, *37*, 326.
- (4) Reed, M. A.; Randall, J. N.; Aggarwal, R. J.; Matyi, R. J.; Moore, T. M.; Wetsel, A. E. *Phys. Rev. Lett.* **1988**, *60*, 535.
- (5) Alivisatos, A. P. *Science* **1996**, *271*, 933.
- (6) G. A. Ozin, A. C. A., L. Cademartiri *Nanochemistry: A Chemical Approach to Nanomaterials*; 2nd ed.; RSCpublishing, 2009.
- (7) White, S.; Cataluna, M. *Photonics* **2015**, *2*, 719.
- (8) Jacak, L.; Hawrylak, P.; Wojs, A. *Quantum Dots*; 1 ed.; Springer-Verlag Berlin Heidelberg, 1998.
- (9) Yin, Y. *Nature* **2005**, *437*, 664.
- (10) Rogach, A. L.; Talapin, D. V.; Shevchenko, E. V.; Kornowski, A.; Haase, M.; Weller, H. *Advanced Functional Materials* **2002**, *12*, 653.
- (11) Cozzoli, P. D.; Pellegrino, T.; Manna, L. *Chemical Society Reviews* **2006**, *35*, 1195.
- (12) Peng, X. *Nano Res.* **2009**, *2*, 425.
- (13) Manna, L.; Scher, E. C.; Alivisatos, A. P. *J. Am. Chem. Soc.* **2000**, *122*, 12700.
- (14) Peng, Z. A.; Peng, X. *J. Am. Chem. Soc.* **2001**, *123*, 1389.
- (15) Murray, C. B.; Norris, D. J.; Bawendi, M. G. *J. Am. Chem. Soc.* **1993**, *115*, 8706.
- (16) Tang, J.; Kemp, K. W.; Hoogland, S.; Jeong, K. S.; Liu, H.; Levina, L.; Furukawa, M.; Wang, X.; Debnath, R.; Cha, D.; Chou, K. W.; Fischer, A.; Amassian, A.; Asbury, J. B.; Sargent, E. H. *Nature Materials* **2011**, *10*, 765.
- (17) Gur, I. *Nano Lett.* **2007**, *7*, 409.
- (18) Kamat, P. V. *The Journal of Physical Chemistry C* **2007**, *111*, 2834.
- (19) Konstantatos, G. *Nature* **2006**, *442*, 180.

Chapter 1

- (20) Rauch, T.; Boeberl, M.; Tedde, S. F.; Fuerst, J.; Kovalenko, M. V.; Hesser, G.; Lemmer, U.; Heiss, W.; Hayden, O. *Nature Photonics* **2009**, *3*, 332.
- (21) Rogach, A. L.; Gaponik, N.; Lupton, J. M.; Bertoni, C.; Gallardo, D. E.; Dunn, S.; Pira, N. L.; Paderi, M.; Repetto, P.; Romanov, S. G.; O'Dwyer, C.; Torres, C. M. S.; Eychmuller, A. *Angew. Chem.-Int. Edit.* **2008**, *47*, 6538.
- (22) Bruchez, M.; Moronne, M.; Gin, P.; Weiss, S.; Alivisatos, A. P. *Science* **1998**, *281*, 2013.
- (23) Michalet, X.; Pinaud, F. F.; Bentolila, L. A.; Tsay, J. M.; Doose, S.; Li, J. J.; Sundaresan, G.; Wu, A. M.; Gambhir, S. S.; Weiss, S. *Science* **2005**, *307*, 538.
- (24) Smith, A. M.; Duan, H.; Mohs, A. M.; Nie, S. *Advanced Drug Delivery Reviews* **2008**, *60*, 1226.
- (25) Medintz, I. L.; Uyeda, H. T.; Goldman, E. R.; Mattoussi, H. *Nature Materials* **2005**, *4*, 435.
- (26) Fu, A.; Gu, W.; Bousset, B.; Koski, K.; Gerion, D.; Manna, L.; Le Gros, M.; Larabell, C. A.; Alivisatos, A. P. *Nano Lett.* **2006**, *7*, 179.
- (27) Yu, W. W.; Falkner, J. C.; Shih, B. S.; Colvin, V. L. *Chem. Mat.* **2004**, *16*, 3318.
- (28) Du, H.; Chen, C.; Krishnan, R.; Krauss, T. D.; Harbold, J. M.; Wise, F. W.; Thomas, M. G.; Silcox, J. *Nano Lett.* **2002**, *2*, 1321.
- (29) de Mello Donegá, C.; Hickey, S. G.; Wuister, S. F.; Vanmaekelbergh, D.; Meijerink, A. *The Journal of Physical Chemistry B* **2002**, *107*, 489.
- (30) Kalyuzhny, G.; Murray, R. W. *J. Phys. Chem. B* **2005**, *109*, 7012.
- (31) Hassinen, A.; Moreels, I.; De Nolf, K.; Smet, P. F.; Martins, J. C.; Hens, Z. *J. Am. Chem. Soc.* **2012**, *134*, 20705.
- (32) Jiang, C. Y.; Lee, J. S.; Talapin, D. V. *J. Am. Chem. Soc.* **2012**, *134*, 5010.
- (33) Hens, Z.; Martins, J. C. *Chem. Mat.* **2013**, *25*, 1211.
- (34) Anderson, N. C.; Hendricks, M. P.; Choi, J. J.; Owen, J. S. *J. Am. Chem. Soc.* **2013**, *135*, 18536.
- (35) Moreels, I.; Fritzing, B.; Martins, J. C.; Hens, Z. *J. Am. Chem. Soc.* **2008**, *130*, 15081.
- (36) Fritzing, B.; Capek, R. K.; Lambert, K.; Martins, J. C.; Hens, Z. *J. Am. Chem. Soc.* **2010**, *132*, 10195.
- (37) Moreels, I.; Martins, J. C.; Hens, Z. *ChemPhysChem* **2006**, *7*, 1028.
- (38) Moreels, I.; Justo, Y.; De Geyter, B.; Hastraete, K.; Martins, J. C.; Hens, Z. *ACS Nano* **2011**, *5*, 2004.
- (39) Koole, R.; Schapotschnikow, P.; de Mello Donegá, C.; Vlugt, T. J. H.; Meijerink, A. *ACS Nano* **2008**, *2*, 1703.
- (40) Ji, X.; Copenhaver, D.; Sichmeller, C.; Peng, X. *J. Am. Chem. Soc.* **2008**, *130*, 5726.
- (41) Bullen, C.; Mulvaney, P. *Langmuir* **2006**, *22*, 3007.
- (42) von Holt, B.; Kudera, S.; Weiss, A.; Schrader, T. E.; Manna, L.; Parak, W. J.; Braun, M. *J. Mater. Chem.* **2008**, *18*, 2728.
- (43) Lobo, A.; Möller, T.; Nagel, M.; Borchert, H.; Hickey, S. G.; Weller, H. *The Journal of Physical Chemistry B* **2005**, *109*, 17422.
- (44) Hens, Z.; Moreels, I.; Martins, J. C. *ChemPhysChem* **2005**, *6*, 2578.
- (45) Moreels, I.; Martins, J. C.; Hens, Z. *Sens. Actuator B-Chem.* **2007**, *126*, 283.
- (46) Fritzing, B.; Moreels, I.; Lommens, P.; Koole, R.; Hens, Z.; Martins, J. C. *J. Am. Chem. Soc.* **2009**, *131*, 3024.
- (47) Antti Hassinen, I. M., Celso de Mello Donegá, José C. Martins, and Zeger Hens *J. Phys. Chem. Lett.* **2010**, *1*, 2577.
- (48) Anderson, N. C.; Owen, J. S. *Chem. Mat.* **2013**, *25*, 69.
- (49) Coppel, Y.; Spataro, G.; Pages, C.; Chaudret, B.; Maisonnat, A.; Kahn, M. L. *Chem.-Eur. J.* **2012**, *18*, 5384.
- (50) Hughes, B. K.; Ruddy, D. A.; Blackburn, J. L.; Smith, D. K.; Bergren, M. R.; Nozik, A. J.; Johnson, J. C.; Beard, M. C. *ACS Nano* **2012**, *6*, 5498.
- (51) Damm, H.; Kelchtermans, A.; Bertha, A.; Van den Broeck, F.; Elen, K.; Martins, J. C.; Carleer, R.; D'Haen, J.; De Dobbelaere, C.; Hadermann, J.; Hardy, A.; Van Bael, M. K. *RSC Advances* **2013**, *3*, 23745.

- (52) De Roo, J.; Van den Broeck, F.; De Keukeleere, K.; Martins, J. C.; Van Driessche, I.; Hens, Z. *J. Am. Chem. Soc.* **2014**, *136*, 9650.
- (53) Dierick, R.; Van den Broeck, F.; De Nolf, K.; Zhao, Q.; Vantomme, A.; Martins, J. C.; Hens, Z. *Chem. Mat.* **2014**, *26*, 5950.
- (54) Ozhukil Kollath, V.; Van den Broeck, F.; Fehér, K.; Martins, J. C.; Luyten, J.; Traina, K.; Mullens, S.; Cloots, R. *Chemistry – A European Journal* **2015**, *21*, 10497.

2

NMR TOOLBOX FOR NANOCRYSTALS

In this chapter, the application of the existing NMR toolbox will be illustrated with previously investigated and published colloidal quantumdot systems.

By exploiting chemical shift perturbations, the resonances' line-width and the molecular diffusion coefficient, interacting species may be distinguished from non-interacting ones in the dispersion. Information regarding the identity and quantity of the interacting ligands at the NC surface can be obtained.

2.1 Different types of colloidal quantumdot systems

As mentioned in chapter 1, several different types of colloidal nanoparticle systems exist and have been studied with NMR spectroscopy by our and other research groups.¹⁻¹⁴ However, these systems can all be divided into three separate categories depending on the exchange dynamics of the surface associated ligands. These different categories all have different spectral characteristics and demand for the use of specific NMR experiments as will be elaborated in this chapter.

One-step exchange

The simplest dynamic exchange situation is a one-step exchange. This situation is illustrated in figure 2.1 for a ligand L_a that exchanges between a bound and a free state. Depending on the activation energy barrier and kinetics of this process, one-step exchange can still be divided into 3 distinct possibilities that give rise to different spectral observations: no, slow or fast exchange.

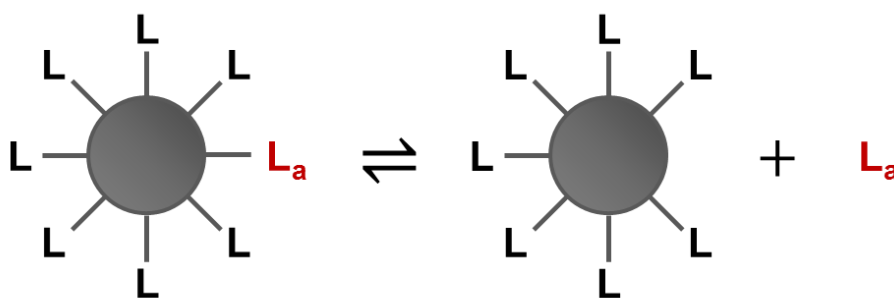


Figure 2.1. Illustration of one-step exchange of a ligand L_a with an NC surface

No exchange

In this situation, two cases need to be considered. If L_a does not act as a ligand for the NC, it will remain free in solution and display all the NMR

characteristics of a solvated and free molecular species. This typically occurs with non-solvents used during work-up procedure that were not completely washed away. Their contribution will be apparent from the contribution of sharp resonances, typically showing scalar coupling fine structure.

A second possibility is that L_a is strongly bound and is only found on the surface. In this case, only a broad resonance will be observed for each proton of the ligand. This is the case for oleic acid capping ligands on CdSe or PbSe NCs in a purified suspension.^{4,7}

Slow or fast exchange

In the case that exchange according to Figure 2.1 does occur, there are still different possibilities that should be distinguished when interpreting the NMR spectra. Depending on the kinetics of the exchange with respect to the NMR time scale, the appearance of the exchanging species in the spectra may be quite different.

Two-step exchange

Previous work has shown that also two-step exchange may exist for a capping ligand with an NC surface, each with a different exchange dynamics. An illustration of the two steps involved is given in figure 2.3. First, an equilibrium exists between the ligand bound to the NC surface (chemisorbed) and entangled in the ligand shell (physisorbed). Because this equilibrium typically involves a protonation/deprotonation step, the activation barrier involved is considerable and the exchange dynamics is usually slow on the NMR time scale. The source of the proton is usually another ligand which is entangled. After deprotonation, it becomes bound to the surface, effectively swapping states with the previously bound and now protonated ligand, that moves to the entangled state. A second

equilibrium now exists between the ligand in the entangled state and those free in solution. As this only involves non-bonding interactions, the kinetics of this exchange is much faster, causing it to be fast on the NMR timescale.

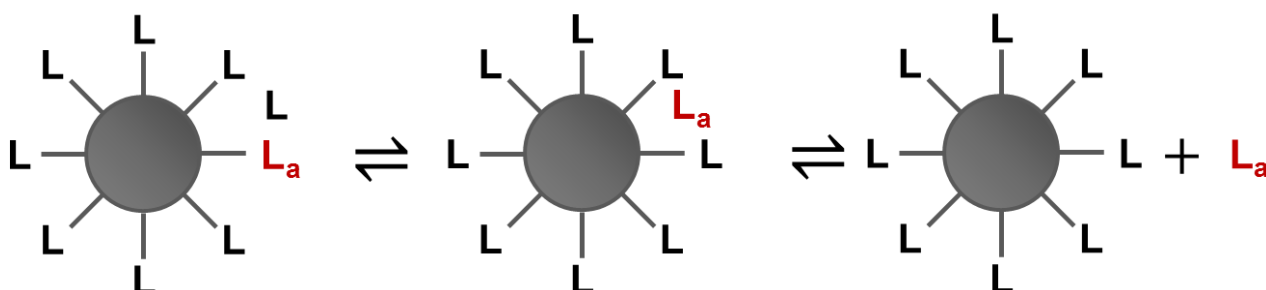


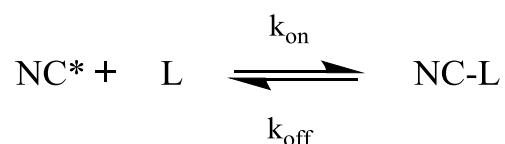
Figure 2.2. Illustration of two-step exchange of a ligand L_a with the NC surface

This behavior is observed in this work and was previously published by our group for oleic acid capped CdSe NCs when additional oleic acid is added to the suspension.⁷

2.2 Effects of exchange on resonance appearance

The theory of the exchange of ligands between free and bound states and the impact it has on resonance appearance, is well-described in literature, especially for the case of host-guest and protein-ligand interactions of interest in chemistry and biology.¹⁶ Conceptually, there is little difference between these systems and that of a ligand interacting with a nanoparticle surface. Therefore, the same theoretical treatment can be followed.⁵

The association/dissociation is given by following chemical equilibrium:



Where L represents the ligand and NC* represents an available binding site on the nanocrystal. The dissociation constant K_D is in that case given by:

$$K_D = \frac{[NC^*][L]}{[NC-L]} = \frac{k_{off}}{k_{on}} \quad (2.1)$$

Assuming association is diffusion controlled, the K_D value is mostly influenced by the k_{off} rate constant. Low off rates will lead to smaller KD values and be indicative of tight binding, while high off rates will lead to large KD values and be indicative of weaker binding for otherwise unaffected concentration of interacting species.

To discuss the impact of the exchange rates on the spectroscopic manifestation of the ligand resonances involved, the total exchange rate constant k_{ex} for the entire process is typically used and defined as:

$$k_{ex} = k_{on} + k_{off}$$

When ligands bind tightly, then $k_{ex} \ll \Delta\nu$ and no or slow exchange is observed. When ligands bind weakly to the NC, $k_{ex} \gg \Delta\nu$ and fast exchange is observed. $\Delta\nu$ refers to the frequency difference (in Hz) between both environments. These different cases are illustrated in figure 2.2 that depicts the impact of such dynamic exchange on the spectral properties. In both illustrated cases (a and b) the resonance of a particular hydrogen nucleus part of a ligand is monitored as the associated molecular species exchanges between two environments, here the free and NC bound ones.

In figure 2.2 a, both environments are equally populated by the exchanging species. As a result, two separate signals of equal integrated peak area are observed when no or slow exchange kinetics apply, i.e. when $\Delta\nu > k_{ex}$. In the case of fast exchange kinetics, i.e. $\Delta\nu < k_{ex}$, only one single

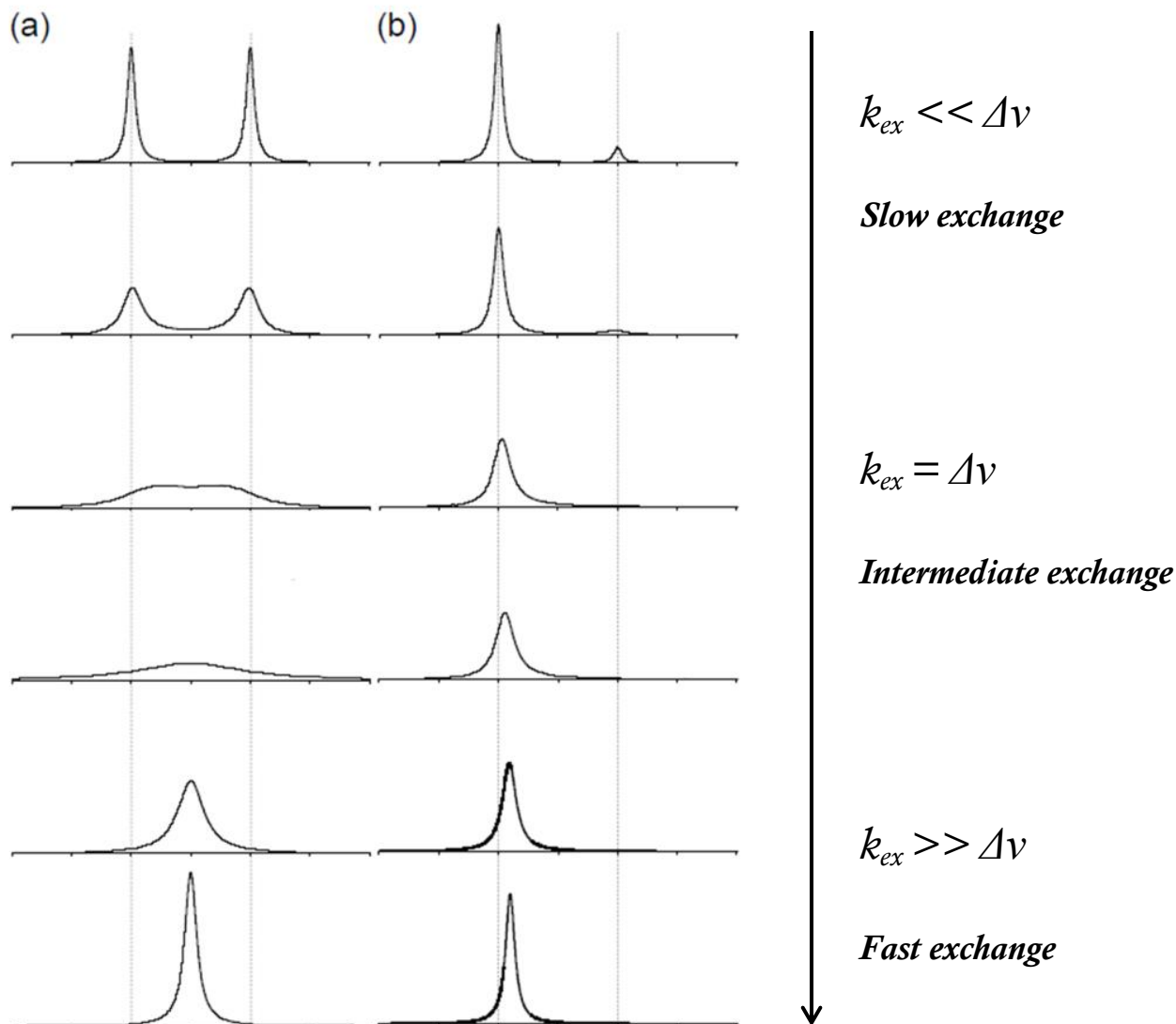


Figure 2.3. Two-site exchange for different k_{ex} values, ranging from slow to fast exchange, for both a system in which both environments are equally populated (a) and in which one environment is more heavily populated (b).¹⁵ The frequency difference between both sites is 400 Hz ($\Delta\omega = 2513 \text{ rad}\cdot\text{s}^{-1}$). Defining the relative populations of the two forms as α_A and α_B , the relative populations for (a) are $\alpha_A = \alpha_B = 0.5$ (b) $\alpha_A = 0.9$ and $\alpha_B = 0.1$.

resonance is observed. Its frequency corresponds to the population average of both individual frequencies.

$$\delta_{obs} = x_a \delta_a + x_b \delta_b \quad (2.2)$$

Here, x_a and x_b represent the fraction of respectively species a and b, and δ_a and δ_b the resonance frequencies expressed as chemical shifts. Since the

populations are considered equal, the resonance appears exactly halfway between the frequencies adopted in each environment. When the exchange rate approaches the frequency difference, considerable broadening occurs and coalescence is apparent when they are equal. This picture changes somewhat when one species is much more abundant than the other (e.g. in the case of a large pool of free ligand compared to a small amount of bound ligand) (figure 2.2 b). In this case, at slow exchange, both resonances are observed with their respective integral. When the exchange is fast on the NMR time scale, one single resonance is observed at a position closer to that of the most abundant species.^{15,17}

Some examples of ligands that are in fast exchange between the free and bound state are oleylamine capped PbS NCs, octylamine capped ZnO NCs and dodecylamine capped CdTe NCs.^{5,8} An example of a capping ligand that is in slow exchange between the free and bound state is TOPO capped InP NCs.³

2.3 1D ¹H NMR

Figure 2.4a depicts the 1D ¹H spectrum of oleic acid in toluene-d₈. The different OA resonances are assigned as indicated. Assignment is performed using chemical shift information and different 2D experiments, such as ¹H-HSQC and COSY (details are not provided here but can be found elsewhere in literature).⁴ Notice the resonance of the alkene protons at 5.4 ppm and the methyl resonance at 0.9 ppm, both fully resolved, making them the most interesting ones from the NMR point of view. They will be typically monitored in most systems studied in this work both for quantitation and for the study of the surface chemistry. Figure 2.4b depicts the same oleic acid but now as a non-exchanging capping ligand on CdSe NCs with a diameter of ~6 nm. Several changes are observed in the spectrum with

respect to the reference spectrum of oleic acid. One can clearly see that the resonances of the oleic acid protons are broadened and show a downfield shift (illustrated with the dashed line for the alkene resonance). These two characteristic spectral changes are mentioned excessively throughout literature.^{1,3,4,7,8,18-23} From theory²⁴, it is known that line broadening is inversely proportional to the transverse relaxation time, T_2 , according to

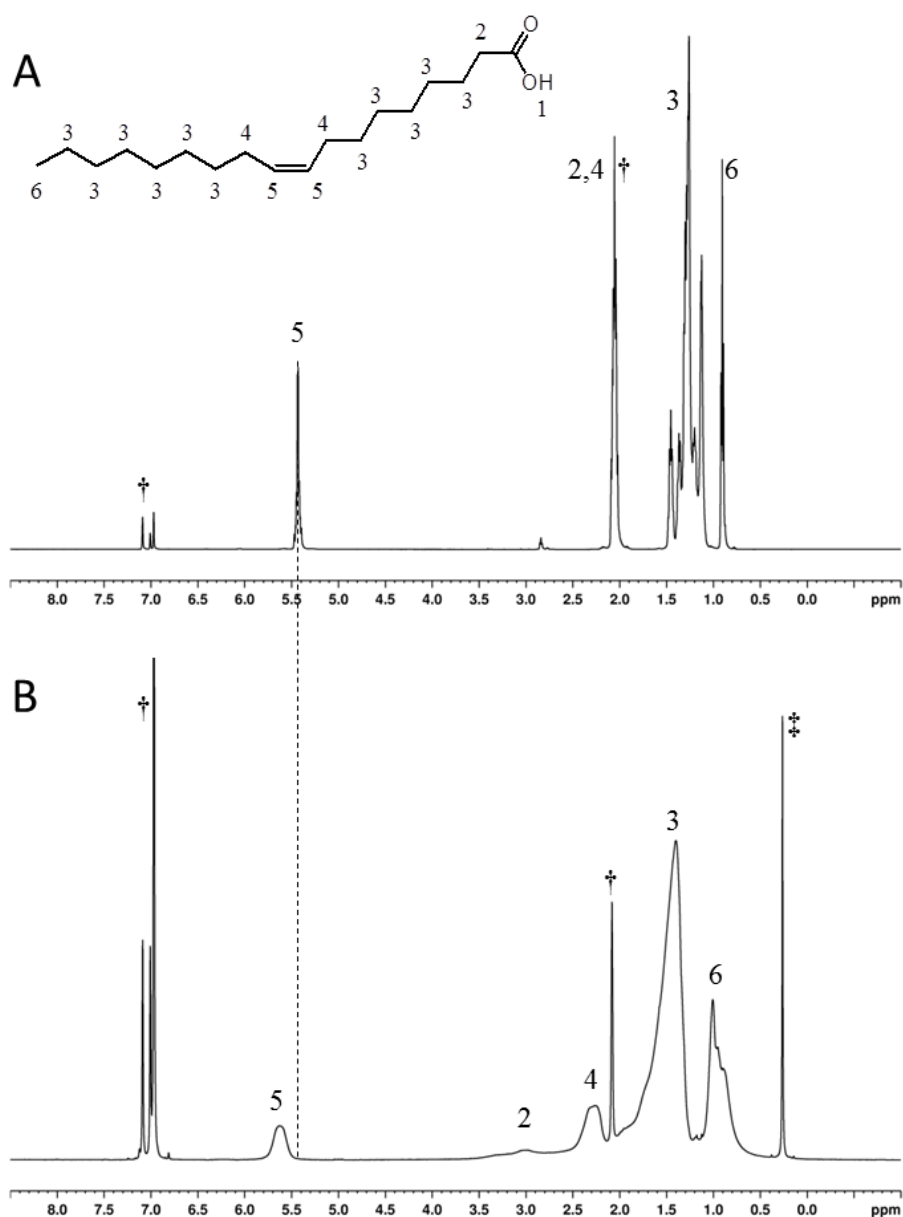


Figure 2.4. (a) 1D ¹H spectrum of oleic acid in toluene-d₈ at 298.2 K (b) 1D ¹H spectrum of oleic acid capping CdSe nanocrystals in toluene-d₈ at 298.2 K

equation 2.2. This transversal interproton dipolar relaxation is typically more efficient with a decreased rotational mobility of the ligands, i.e. when they are bound to the nanocrystal's surface.

$$\Delta\nu_{1/2} = \frac{1}{\pi T_2} \quad (2.2)$$

When recording the 1D ^1H spectrum in a quantitative fashion, i.e. with a relaxation delay d_1 of 30 seconds, which allows full T_1 relaxation ($d_1 > 5T_1$), it is also possible to determine the amount of bound ligands. For this quantification the integrated intensity of the resonance is weighed against an internal calibration of the spectrometer using the Electronic Reference To access In vivo Concentrations (ERETIC) method, which is based on PULse Length based CONcentration (PULCON) Determination.²⁵ The broadening of the resonances upon binding may raise questions about the precision of the integration. However, if both edges of the signal are clearly observed one can take the whole resonance in consideration. However when broadening increases even more due to binding to very large particles or exchange phenomena, it becomes harder to define the edges of the resonance and integration may in these cases cause an underestimation of the amount of bound ligands. In the worst case, broadening can cause the signal to be no longer detectable. Then, an indirect way to quantify the amount of bound ligand is by adding an excess of a different ligand with higher affinity to the solution and quantifying the released ligand in the free state.

2.4 Nuclear Overhauser enhancement spectroscopy (NOESY)^{24,26,27}

NOESY is a 2D NMR technique that is very widely used for characterizing molecular stereochemistry and conformation because it gives information on the short internuclear distances. The NOE can be defined as

the change in intensity of one resonance when the spin transitions of another, dipolarly coupled spin are perturbed from their original populations.

The mechanism behind this can be illustrated if we consider the energy level diagram of a two-spin system (figure 2.5). Now suppose that spin S is saturated, i.e. population differences across the S transitions are forced to 0. Clearly, the system is now perturbed from its equilibrium and will try to regain this by altering its spin populations. There are 6 different relaxation pathways that make this possible. Four of these pathways are single-quantum transitions that are labeled by a transition probability W_1 . The two other transitions involve the simultaneous flipping of both I and S spins. The $\alpha\beta$ - $\beta\alpha$ W_0 process is referred to as a zero-quantum transition and the $\alpha\alpha$ - $\beta\beta$ W_2 process is the double-quantum transition. It is these two cross-relaxation pathways that are responsible for the NOE. A W_2 process will remove spins from the $\beta\beta$ state to the $\alpha\alpha$ state in an attempt to recover the

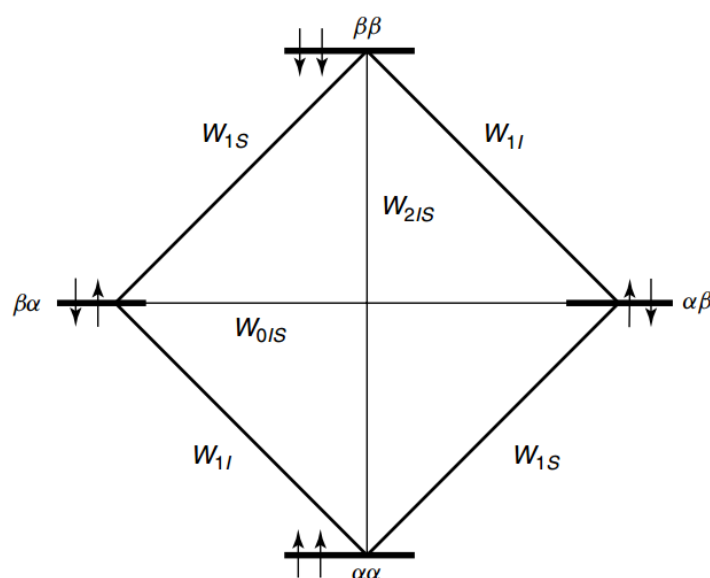


Figure 2.5. Energy level diagram for a two-spin system, showing the definitions of transition probabilities (W_0 , W_1 , and W_2) and spin states ($\alpha\alpha$, $\alpha\beta$, $\beta\alpha$ and $\beta\beta$). Spin states are written with the state of I first and that of S second, i.e., $\alpha\beta$ means spin I is in the α state, and spin S in the β state (from ref. 24)

population differences across the S transitions. Doing so, it increases the population difference across the two I transitions. This will result in a net increase of the I spin resonance intensities in the spectrum, i.e. create a positive NOE. A W_0 process will transfer spins from the $\beta\alpha$ to the $\alpha\beta$ state also attempting to recover population differences across S transitions. In this case however, the population difference across the I transitions will decrease, leading to a reduction of the I spin resonance intensities in the spectrum, i.e. a negative NOE. The W_1^I process will attempt to re-establish the equilibrium population differences for the I transitions as soon as the NOE begins to develop and will act against the NOE build-up.

Considering all the various rate processes involved in the population changes, following expression can be derived for the steady-state NOE:

$$\eta_I\{S\} = \frac{\gamma_S}{\gamma_I} \left[\frac{W_2 - W_0}{W_0 + 2W_1^I + W_2} \right] \equiv \frac{\gamma_S}{\gamma_I} \left[\frac{\sigma_{IS}}{\rho_{IS}} \right] \quad (2.4)$$

In this equation for the steady-state NOE, all the important factors needed for interpreting NOE data are present, making it very useful even though NOE enhancements in NOESY spectra are measured under transient-state spin perturbations.

Quantitative expressions for the relaxation rates for the case of two spins $\frac{1}{2}$ relaxing exclusively via their mutual dipole-dipole interaction are the following:

$$W_{0IS} = \frac{1}{20} K^2 J(\omega_I - \omega_S) \quad (2.5)$$

$$W_{1I} = \frac{3}{40} K^2 J(\omega_I) \quad (2.6)$$

$$W_{2IS} = \frac{3}{10} K^2 J(\omega_I + \omega_S) \quad (2.7)$$

Where $K = (\mu_0/4\pi)\hbar\gamma_I\gamma_S r_{IS}^{-3}$.

The various spectral density functions $J(\omega_x)$ in these equations each describe how good the local magnetic fields oscillating at the frequency ω_x due to molecular motions can stimulate relaxation. Via these spectral density functions, we can link the molecular tumbling with the transition probabilities. Assuming isotropic tumbling of a rigid molecule, the spectral density can be said to be:

$$J(\omega_X) = \frac{2\tau_c}{(1+\omega_X^2\tau_c^2)} \quad (2.8)$$

For small molecules, molecular tumbling is very rapid and $\omega_X\tau_c \ll 1$. This is called the extreme narrowing limit and in this case, the denominators of all spectral density expressions can be set to 1 which simplifies the expression of the NOE enhancement in Eq. 2.4 to + 50 % in

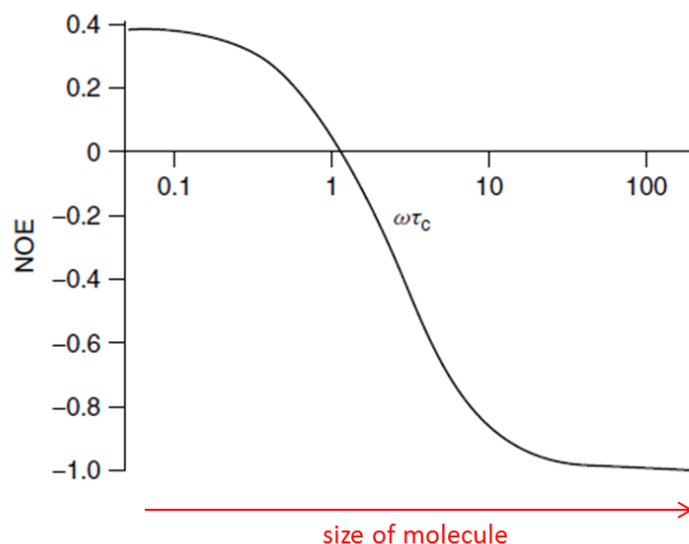


Figure 2.6. NOE enhancement in function of molecular size (figure from ref 24)

the homonuclear case. W_2 processes are dominant in this case, thus the NOE enhancement is positive. When molecular weight increases and $\omega_X\tau_c \approx 1$, the number of W_2 and W_0 transitions are nearly equal and NOE

enhancements reduce to zero. In larger molecules when $\omega_X\tau_c \gg 1$, all spectral densities other than $J(\omega_I - \omega_S)$ become insignificant and W_0 transitions will now become dominant, leading to negative NOE enhancements that build up rapidly. This limit is known as the spin-diffusion limit. Figure 2.6 illustrates this dependence of the NOE enhancement on molecular weight.

Unwanted signals remaining from the NOESY sequence are zero-quantum coherences (ZQCs) that existed during the mixing time and which are subsequently transformed to observable signals by the last 90° pulse. These are COSY-like peaks with anti-phase multiplet appearance. When applied to the case of nanocrystal research, the following observations can be expected.

A ligand that is free in solution behaves as a small molecule and will develop weak, positive NOEs, as shown for oleic acid in toluene- d_8 in figure 2.7a. On the other hand, ligands that are tightly bound to the surface (no or slow exchange) will develop large negative NOEs, as shown for oleic acid capping ligands on CdSe NCs in figure 2.3b. It is important to clarify that positive NOEs have opposite signs from the diagonal peaks and negative NOEs have the same sign as the diagonal peaks. Also, clear and negative NOEs will typically be observed between all resolved resonances, even if the distance between the spins is larger than the normal distance for NOE build-up. This phenomenon is caused by efficient multistep transfers involving spin diffusion.⁷ These spectra illustrate the applicability of 2D NOESY to identify ligands bound to a nanocrystal versus non-interacting ligands that are free in solution. This has also been demonstrated already several times in literature for different types of nanocrystals.^{5,6,8,23}

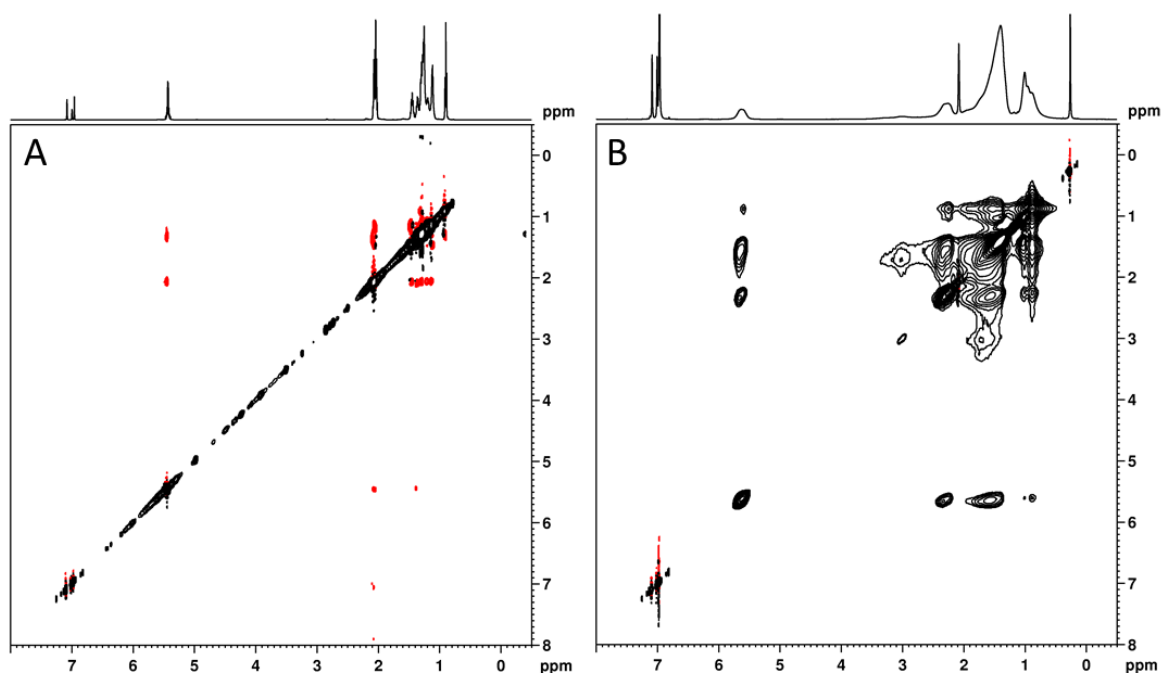


Figure 2.7. 2D NOESY spectrum of (a) oleic acid in tol-d₈, recorded with 450 ms mixing time, (b) oleic acid capping ligands on CdSe NCs in tol-d₈, recorded with a 300 ms mixing time

In the case of oleic acid capping ligands on CdSe NCs, the ligands are tightly bound to the surface and negative NOEs are easily interpreted as the result of the ligand's behavior as part of one large system. In case a molecule or ligand is in fast exchange with the surface, NOESY remains a suitable technique to identify this case thanks to the occurrence of the transfer NOE.^{5,6,27} The trNOE concept can be explained conveniently using the depiction in figure 2.8. Upon adsorption on the NC surface, the tumbling rate of the ligand slows down and an initial polarization located at specific protons can be efficiently distributed via the NOE effect to neighboring protons during the mixing time. This distributed polarization is maintained after desorption, when the ligand's tumbling rate increases again, and appears as a cross peak in the 2D NOESY spectrum. Negative NOEs generated in the bound state are thus easily transferred to the free state. An example of this was reported in literature by our research groups for DDA (dodecylamine) capped CdTe NCs where the DDA is in fast exchange

between the bound and free state, but strong negative trNOE cross peaks are observed (figure 2.9).⁵

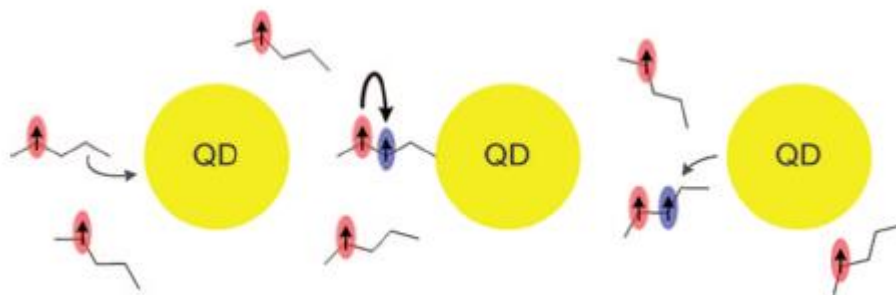


Figure 2.8. The trNOE concept (figure from ref 5)

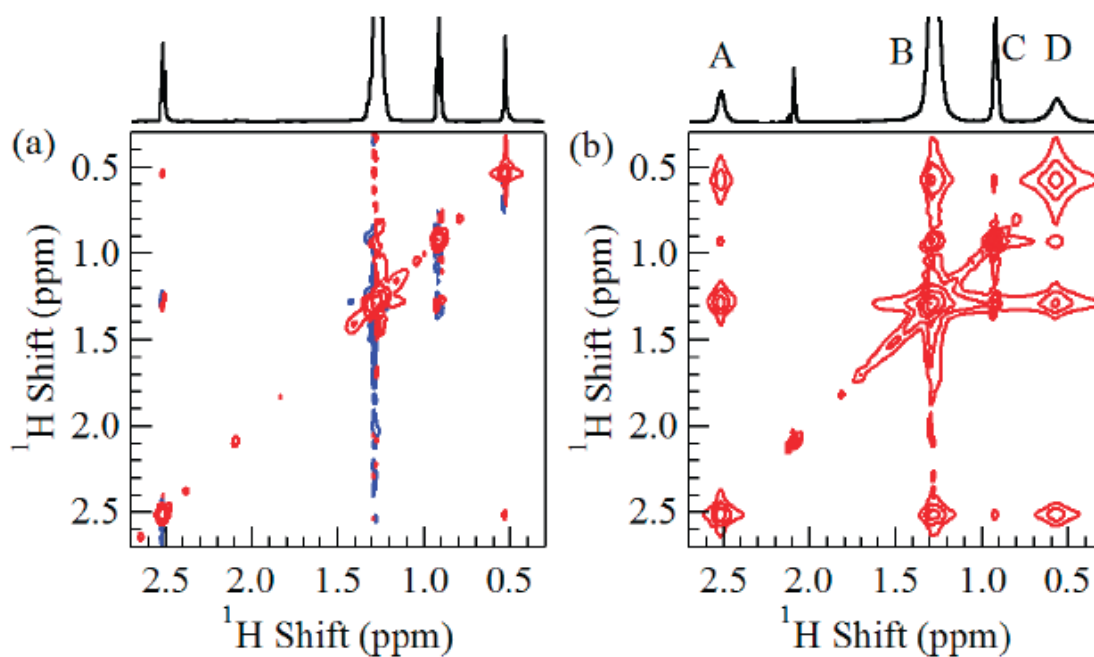


Figure 2.9. 2D NOESY spectra at 100 ms mixing time of a reference DDA sample in toluene (a) and of Q-CdTe with DDA (b). Whereas zero-quantum coherence artifacts typical for small molecules are visible in the reference sample, strong, negative trNOE cross-peaks are apparent in Q-CdTe|DDA. (from ref 5)

2.5 Rotating frame Overhauser Enhancement Spectroscopy (ROESY)²⁸

The ROESY experiment was originally designed to study the structure of intermediate sized molecules, since the NOE build-up curve crosses zero for those molecules.^{29,30} As shown in figure 2.10, in contrast to the NOE, the

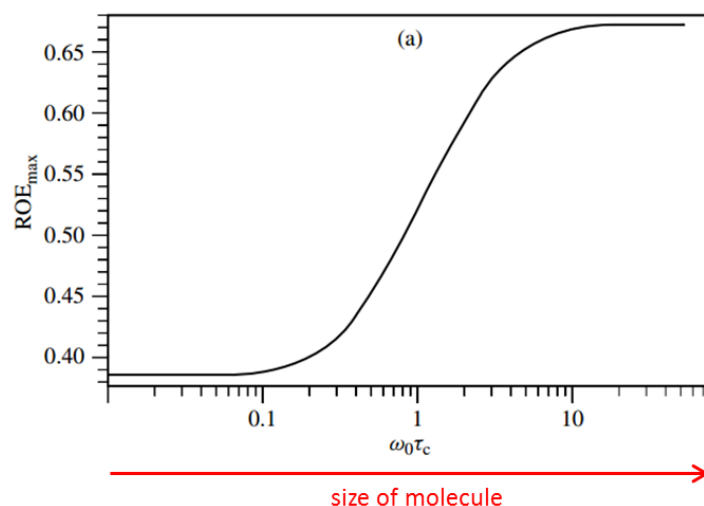


Figure 2.10. ROE enhancement in function of molecular size (figure from ref 6)

ROE build-up curve is positive for all sizes of molecules. For the study of nanocrystals, a secondary advantage of ROESY is being used, i.e. the possibility to distinguish cross relaxation from chemical exchange effects. ROE cross peaks will always be positive, i.e. display a sign opposite to the diagonal peaks, while chemical exchange cross peaks will be negative, i.e. have the same sign as the diagonal peaks. Practically, the experiments used throughout this thesis are off-resonance ROESY experiments, since these lack the unwanted TOCSY (or HOHAHA) transfers.³¹ The value of this technique was demonstrated by our research groups in a paper on self-exchange of carboxylic acid ligands on CdSe QDs (figure 2.11).⁷ When oleic acid is added to a suspension of oleic acid capped CdSe NCs, a two-step exchange occurs (*cf. supra*). In the 2D NOESY spectrum (figure 2.11 a), no distinction can be made between cross-peaks resulting from slow exchange (see inset) or from NOEs occurring between the different resonances of one

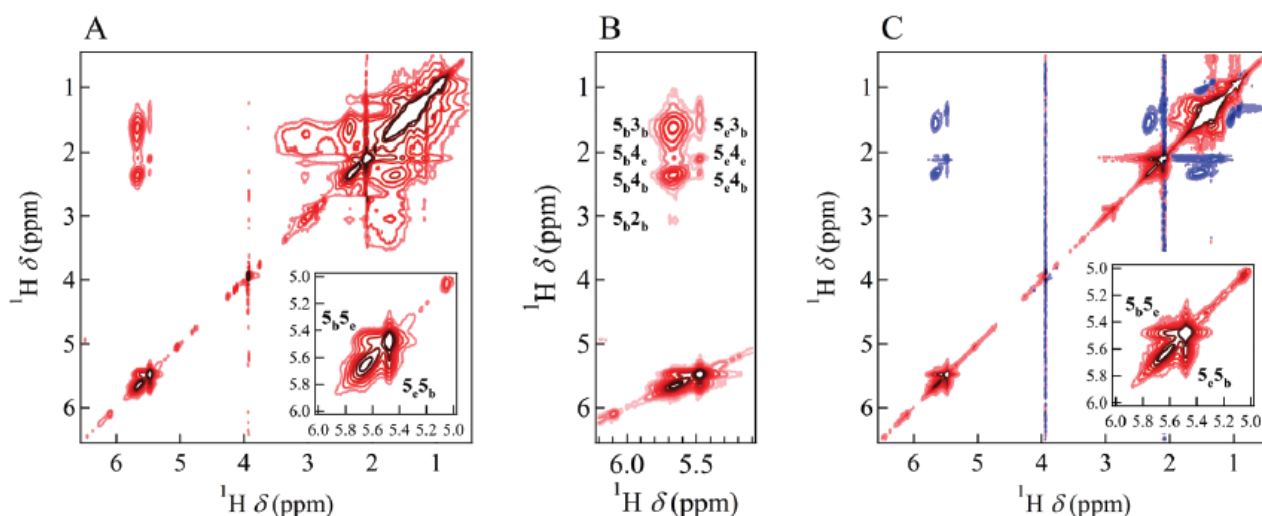


Figure 2.11. Suspension of oleic acid capped CdSe NCs with additional oleic acid added in a two-step exchange equilibrium, 2D NOESY spectrum (A), zoom of alkene region (B), 2D ROESY spectrum (C). (from ref 7)

species: they are all negative, *i.e.* they have the same sign as the diagonal peaks. In the 2D off-resonance ROESY however (figure 2.11 c), the ROE cross peaks are positive while the cross peak between the bound and “free” pool of OLAc is clearly negative (see inset), indicating that this peak originates from chemical exchange.

2.6 Diffusion Ordered Spectroscopy (DOSY)³²⁻³⁷

Self-diffusion arises from the random translational (Brownian) motion of molecules in physically homogenous solutions. The diffusion coefficient is a measure of the rate of mean square displacement of a molecule and has units of m^2s^{-1} . The principle of a simple diffusion measurement using a Pulsed-Field Gradient (PFG) approach is shown in figure 2.7.³⁴ First, the magnetization is rotated from the z-axis into the x-y plane with a $\pi/2$ rf pulse. Then, a gradient pulse with duration δ and strength g_z is applied. At the end of the first period τ , a π rf pulse reverses the sign of precession. Finally, at time $t_1 + \Delta$, a second gradient pulse with same duration δ and strength g_z is applied. If the spins have not undergone any translational

motion with respect to the z-axis, all spins will refocus and maximum signal intensity is obtained. If however part of the spins have moved over the z-axis during the diffusion time Δ , these spins are not refocused and the final signal is attenuated. You might think of it as creating a magnetization helix during the first gradient and unwinding this helix during the second gradient pulse (since the phase angle was changed during the π rf pulse). If the spins stay on their z-position, the echo signal is the same before and after this “helix formation”. If on the other hand, the spins diffuse through the z-axis,

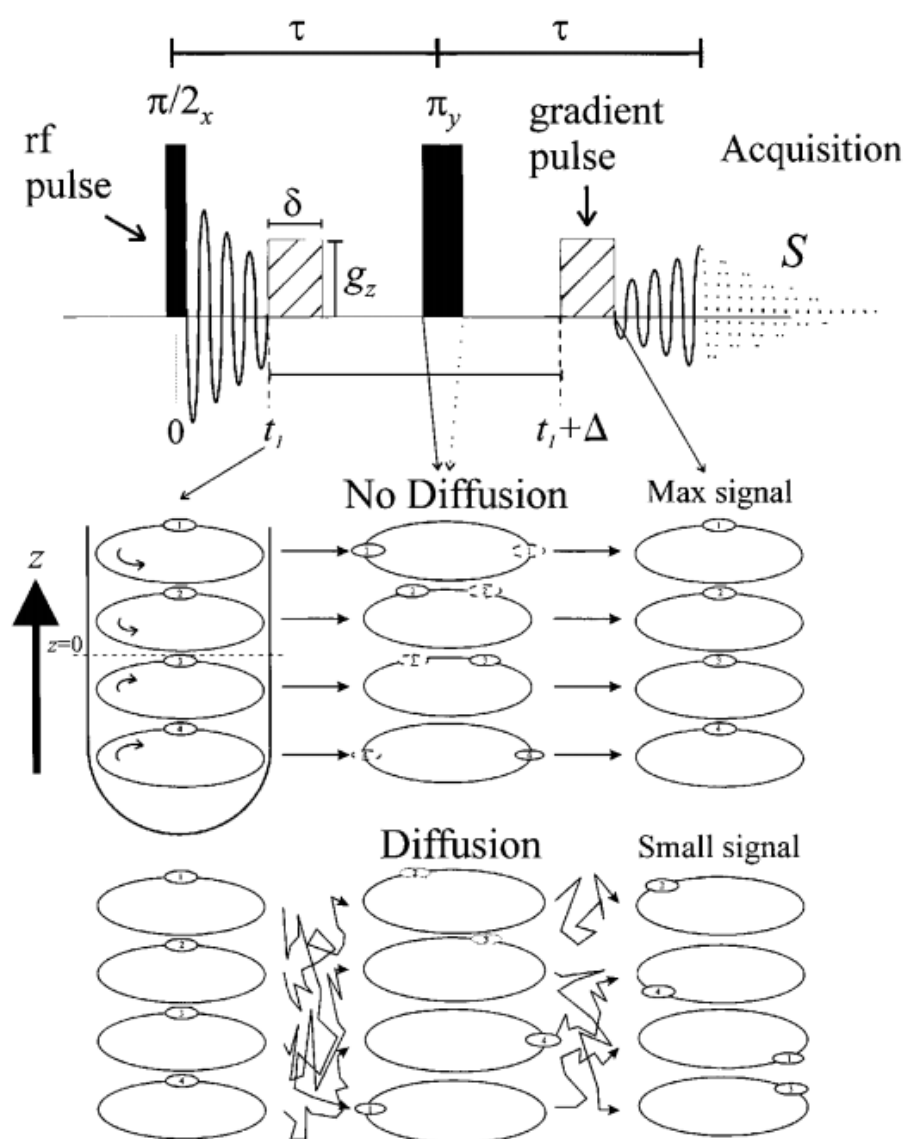


Figure 2.12. Depiction of a simple PFG NMR experiment and the effect of diffusion on the signal intensity (from ref 32)

the winding and unwinding of the helix are scrambled resulting in a smaller echo signal. Two important parameters in this pulse sequence that can be optimized are the duration of the gradient pulse δ and the time between the two gradient pulses Δ . For all the experiments in this thesis, these values are optimized to get signal attenuation at the maximal gradient strength of at least 90%, with $\delta < 2500 \mu\text{s}$ and $\Delta < 0.35 \text{ s}$. It is important to get this attenuation in order to have a correct sampling of the Gaussian decay of the resonance intensity. During the experiment, the gradient strength is systematically varied to its maximum in 32 or 64 steps. For ligand-nanocrystal systems, it is important to keep δ as low as possible since effective relaxation causes these resonances to decay rapidly during this delay time. Therefore, we optimized to a maximized Δ (maximum due to probe safety limitations) and kept δ as low as possible. For the ligand-nanocrystal systems studied in this thesis, the normal probe (Z gradient of 50 G/cm) was sufficient to obtain good signal decay and fitting. Larger systems with reduced diffusivity may not satisfy the 90% or more attenuation criterion. In this case, the use of a dedicated diffusion probe (1200 G/cm) may be considered.

From the results of the PFG experiment, a diffusion coefficient D is calculated using the appropriate Stejskal-Tanner equation.³⁷ [ENREF_36](#) As the convection compensated diffusion experiment using smoothed rectangle gradient shape functions were mostly used in this work, this was mostly the following equation:

$$I = I_0 \exp \left\{ -D\gamma^2 \delta^2 g^2 \frac{81}{100} \left(\Delta - \frac{6.344\pi^2 - 207}{9.720\pi^2} \delta - \frac{\tau_1 + \tau_2}{2} \right) \right\} \quad (2.9)$$

The calculations were always performed using an in-house MatLab-script. Fitting can be mono or bi-exponential, according to the presence of overlapping signals with different diffusion coefficients.

In the case of CdSe NCs capped with oleic acid ligands, the resulting data points and fitting curves are depicted in figure 2.13. These curves belong to the alkene signal at 5.4 ppm only, but the same result is obtained when processing the attenuation of the other resonances. In the logarithmic plot a linear decay is visible, which points to a mono exponential decay. The calculated diffusion coefficient is $99.6 \pm 0.7 \mu\text{m}^2/\text{s}$. From the diffusion

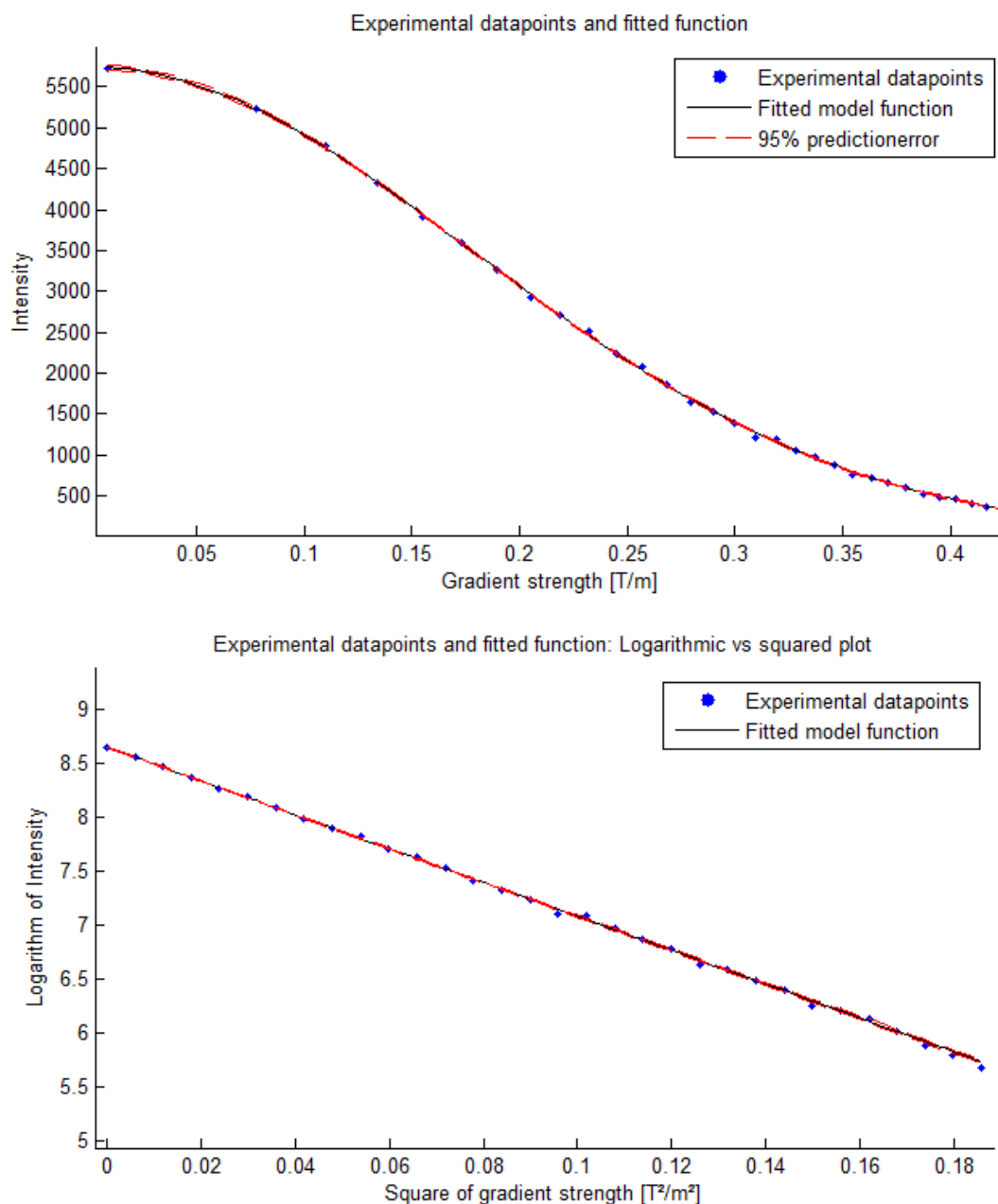


Figure 2.13. Decay of the signal intensity at increasing gradient strength during the 2D DOSY sequence of the alkene resonance of strongly bound oleic acid capping ligands on CdSe NCs in toluene-d₈ at 298 K.

coefficient, a hydrodynamic radius is calculated using the Stokes-Einstein equation for spherical particles.

$$r_H = \frac{k_B T}{6\pi\eta D} \quad (2.10)$$

Here k_B is the Boltzmann constant, T is the temperature in Kelvin, η the viscosity of the solvent in mPa.s and D the diffusion coefficient in m^2/s . The different values of the viscosities used in this thesis are given in table 2.1. For our example of CdSe capped with oleic acid ligands, the resulting hydrodynamic radius is 3.71 nm.

For comparison, the diffusion coefficient of a reference sample of oleic acid in toluene is also measured and calculated. Figure 2.14 shows the mono exponential decay of the signal intensity of the alkene resonance. Again only the logarithmic plot is shown since this provides a most convenient visual inspection of the information. Also in the course of this thesis, logarithmic plots will be given. The diffusion coefficient is equal to $556.8 \pm 0.4 \mu\text{m}^2/\text{s}$, which correlates with a hydrodynamic radius of 0.66 nm.

Table 2.1. Viscosities of solvents used in this thesis

solvent	viscosity (mPa.s)
toluene	0.59
chloroform	0.54
water	0.89
1,2-dichlorobenzene	1.32

In the case of fast chemical exchange on the diffusion time scale (defined by Δ^{-1}), the observed diffusion coefficient will be a weighted average between the two states, according to the following equation:

$$D_{obs} = x_A D_A + x_B D_B \quad (2.11)$$

With A and B the two possible states of the molecule, i.e. in our case free

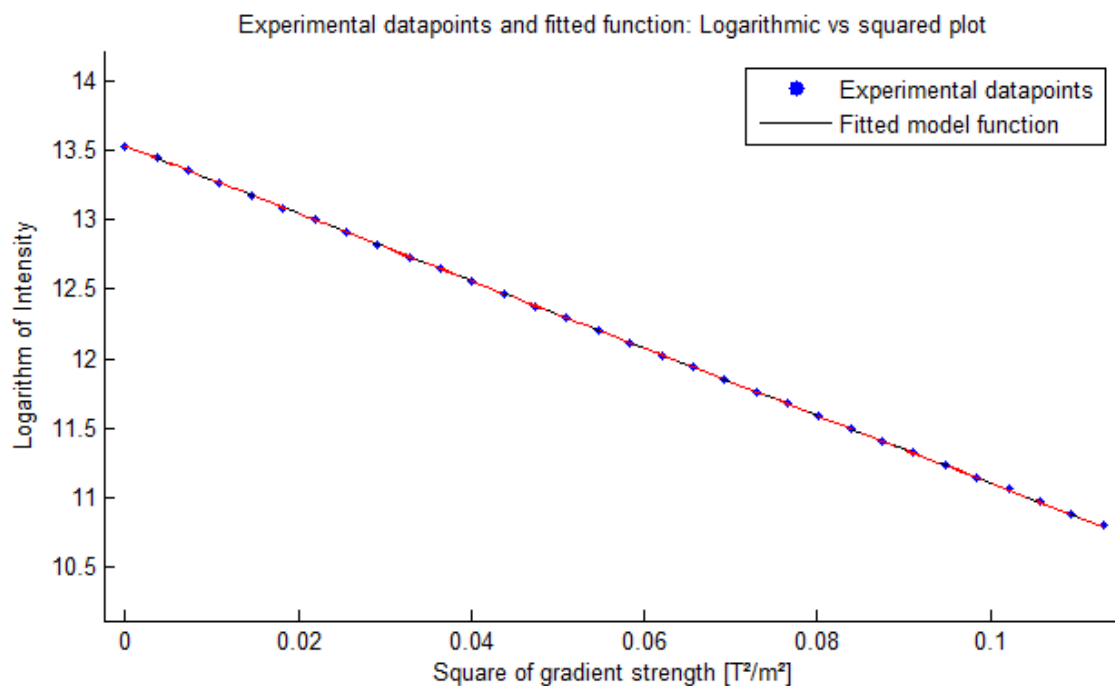


Figure 2.14. Decay of the signal intensity at increasing gradient strength during the 2D DOSY sequence of the alkene resonance of oleic acid in toluene-d₈ at 298 K.

and bound ligands.

2.7 References

- (1) Hens, Z.; Moreels, I.; Martins, J. C. *ChemPhysChem* **2005**, *6*, 2578.
- (2) Moreels, I.; Martins, J. C.; Hens, Z. *ChemPhysChem* **2006**, *7*, 1028.
- (3) Moreels, I.; Martins, J. C.; Hens, Z. *Sens. Actuator B-Chem.* **2007**, *126*, 283.
- (4) Moreels, I.; Fritzing, B.; Martins, J. C.; Hens, Z. *J. Am. Chem. Soc.* **2008**, *130*, 15081.
- (5) Fritzing, B.; Moreels, I.; Lommens, P.; Koole, R.; Hens, Z.; Martins, J. C. *J. Am. Chem. Soc.* **2009**, *131*, 3024.
- (6) Antti Hassinen, I. M., Celso de Mello Donegá, José C. Martins, and Zeger Hens *J. Phys. Chem. Lett.* **2010**, *1*, 2577.
- (7) Fritzing, B.; Capek, R. K.; Lambert, K.; Martins, J. C.; Hens, Z. *J. Am. Chem. Soc.* **2010**, *132*, 10195.
- (8) Moreels, I.; Justo, Y.; De Geyter, B.; Haustraete, K.; Martins, J. C.; Hens, Z. *ACS Nano* **2011**, *5*, 2004.
- (9) Hassinen, A.; Moreels, I.; De Nolf, K.; Smet, P. F.; Martins, J. C.; Hens, Z. *J. Am. Chem. Soc.* **2012**, *134*, 20705.

- (10) Kalyuzhny, G.; Murray, R. W. *J. Phys. Chem. B* **2005**, *109*, 7012.
- (11) Anderson, N. C.; Hendricks, M. P.; Choi, J. J.; Owen, J. S. *J. Am. Chem. Soc.* **2013**, *135*, 18536.
- (12) Anderson, N. C.; Owen, J. S. *Chem. Mat.* **2013**, *25*, 69.
- (13) Coppel, Y.; Spataro, G.; Pages, C.; Chaudret, B.; Maisonnat, A.; Kahn, M. L. *Chem.-Eur. J.* **2012**, *18*, 5384.
- (14) Hughes, B. K.; Ruddy, D. A.; Blackburn, J. L.; Smith, D. K.; Bergren, M. R.; Nozik, A. J.; Johnson, J. C.; Beard, M. C. *ACS Nano* **2012**, *6*, 5498.
- (15) Sinnaeve, D., Ghent University, 2010.
- (16) Meyer, B.; Peters, T. *Angewandte Chemie International Edition* **2003**, *42*, 864.
- (17) Bain, A. D. *Prog. Nucl. Magn. Reson. Spectrosc.* **2003**, *43*, 63.
- (18) Sachleben, J. R.; Wooten, E. W.; Emsley, L.; Pines, A.; Colvin, V. L.; Alivisatos, A. P. *Chemical Physics Letters* **1992**, *198*, 431.
- (19) Sachleben, J. R.; Colvin, V.; Emsley, L.; Wooten, E. W.; Alivisatos, A. P. *J. Phys. Chem. B* **1998**, *102*, 10117.
- (20) Kohlmann, O.; Steinmetz, W. E.; Mao, X. A.; Wuelfing, W. P.; Templeton, A. C.; Murray, R. W.; Johnson, C. S. *J. Phys. Chem. B* **2001**, *105*, 8801.
- (21) Shon, Y. S.; Wuelfing, W. P.; Murray, R. W. *Langmuir* **2001**, *17*, 1255.
- (22) Shaffer, A. W.; Worden, J. G.; Huo, Q. *Langmuir* **2004**, *20*, 8343.
- (23) Cros-Gagneux, A.; Delpech, F.; Nayral, C.; Cornejo, A.; Coppel, Y.; Chaudret, B. *J. Am. Chem. Soc.* **2010**, *132*, 18147.
- (24) Claridge, T. In *High-Resolution NMR Techniques in Organic Chemistry*; Elsevier: 2009; Vol. 27.
- (25) Wider, G.; Dreier, L. *J. Am. Chem. Soc.* **2006**, *128*, 2571.
- (26) Williamson, M. P. In *eMagRes*; John Wiley & Sons, Ltd: 2007.
- (27) Neuhaus, D. In *eMagRes*; John Wiley & Sons, Ltd: 2007.
- (28) Bax, A.; Grzesiek, S. In *eMagRes*; John Wiley & Sons, Ltd: 2007.
- (29) Bothner-By, A. A.; Stephens, R. L.; Lee, J.; Warren, C. D.; Jeanloz, R. W. *J. Am. Chem. Soc.* **1984**, *106*, 811.
- (30) Bax, A.; Davis, D. G. *Journal of Magnetic Resonance (1969)* **1985**, *63*, 207.
- (31) Desvaux, H.; Berthault, P.; Birlirakis, N.; Goldman, M. *Journal of Magnetic Resonance, Series A* **1994**, *108*, 219.
- (32) Stejskal, E. O.; Tanner, J. E. *The Journal of Chemical Physics* **1965**, *42*, 288.
- (33) Stilbs, P. *Prog. Nucl. Magn. Reson. Spectrosc.* **1987**, *19*, 1.
- (34) Price, W. S. *Concepts Magn. Resonance* **1997**, *9*, 299.
- (35) Ribot, F.; Escax, V.; Roiland, C.; Sanchez, C.; Martins, J. C.; Biesemans, M.; Verbruggen, I.; Willem, R. *Chem. Commun.* **2005**, 1019.
- (36) Morris, G. A. In *eMagRes*; John Wiley & Sons, Ltd: 2007.
- (37) Sinnaeve, D. *Concepts in Magnetic Resonance Part A* **2012**, *40A*, 39.

3

ALUMINIUM-ZINC-OXIDE NANOCRYSTALS

In this chapter, Aluminium doped Zinc Oxide NCs synthesized with both oleic acid and oleylamine are characterized. First, the project is situated in the current research area of transparent conductive oxides. Next, a full characterization using the NMR toolbox on this specific system is presented. This work was published in RSC advances.¹

3.1 Introduction

Transparent Conductive Oxides (TCOs) have received considerable attention in recent years because of their interesting properties in thin film optoelectronic devices such as solar cells², light emitting diodes^{3,4}, laser diodes^{5,6}, transistors⁷,... Tin doped Indium Oxide (ITO) is the most commercialized TCO material to date because of its high conductivity and transparency.⁸ However, concerns about its toxicity and the limited availability of Indium, forces researchers to consider different alternatives.

Aluminium doped Zinc Oxide (AZO) is seen as a promising alternative ITO and much research is performed in order to improve its characteristics and applicability.⁹⁻¹³ AZO has been reported with conductivities up to 10^4 S cm^{-1} and a transparency of 90%.¹⁴

In the research presented here, focus is placed on solution based methods instead of vacuum based physical routes because of valorization towards industrial applications. A thermal decomposition route yields monodisperse NCs with high colloidal stability. There are two types of thermal decomposition syntheses: the hot-injection method and the heating method.¹⁵ For this work, the heating method was explored since there was a lack of insight in the stabilization mechanisms occurring during the reaction and after stabilization with long-chain amines and carboxylic acids. AZO NCs were synthesized by thermal decomposition of Zn and Al acetylacetonates, as adapted from an original thermal decomposition synthesis route for ferrites.¹⁶ For the stabilization of these AZO NCs, the combination of two surfactants is often used, oleic acid and oleylamine, providing high colloidal stability.

The synthetic route is schematically presented in figure 3.1. Synthesis was carried out with 2 mmol of $\text{Zn}(\text{acac})_2 \cdot x\text{H}_2\text{O}$ in combination with 2 mol% $\text{Al}(\text{acac})_3$. Former reagents were mixed with 10 mmol 1,2-hexadecanediol and dissolved in a mixture of 6 mmol oleic acid, 6 mmol oleyl amine and 25 mL dibenzyl ether. The solution in the three-neck round bottom flask was magnetically stirred and flushed with nitrogen while heating to 60 °C with a heating mantle coupled to a JKEM scientific 310 controller. After obtaining a clear solution at 60 °C, the three-neck flask was closed under nitrogen and the temperature raised further up to 200 °C. The solution was maintained at 200 °C for 2 h and afterwards 1 h at 300 °C. After reflux, the obtained sol was cooled down to room temperature in the closed N_2 setup. Absolute ethanol (180 mL) was added (in atmospheric conditions) to destabilize the sol and to induce precipitation of the NCs. The precipitated particles were purified by means of centrifugation in an Eppendorf microcentrifuge (30' at 4000 rpm). The supernatant was discarded and the white powder with NCs was resuspended in 8 mL of hexane. The precipitation and centrifugation steps were repeated once. The resulting purified NCs were finally suspended in hexane (16 mL) and again centrifugated for 30' at 4000 rpm to remove larger NCs. In this final step, the precipitated pellet with the excess population was discarded and the

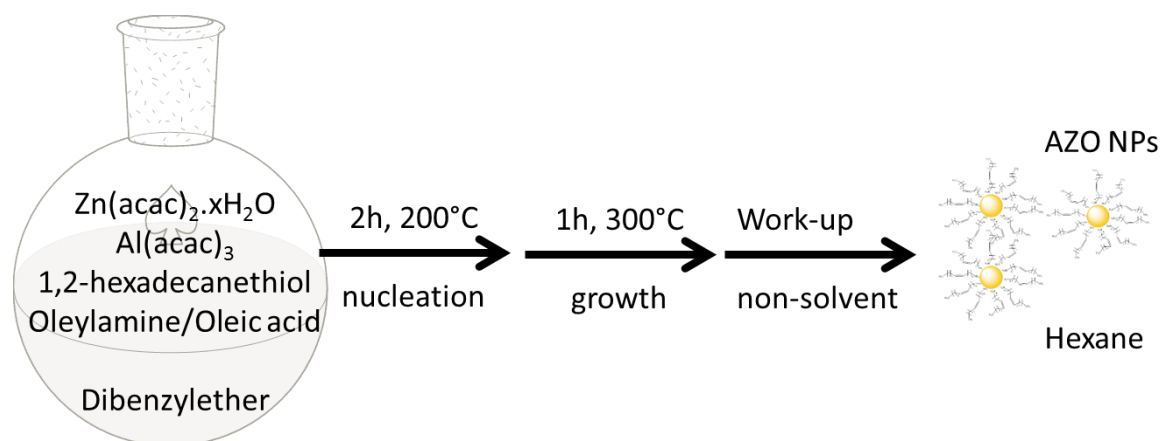


Figure 3.1. Schematic depiction of the synthesis and work-up procedure of AZO NCs.

supernatant, containing the desired NCs, is transferred into a container to be stored for further use. For the NMR characterization, the suspensions are first completely dried, using a rotary evaporator and subsequently an oil pump. Afterwards, the samples are redissolved in deuterated toluene and 600 μl is put in an NMR tube.

More information on the development and implementation of the synthesis strategies of AZO NCs and the processing towards different applications is available from the PhD thesis of Hanne Damm, whom did her PhD research on these materials at UHasselt and provided all the samples studied during our collaboration. In this thesis, focus is put solely on the characterization of the AZO NC colloidal suspensions using the NMR-toolbox. Different research questions were formulated in this collaboration. To address these, a full NMR characterization of the material was conducted first, since this already reveals some important information, such as nanoparticle size and dynamic ligand behavior.

After this initial study, we were challenged to determine the role of the two surfactants used, oleylamine and oleic acid. Both surfactants appear necessary during synthesis and stabilization, but their specific role was unclear. To explain why both are indispensable, we aimed at determining the composition of the final ligand shell, in order to determine whether they are both present there or not. Given the strong resemblance of their spectroscopic properties, we designed different experiments that allowed us to make a distinction between both. This work was the first in-depth study on the surfactants behavior of AZO NCs and provides important information for better understanding of the thermal decomposition synthesis. The main results were published in RSC advances.¹

3.2 Basic characterization

First, a basic characterization was performed on the AZO NCs synthesized via a heating synthesis using both oleic acid (OLAc) and oleylamine (OLAm) as surfactants.

In figure 3.2, the structural formula and 1D ^1H reference spectra of OLAc and OLAm in toluene- d_8 are shown. The assignment was carried out using 2D ^1H - ^1H COSY and 2D ^1H - $\{^{13}\text{C}\}$ HSQC. Given the structural similarities between both molecules, only few differences between both 1D ^1H spectra can be observed. Proton resonances 2 and 3 are overlapping in the spectrum of OLAc, while in the spectrum of OLAm, they are completely resolved due to the downfield shift of the proton resonances on the carbon next to nitrogen. Also, for OLAc, a small broad signal at 12 ppm

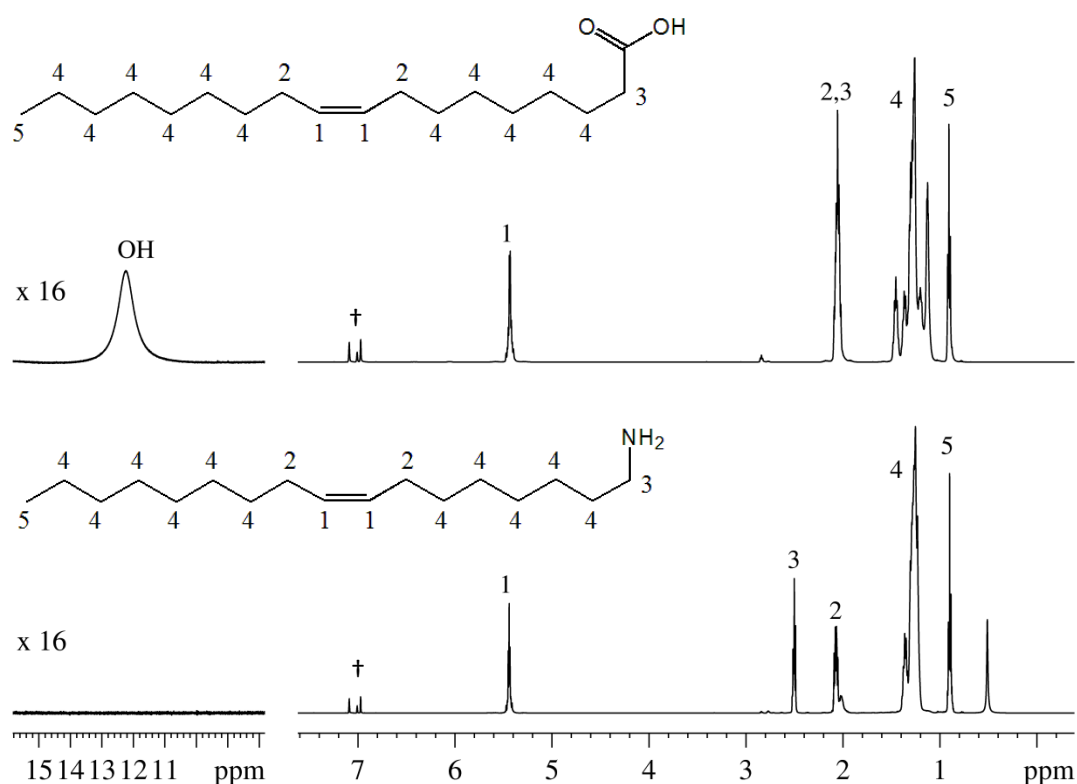


Figure 3.2. Structural formula and 1D ^1H spectra of OLAc (top) and OLAm (bottom) in toluene- d_8 (\dagger) at room temperature

is observed, typical for the carboxylic acid (COOH) resonance. For OLAm, we could expect a signal around 2 ppm for the amine NH_2 , but this is not observed in this reference sample. However, there is a small signal visible at 0.5 ppm, indicating the presence of some residual water in the sample. This causes fast exchange between the amine protons and the water pool, leading to a single exchange averaged resonance at 0,5 ppm.

Considering the spectrum of the AZO sample synthesized with both OLAc and OLAm and thus containing either one or both as capping ligand (figure 3.3), different observations can be made. First, all signals are severely broadened, indicating that the ligand(s) contributing to the spectrum is(are) bound to the AZO surface. Also, there is no additional free ligand pool, since no additional sharp signals are observed. This suggests that the ligand(s) is(are) bound at the surface (cfr. Chapter 2), which is also supported by DOSY measurements, *vide infra*. Second, resonances 1, 2, 4 and 5 are assigned using their chemical shift value and 2D ^1H - ^1H COSY and

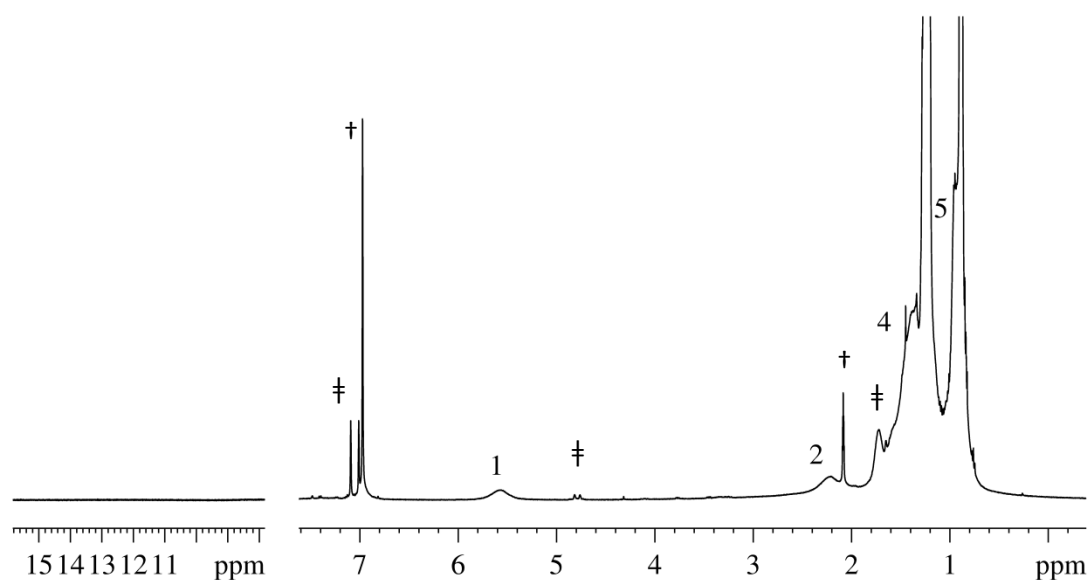


Figure 3.3. 1D ^1H spectrum of AZO NCs with OLAc and/or OLAm ligands in toluene- d_8 (†) at room temperature.

2D $^1\text{H}\{-^{13}\text{C}\}$ HSQC. Resonance 3, corresponding to the $\alpha\text{-CH}_2$ is not observed, which is also what we expect from a resonance that is this close to the surface (cfr. Chapter 2). Third, no labile carboxylic acid (COOH) signal is observed between 8 and 15 ppm. This can be explained in three possible ways: first, it is possible that only OLAm is present and therefore this proton is simply not present. Second, OLAc could be bound as an oleate or third, this proton is not observed due to severe broadening since it is too close to the NC surface. Finally, some impurities are observed: dibenzylether at 7.0 and 4.8 ppm and hexanediol in the alkyl region; the resonances assigned to these impurities are denoted with ‡ in the spectrum. These organic moieties are used during synthesis and were not removed during work-up. The 1D ^1H spectrum as such does not allow determination of the precise identity of the interacting ligand(s) on the surface. Either OLAm, or OLAc as an oleate or actually even OLAc as acid can (though highly unlikely), not be excluded as ligand from the 1D ^1H spectrum data above.

2D DOSY measurements are also conducted on the sample. Calculation of the diffusion coefficient is performed on the alkene signal using a mono exponential fitting (figure 3.4). A diffusion coefficient of $119.5 \cdot 10^{-12} \mu\text{m}^2/\text{s}$ is calculated, which matches a hydrodynamic diameter of 6.2 nm. This value is rather small when compared to DLS and TEM measurements, where a range of sizes is obtained around 10-15 nm. These measurements were however performed on different batches from those used for NMR study, which most likely explains the difference. Nevertheless, the mono-exponential decay does support our hypothesis that the surfactant is bound to the surface and no free pool of ligand is present (cfr. chapter 2).

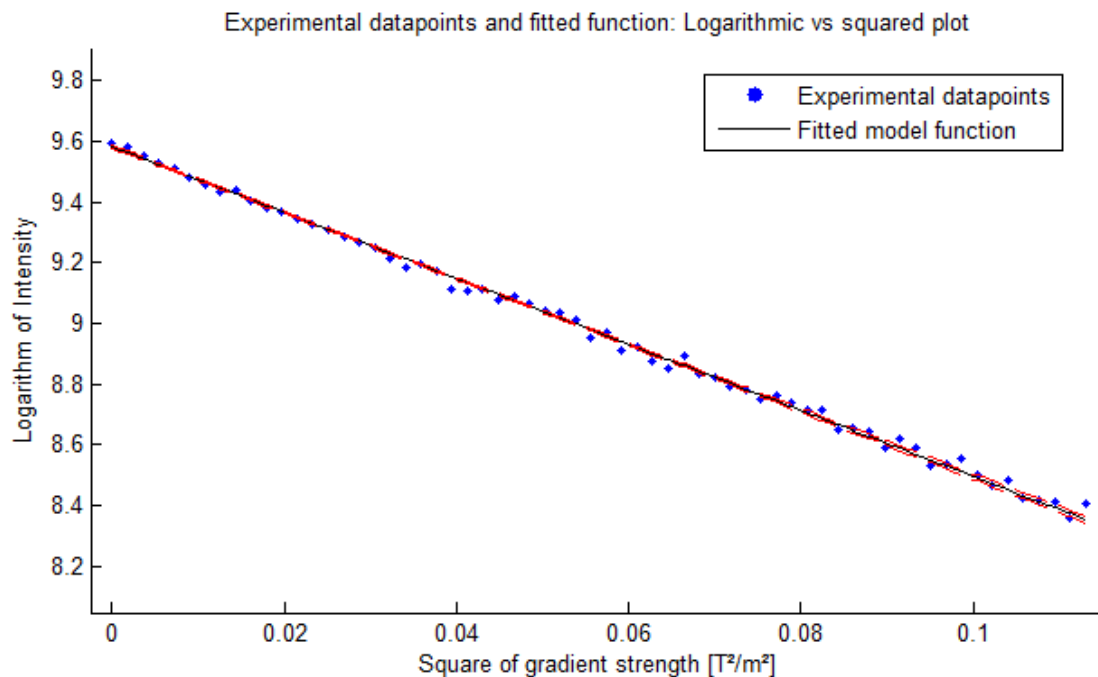


Figure 3.4. Logarithmic decay curve of the signal intensity of the alkene signal during the DOSY measurement.

The 2D NOESY spectrum (figure 3.5) confirms ligand binding on the AZO surface, given the presence of large negative NOEs between the different OLAc and/or OLAm resonances. In figure 3.5 B, the NOE cross peaks from resonance 1 to resonance 2, 4 and 5 are indicated. In figure 3.5 C, the NOE cross peaks from resonance 2 to resonance 4 and 5, and from resonance 4 to resonance 5 are indicated. Small positive NOEs are present between the hexanediol resonances indicating this is a small, non-interacting molecule present in the sample (figure 3.6 C). In between the different dibenzylether resonances, no NOE cross peaks are observed. This is probably due to the small quantity present in the sample but this notwithstanding, it indicates that it does not interact with the NC surface.

Combining all the observations from the first experiments, it can be concluded that the capping ligand is tightly bound to the AZO surface with no or slow exchange to a free molecular species in solution. The assignment of the capping ligand to both or either OLAc and OLAm is not possible

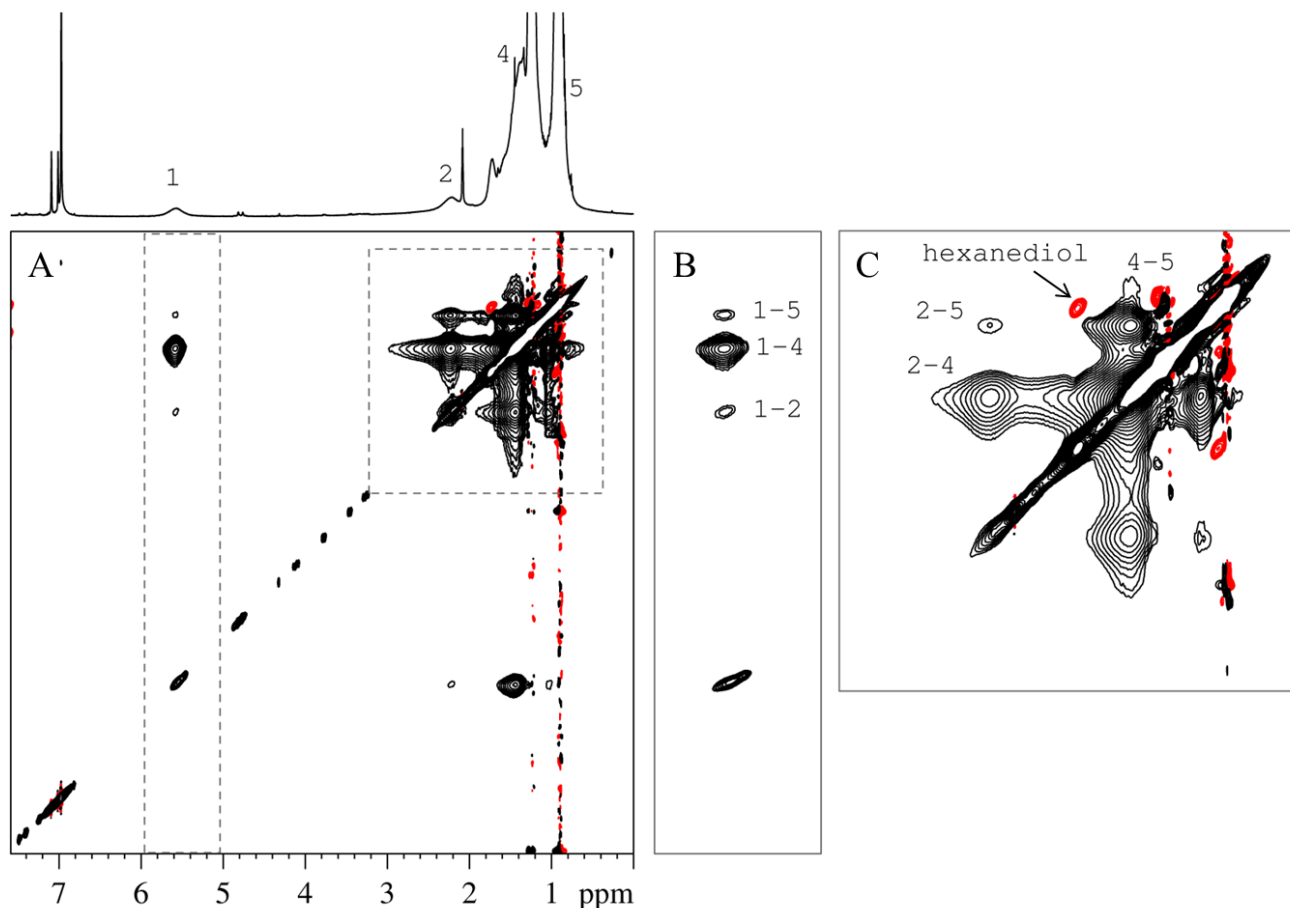


Figure 3.5. 2D NOESY spectrum of AZO NCs with OLAc and/or OLAm ligands in toluene-d₈ at room temperature, recorded with a mixing time of 300 ms.

based on the current measurements solely. For the latter, a different approach was considered.

3.3 Distinguishing OLAc and OLAm

Both OLAc and OLAm are added during the thermal decomposition synthesis to control size and shape and provide colloidal stability. The basic sample that we studied was synthesized using OLAc and OLAm in equimolar quantities (cfr. synthesis). Both the exclusive use of OLAc or OLAm leads to low yields and unstable suspensions, preventing any useful NMR investigation. Thus, it remains to be established if both or either one ends up capping the AZO surface in the stabilized colloid.

To address this, a sample was prepared using stearic acid (SteAc) instead of OLAc, but keeping OLAm in the synthesis. SteAc was chosen as an alternative carboxylic acid for several reasons. First, the synthesis yield was found to be similar and a stable colloid was obtained. Second, it allows selective observation of OLAm since only the latter will contribute an alkene resonance (cfr. Chapter 2).

In figure 3.6, the structural formula of stearic acid is shown together with the assigned reference spectrum in toluene-d₈. This assignment was carried out using 2D ¹H-¹H COSY and 2D ¹H-¹³C HSQC. Also, the 1D ¹H spectrum of the AZO NCs synthesized with both SteAc and OLAm is

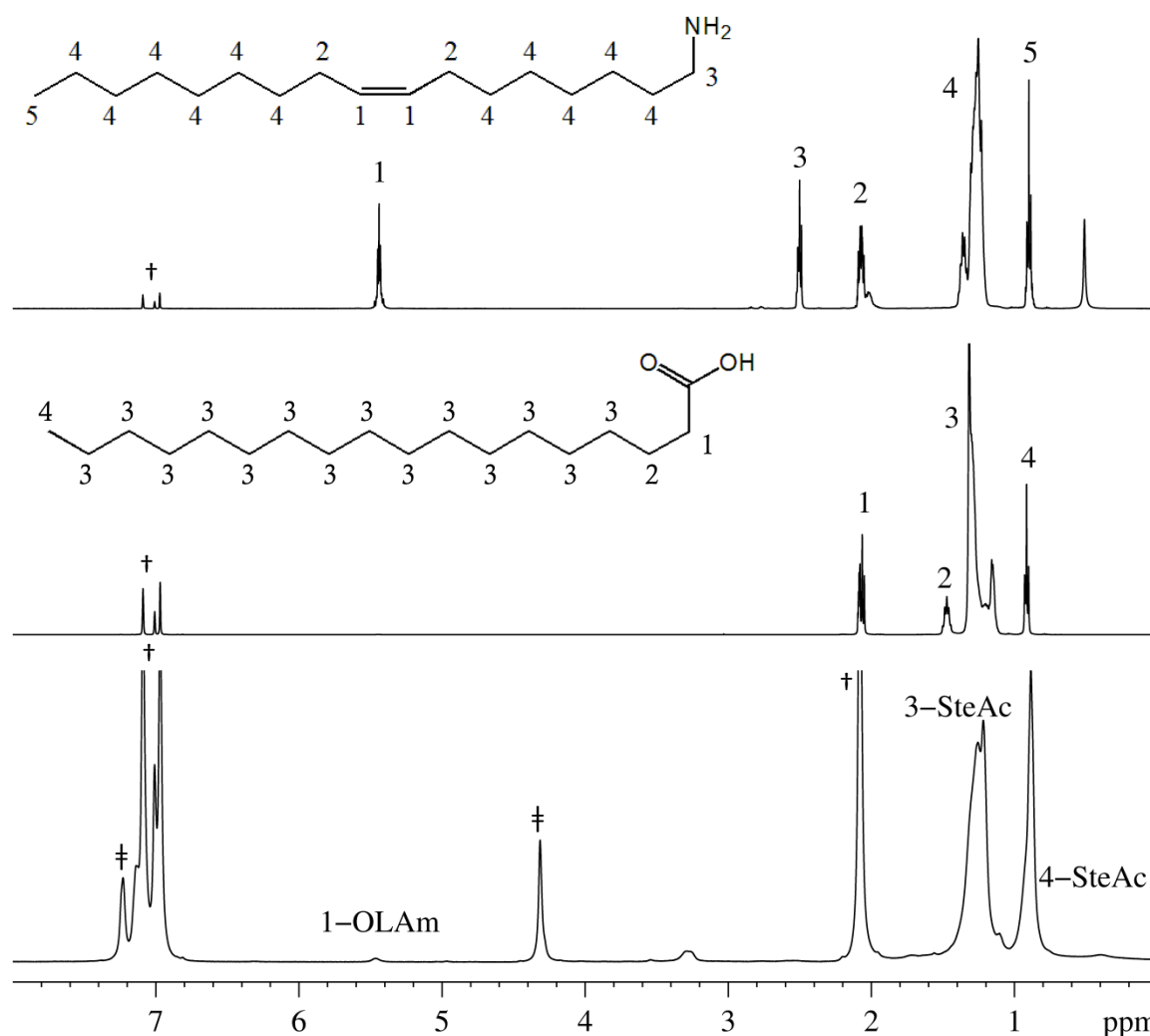


Figure 3.6. Structural formula and 1D ¹H spectrum of a reference sample of SteAc (top), of OLAm (middle) and of SteAc capped AZO NCs in toluene-d₈ (†) (bottom) recorded at room temperature

shown. Several observations can be made from this spectrum. First, the signal intensities of OLAm are very small. This can be due to a loss of OLAm during work-up since it is not captured in the ligand shell, *vide infra*. Second, the signals of stearic acid are visible and are broadened, indicating interaction. Third, also large signals from residual toluene (7.09, 7.00, 6.98 and 2.09 ppm) and dichlorobenzene (7.17, 7.05 and 4.40 ppm) are present in the spectrum.

In the 2D NOESY spectrum (figure 3.7), no negative NOEs are observed from the small alkene resonance at 5.5 ppm, that is assigned as 1-OLAm, to the alkyl region. This is especially visible when focusing on the region from the alkene to the alkyl region, as in figure 3.7 C. The fact that no positive

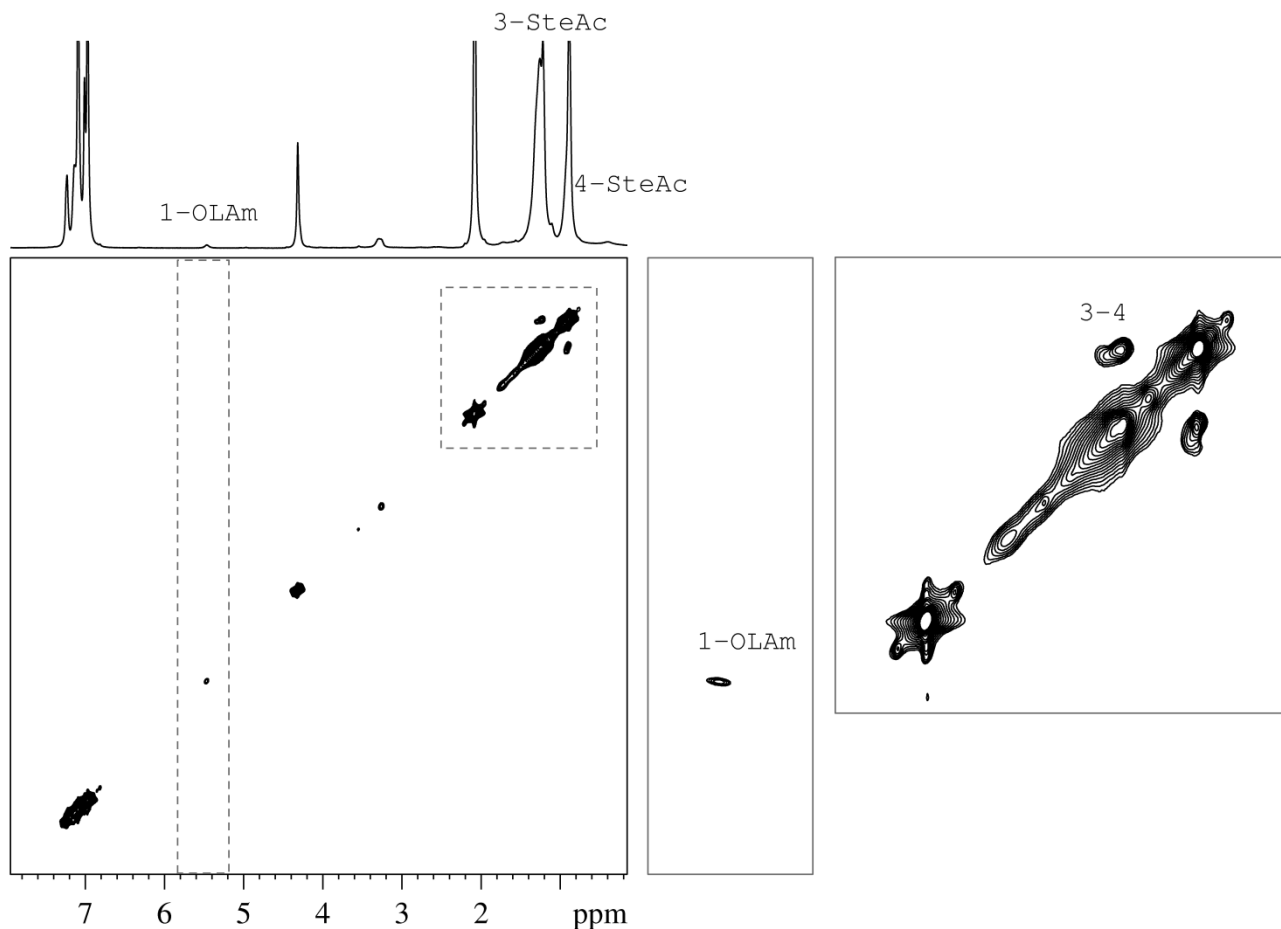


Figure 3.7. 2D NOESY spectrum of AZO NCs with SteAc and OLAm in toluene-d8 at room temperature, recorded with a mixing time of 300 ms

NOE cross-peaks are observed either between the OLAm resonances (as would be expected for a small molecule, cfr. Chapter 2) can be explained from the very low signal intensity of the alkene resonance, causing the already weak positive NOEs which build-up slowly to become unobservable. Based on this observation together with the small signal intensities of OLAm in the 1D ^1H , it is concluded that OLAm is not present in the ligand shell of the AZO NCs and is almost completely removed during work-up (cfr. synthesis). In between the alkyl resonances 3 and 4 of SteAc on the other hand, strong negative NOEs are observed. This proves that SteAc is bound on the AZO NC surface.

By performing a synthesis with SteAc instead of OLAc, we were thus able to determine that the amine is washed away during work-up and only the carboxylic acid is providing colloidal stability of the AZO NCs in the ligand shell. Furthermore, infrared analysis was performed on a suspension of AZO NCs capped with OLAc.¹ In the spectrum, 2 carboxylate stretch vibrations are visible at 1500-1400 cm^{-1} which indicates that the OLAc is bound as a carboxylate, i.e. an X-type ligand (cfr. chapter 1).

3.4 Dynamic behavior of OLAc on the AZO NC surface

Once it was established that OLAc is the sole capping ligand in the final colloidal suspension of AZO NCs, the dynamic behavior of OLAc on the AZO NC surface could be studied. To do this, a sample was synthesized as described in section 3.1 with OLAc and OLAm. Afterwards, the sample was prepared for NMR and OLAc was gradually added to the sample *in situ*, while monitoring the sample with ^1H NMR.

Focusing on the alkene resonance of OLAc in the 1D ^1H spectra recorded after each addition, several observations can be made (figure 3.8). First, the signal intensity of the resonance does not merely increase when

adding OLAc to the sample. Instead, a shoulder appears on top of the bound signal, on the right hand side. The chemical shift value of this shoulder does not match the chemical shift of the alkene resonance in the reference sample of OLAc in toluene-d₈. Also, this shoulder shows no fine structure but is a rather broad signal. Monitoring the chemical shift value of the shoulder over several additions, it is observed that the chemical shift value of the shoulder peak gradually evolves towards that of free OLAc in toluene-d₈, but does not reach it. This type of behavior has already been observed previously in our research group for a different system, namely CdSe NCs capped with OLAc, and the study of it was published in JACS¹⁷ see also chapter 2. In this previous work, the dynamic behavior of the system is categorized as a two-step exchange (cfr. Figure 2.3). In the system, there are three pools of OLAc present. First, there is the bound OLAc on

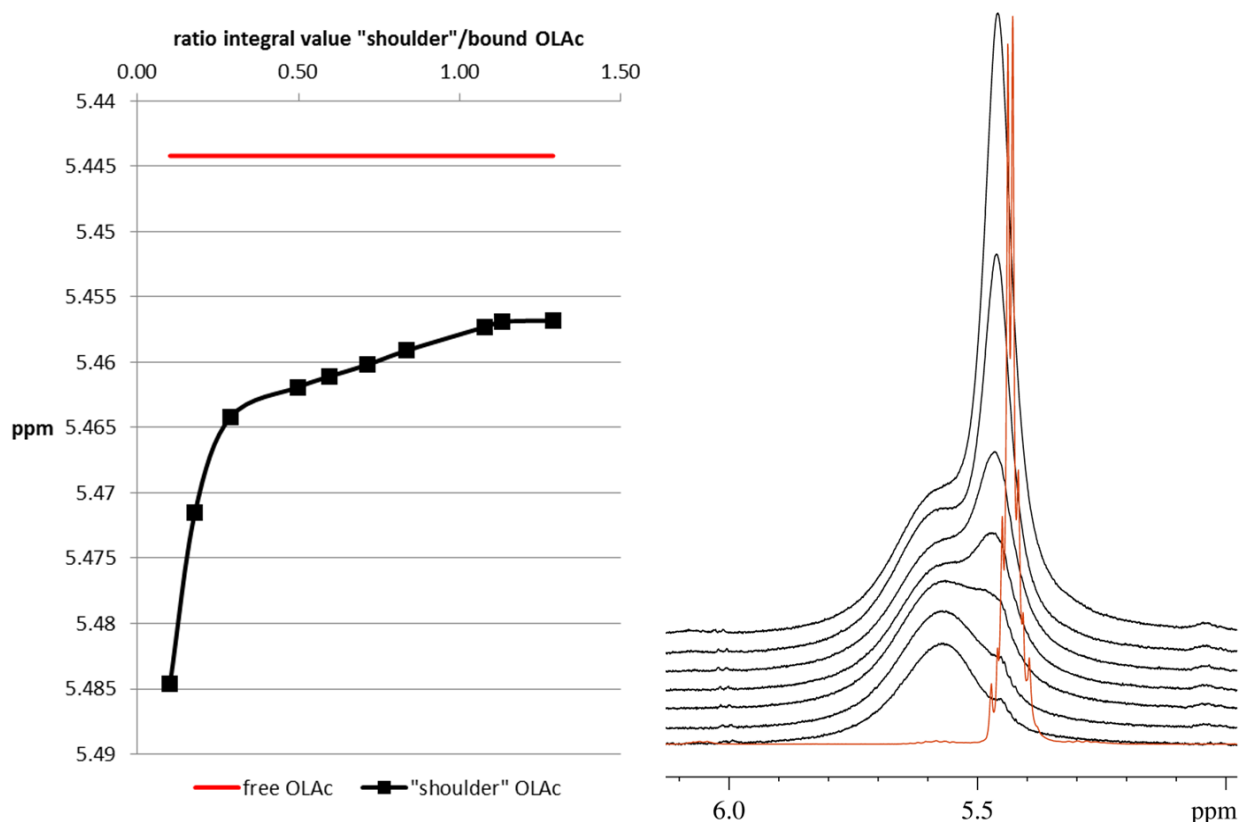


Figure 3.8. Stacked plot of 1D ¹H spectra of OLAc capped AZO NCs after stepwise additions of OLAc *in situ* in toluene-d₈, at room temperature (left). For good comparison, a graph is added that depicts the shift of ppm value of the shoulder towards that of free OLAc in toluene-d₈ (right)

the NC surface. Second, part of the added OLAc is entangled in the ligand shell and third the other part of the added OLAc is free in solution. Between the latter two, a fast exchange exists, which is why only one peak is observed with a concentration dependent chemical shift value in between both. Between the entangled and the bound pool, a slow exchange is present. This explains why the bound resonance and the shoulder can both be observed separately. However, to make this conclusion based solely on the 1D ^1H spectra would be rather expeditious. Thus, we performed some additional measurements on the sample after the addition of extra OLAc.

The first additional experiment was to record a NOESY to visualize the NOE cross peaks connecting the resonances of the added OLAc signal (figure 3.9). In the full spectrum and the zoom of cross peaks of the alkene resonances towards the alkyl resonances (figure 3.9 B), it is obvious that both the added and the bound signals of OLAc have strong negative NOEs between all their resonances respectively. This agrees with the previous observation that the added OLAc is not just free in solution, as weak positive NOEs would then be expected. If we zoom in on the alkene resonances (figure 3.9 C), a strong negative cross peak is visible between the added and bound OLAc signal. However, since this peak connects two different molecular species, this can be explained from two different sources. Either there is a mutual proximity between both ligands allowing intermolecular NOE contacts to be generated, or they chemically exchange with each other, the likely source if the two step exchange model applies. Both possibilities are depicted in figure 3.10. There is thus a clear need to distinguish between the NOE/exchange character.

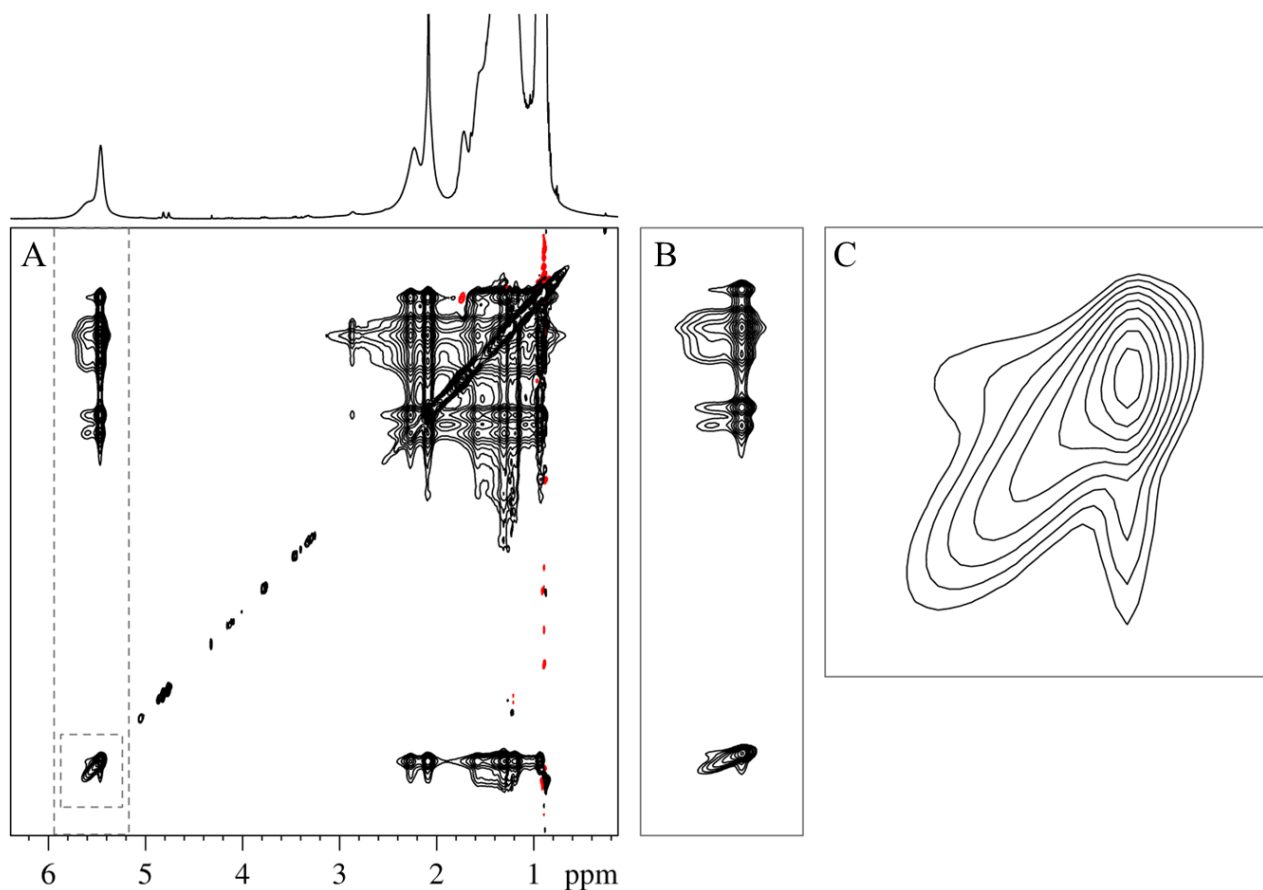


Figure 3.9. 2D NOESY spectrum of OLAc capped AZO NCs in toluene-d₈ with additional OLAc added *in situ* recorded at room temperature and with a mixing time of 300 ms (A), zoom on the cross peaks from the alkene resonances to the other resonances (B) and zoom on the alkene resonances of bound OLAc and the added OLAc (C)

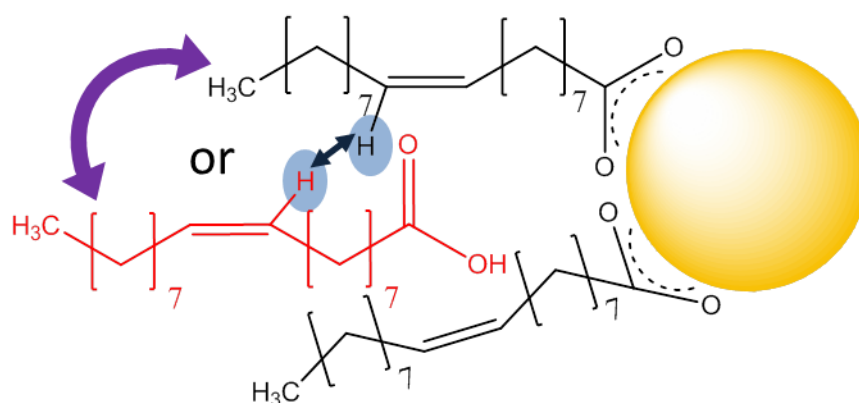


Figure 3.10. Cartoon of two possible interactions of the added OLAc with the capping OLAc derived from the cross peak in between the two alkene resonances. This cross peak can be either caused by mutual proximity or chemical exchange between both.

In order to determine the origin of the cross peak between the added and bound OLAc, a 2D ROESY spectrum was recorded. In contrast to NOESY, ROESY produces cross peaks with a different sign for ROE and exchange peaks allowing their discrimination, cfr. 2.6. ROE cross peaks from mutual proximity are always positive, even for large molecules. Negative cross peaks therefore can only arise from chemical exchange between the two molecules involved. In the 2D ROESY spectrum (figure 3.11), positive ROE cross peaks are observed between the different OLAc resonances of the bound pool on the one hand and the pool of added OLAc on the other hand. These peaks are rather weak, but this is due to the long mixing time of 400 ms in which the intensity of the cross peaks already decays due to relaxation mechanisms acting during the spin lock. Between the alkene

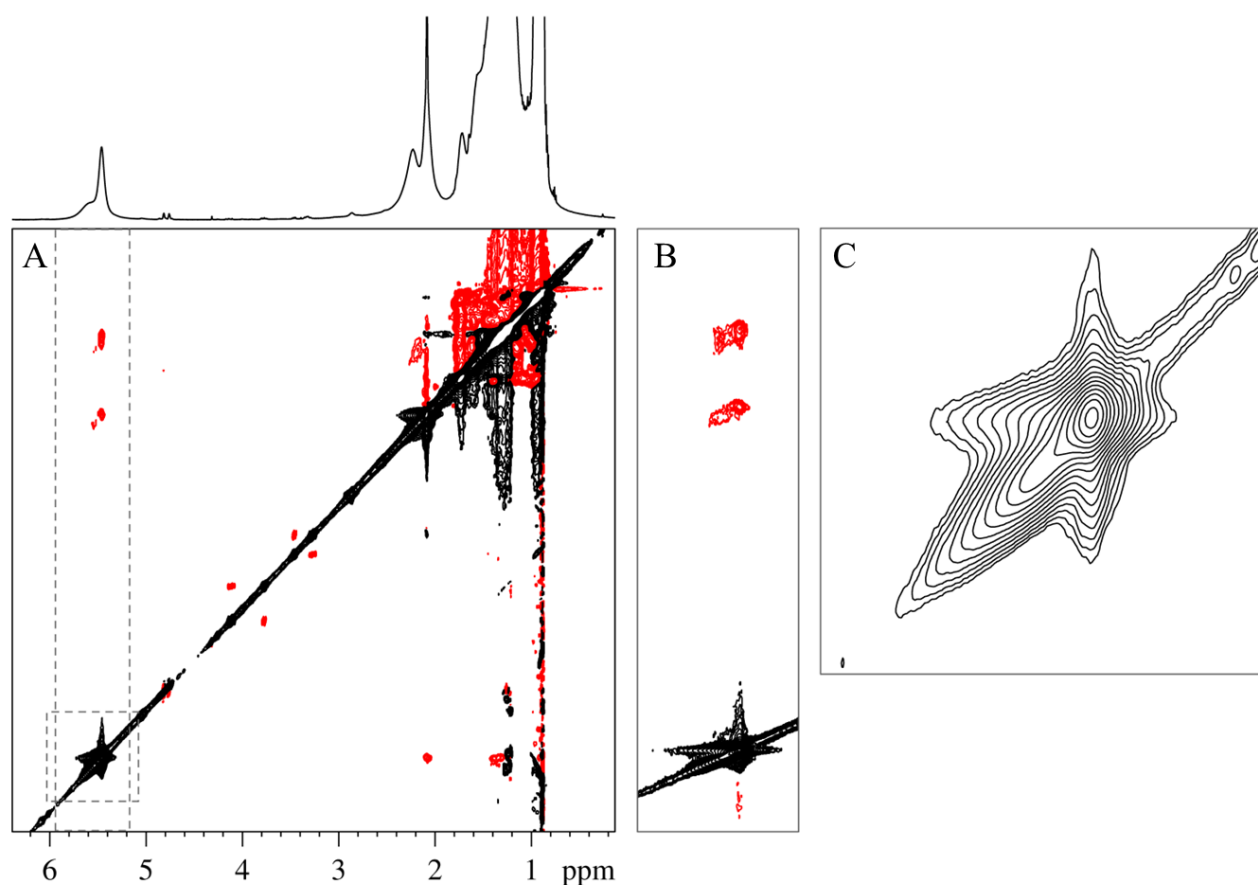


Figure 3.11. 2D ROESY spectrum of OLAc capped AZO NCs in toluene-d₈ with additional OLAc added *in situ* recorded at room temperature and with a mixing time of 400 ms (A), zoom on the cross peaks from the alkene resonances to the other resonances (B) and zoom on the alkene resonances of bound OLAc and the added OLAc (C)

resonance of the added OLAc and the bound OLAc however (figure 3.11 C), a clear negative cross peak is observed, indicative of chemical exchange between the bound and added OLAc. Thus, the ROESY spectrum effectively demonstrates that OLAc molecules exchange between the bound surface state and a non-bound state on a timescale on the order of at most a few hundred ms.

These observations together with the 1D ^1H spectra lead to a total dynamic description of the system. Apparently, OLAc is tightly bound to the AZO NCs but can be exchanged by additional OLAc in the sample. This added OLAc is in fast exchange between two states, free in solution and entangled in the ligand shell, as was already studied by our groups in previous published research, *vide supra*. For our system, the dynamic behavior is schematically illustrated in figure 3.12.

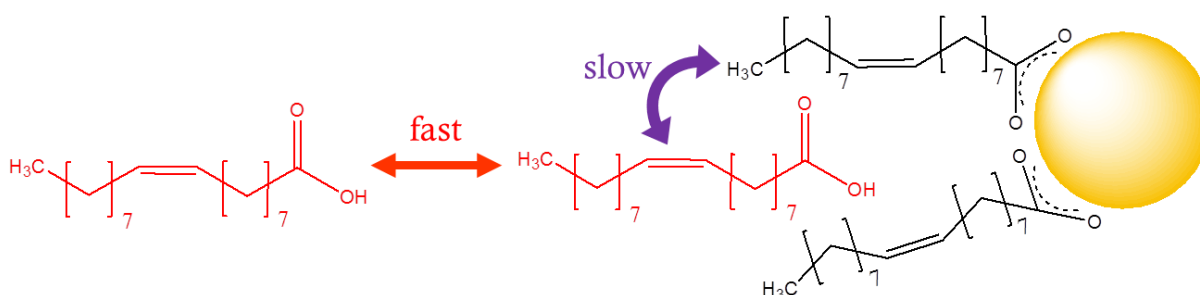


Figure 3.12. Cartoon of the two-step exchange mechanism of the OLAc capped AZO NCs with added OLAc

3.5 Conclusion

Our NMR study on AZO NCs synthesized using both oleic acid and oleylamine revealed the role of both surfactants in the final stabilized colloid. Oleic acid is capping the AZO surface as an oleate, while oleylamine is mostly washed away during work-up.

If more oleic acid is added to the colloid, a two-step exchange system initiates. The added oleic acid is in fast exchange between two states: free in solution or entangled in the ligand shell. These entangled molecules in turn, are in slow exchange with the ones bound to the AZO surface, the latter indicative of the occurrence of a proton transfer involving the bound and entangled species.

3.6 References

- (1) Damm, H.; Kelchtermans, A.; Bertha, A.; Van den Broeck, F.; Elen, K.; Martins, J. C.; Carleer, R.; D'Haen, J.; De Dobbelaere, C.; Hadermann, J.; Hardy, A.; Van Bael, M. K. *RSC Advances* **2013**, *3*, 23745.
- (2) Ben Ayadi, Z.; Mahdhi, H.; Djessas, K.; Gauffier, J. L.; El Mir, L.; Alaya, S. *Thin Solid Films* **2014**, *553*, 123.
- (3) Bao, J.; Zimmler, M. A.; Capasso, F.; Wang, X.; Ren, Z. F. *Nano Lett.* **2006**, *6*, 1719.
- (4) Yang, Q.; Liu, Y.; Pan, C. F.; Chen, J.; Wen, X. N.; Wang, Z. L. *Nano Lett.* **2013**, *13*, 607.
- (5) Tang, Z. K.; Wong, G. K. L.; Yu, P.; Kawasaki, M.; Ohtomo, A.; Koinuma, H.; Segawa, Y. *Applied Physics Letters* **1998**, *72*, 3270.
- (6) Vanmaekelbergh, D.; van Vugt, L. K. *Nanoscale* **2011**, *3*, 2783.
- (7) Fortunato, E.; Barquinha, P.; Martins, R. *Advanced Materials* **2012**, *24*, 2945.
- (8) Bel Hadj Tahar, R.; Ban, T.; Ohya, Y.; Takahashi, Y. *Journal of applied physics* **1998**, *83*, 2631.
- (9) Keis, K.; Bauer, C.; Boschloo, G.; Hagfeldt, A.; Westermark, K.; Rensmo, H.; Siegbahn, H. *Journal of Photochemistry and Photobiology A: Chemistry* **2002**, *148*, 57.
- (10) Ellmer, K.; Mientus, R. *Thin Solid Films* **2008**, *516*, 5829.
- (11) Wang, F.; Wu, M. Z.; Wang, Y. Y.; Yu, Y. M.; Wu, X. M.; Zhuge, L. J. *Vacuum* **2013**, *89*, 127.
- (12) Xu, Z. Q.; Deng, H.; Li, Y.; Guo, Q. H.; Li, Y. R. *Materials Research Bulletin* **2006**, *41*, 354.
- (13) Tonooka, K.; Bando, H.; Aiura, Y. *Thin Solid Films* **2003**, *445*, 327.
- (14) Park, K. C.; Ma, D. Y.; Kim, K. H. *Thin Solid Films* **1997**, *305*, 201.
- (15) Niederberger M, P. N. *Metal Oxide Nanoparticles in Organic Solvents: Synthesis, Formation, Assembly and Application*; Springer, 2009.
- (16) Sun, S.; Zeng, H.; Robinson, D. B.; Raoux, S.; Rice, P. M.; Wang, S. X.; Li, G. J. *Am. Chem. Soc.* **2003**, *126*, 273.
- (17) Fritzing, B.; Capek, R. K.; Lambert, K.; Martins, J. C.; Hens, Z. *J. Am. Chem. Soc.* **2010**, *132*, 10195.

4

HAFNIUM-OXIDE NANOCRYSTALS

In this chapter, the NMR toolbox is used to analyze the surface chemistry of HfO₂ nanocrystals stabilized with both carboxylic acids and amines. The function of both surfactants in the stabilization of the NCs was studied. Moreover, the surface reaction occurring during the surface stabilization was fully elucidated using NMR, providing a new insight in the stabilization of metal oxide nanocrystal dispersions. This research was published in the Journal of the American Chemical Society.¹

4.1 Introduction

Metal oxide nanocrystals (MONCs) are an important class of nanomaterials with potential applications in medicine,² (photo)catalysis,^{3,4} gas sensing,⁵ magnetic applications,⁶ solar cells,⁷ transparent electrodes,⁸ lithium ion batteries^{9,10} and light emitting diodes.¹¹ Different synthesis strategies are possible, but a surfactant-free non-aqueous synthesis is known to be a chemically robust procedure with high yields.¹² Using microwave heating, reactions are furthermore accelerated considerably.^{13,14} The obtained MONCs however, aggregate and are difficult to redisperse.¹² A post-synthetic stabilization in a nonpolar solvent is a good approach to solve this problem. Several different approaches and recipes are suggested in literature, indicating a lack of rationalized design of surface modification of MONCs. An in-depth understanding of the surface chemistry during all stages of synthesis and functionalization would allow for more intelligent design of surface modification schemes.

Here, the stabilization of Hafnium Oxide NCs was studied. Starting from the observation that two types of surfactants are needed for their stabilization, cfr. Chapter 3, a thorough NMR study allowed us to rationalize the surface chemistry of these materials. Again, NMR proves to be a very useful analysis technique in this research field since it allows the elucidation of the phenomena involved in the surface chemistry.

The synthesis route can be depicted in a very simplified manner as shown in figure 4.1. This synthesis proceeds via an established microwave-assisted solvothermal process which was slightly modified and was executed by Jonathan De Roo, a PhD student from the SCRiPTS inorganic chemistry group.^{1,13} First, 0.5 ml of dibenzylether is added to 0.4 mmol of hafnium chloride under vigorous stirring. Then quickly, 4 ml of benzyl alcohol is added and it is left to stir for 5 min. This solution is subjected to microwave

heating: 5 min at 60°C and 3h at 220°C. Afterwards, 3 ml of diethylether is added, yielding two separate phases. The organic phase is first removed and ethanol is added to the aqueous phase. Finally, for stabilization, the particles are redispersed in chloroform and 0.2 mmol of fatty acid is added to the milky suspension. Under stirring, also amine is added until a colorless and transparent suspension is obtained. Prior to NMR analysis, this suspension is further purified in a work-up procedure using a non-solvent (acetonitrile, acetone) and finally redispersed in a suitable deuterated solvent for NMR.

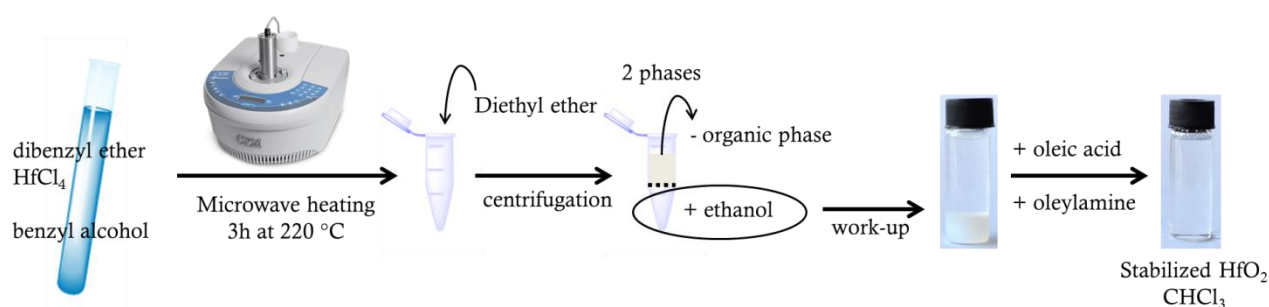


Figure 4.1. Schematic, simplified depiction of the synthesis and postsynthetic stabilization of HfO₂ NCs.

4.2 Characterization of the nanocrystal surface

In order to determine the role of both surfactants, the stabilization of the particles was done using dodecanoic acid (DDAc) as fatty acid and oleylamine (OLAm) as amine. Reference spectra of both molecules are depicted in figure 4.2. As can be observed from these spectra, the amine can be easily followed with ¹H NMR by following its alkene resonance at 5.5 ppm.

Two samples were measured, one that was only purified once (figure 4.3 A) and another that was purified 5 times (figure 4.3 B). First of all, it can be said that in the less purified sample, resonances of both OLAm and DDAc are observed. After 5 purification steps however, the spectrum is devoid of resonances of OLAm and only strongly broadened resonances are present in

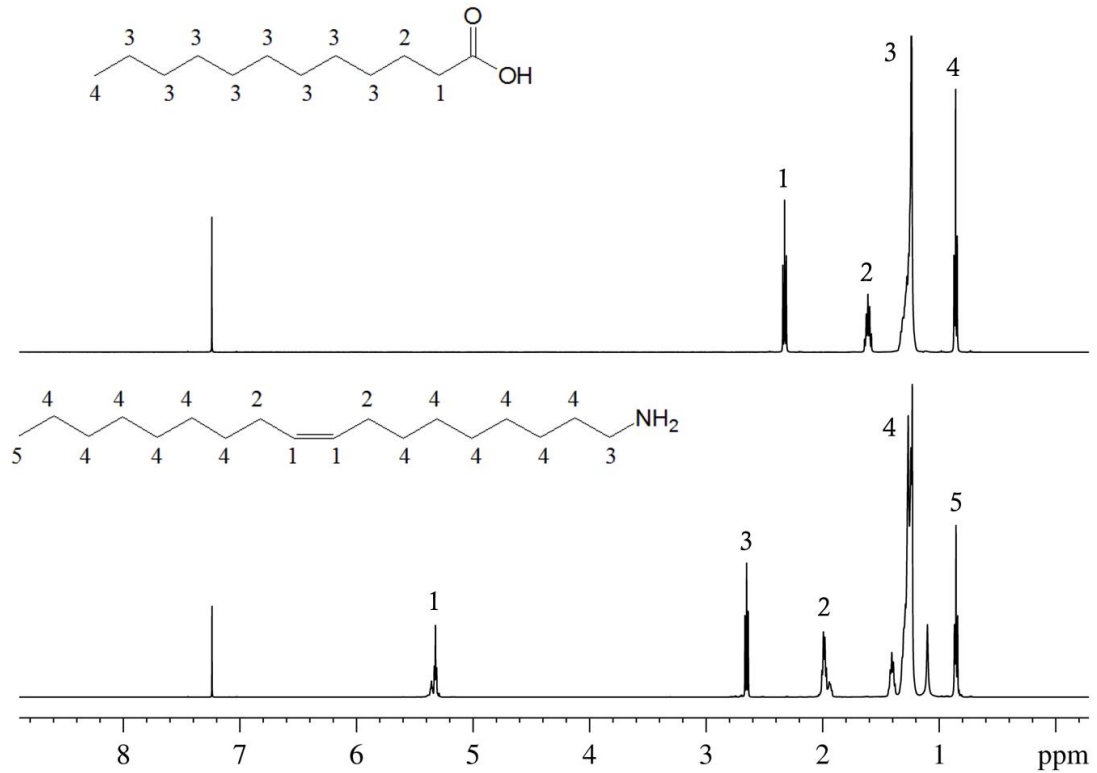


Figure 4.2. Structural formula and reference spectrum of OLAm (bottom) and DDAC (top) in CDCl_3 at 298.2 K

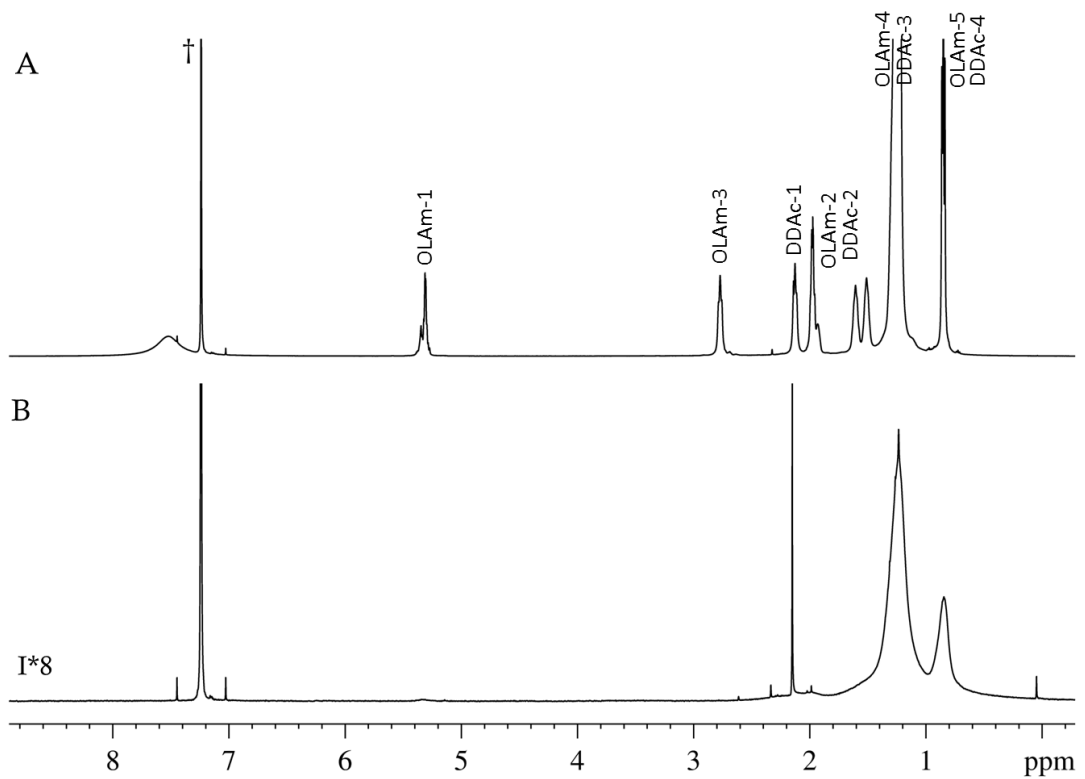


Figure 4.3. $1\text{D } ^1\text{H}$ spectrum of HfO_2 NCs stabilized with OLAm and DDAC in CDCl_3 after one (A) and five consecutive purification steps (B). The intensity of spectrum B was multiplied 8 times with respect to that of spectrum A

the alkyl region. Given the lack of OLAm resonances around 5.5 ppm and 2.8 ppm, it is concluded that these broadened alkyl resonances are from DDAC that is bound to the HfO_2 surface.

For more information on the ligand binding, 2D DOSY and NOESY were recorded on both samples. Considering first the 5-fold purified sample, that only contains DDAC, a diffusion coefficient of $77.1 \pm 0.4 \mu\text{m}^2/\text{s}$ could be extracted from the mono-exponential decay of the methyl resonance during the DOSY measurement. This corresponds to a hydrodynamic radius of 10.5 nm (using the Stokes-Einstein equation), which is in fairly good agreement with results from DLS analysis in chloroform, figure 4.5. Also, clear negative NOE cross peaks are observed between the different DDAC resonances (figure 4.4 B). The DOSY measurement of the sample after one purification on the other hand reveals a diffusion coefficient of 323.9 ± 0.2

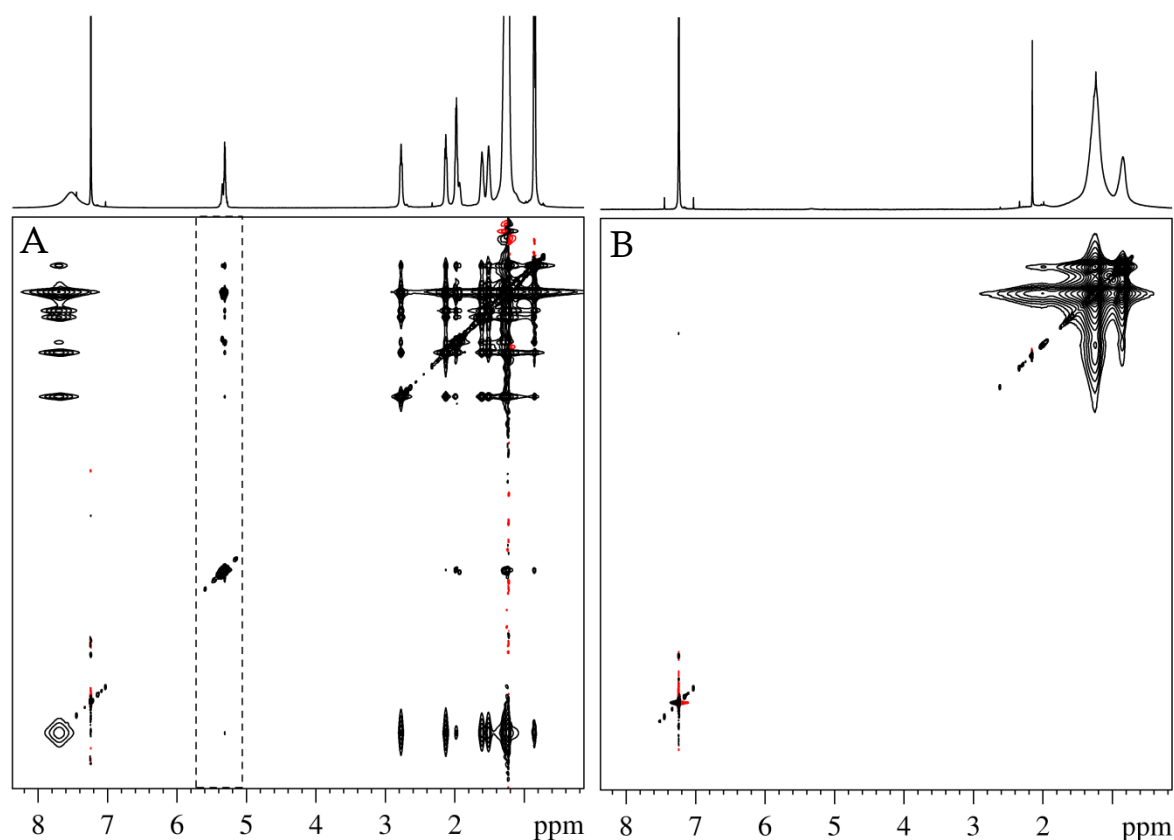


Figure 4.4. 2D NOESY of the HfO_2 suspension stabilized with OLAm and DDAC after 1 (A) and 5 (B) consecutive purification steps

$\mu\text{m}^2/\text{s}$ for OLAm (obtained from the decay of the alkene resonance at 5.5 ppm), which is a value that does not match with a value for the hydrodynamic radius of the HfO_2 NCs, nor with a value of free OLAm in CDCl_3 ($\approx 864 \mu\text{m}^2/\text{s}$). Rather, it represents an averaged value indicating presence of exchange between free and entangled OLAm under fast exchange conditions on the diffusion time scale. The 2D NOESY of the sample also exhibits large negative NOE cross peaks connecting the different OLAm and DDAC resonances respectively (figure 4.4 A). These NOESY and DOSY results are typical for an entangled ligand in the ligand shell, cfr Chapter 2. It is concluded that OLAm is entangled in the ligand shell of DDAC capped HfO_2 NCs and is in a fast dynamic exchange with OLAm free in solution, which explains the ability to completely wash away OLAm following repeated purification cycles. OLAm is apparently not necessary as a capping ligand in providing stability to the HfO_2 NCs. This study however, only provides information on the surface composition after stabilization and purification. To get more insight in the stabilization procedure itself and the necessity of the amine in the process, a titration of both surfactants was performed (*vide infra*).

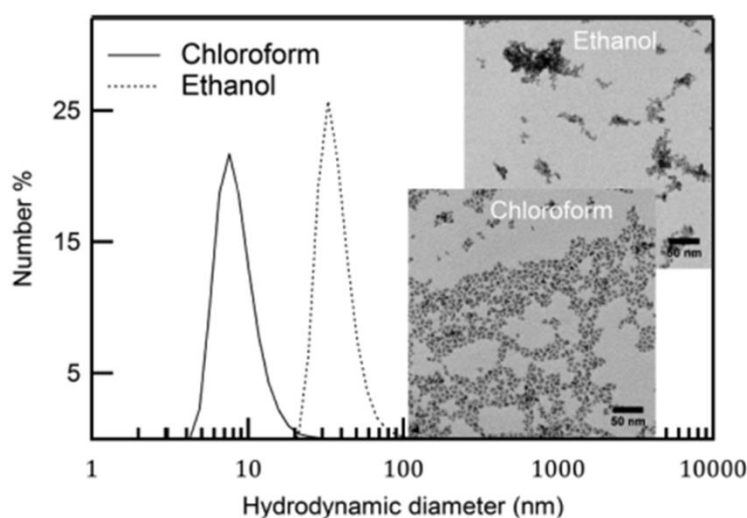


Figure 4.5. Size distribution by DLS of HfO_2 NCs dispersed in either ethanol (as-synthesized) or chloroform (5 times purified suspension)

4.3 Binding mode of the carboxylic acid

First, the binding of the acid on the HfO_2 NCs after stabilization and thorough purification was studied. Since it is clear from the above that OLAm can be washed away completely during purification, stabilization of the HfO_2 NCs was in this case done with OLAm and OLAc instead of DDAC since OLAc is more conveniently followed using ^1H NMR. This means that the resonances in figure 4.6 B can be assigned to OLAc solely. Since only one set of broadened resonances is visible, this also means that all the OLAc is bound to the HfO_2 surface. In order to get some information on the binding mode additional OLAc was added to the sample. One equivalent was used with respect to the bound OLAc. The resulting 1D ^1H spectrum is shown in figure 4.6 A. With respect to the previous spectrum, an additional set of resonances appears on top of the broadened ones. These are

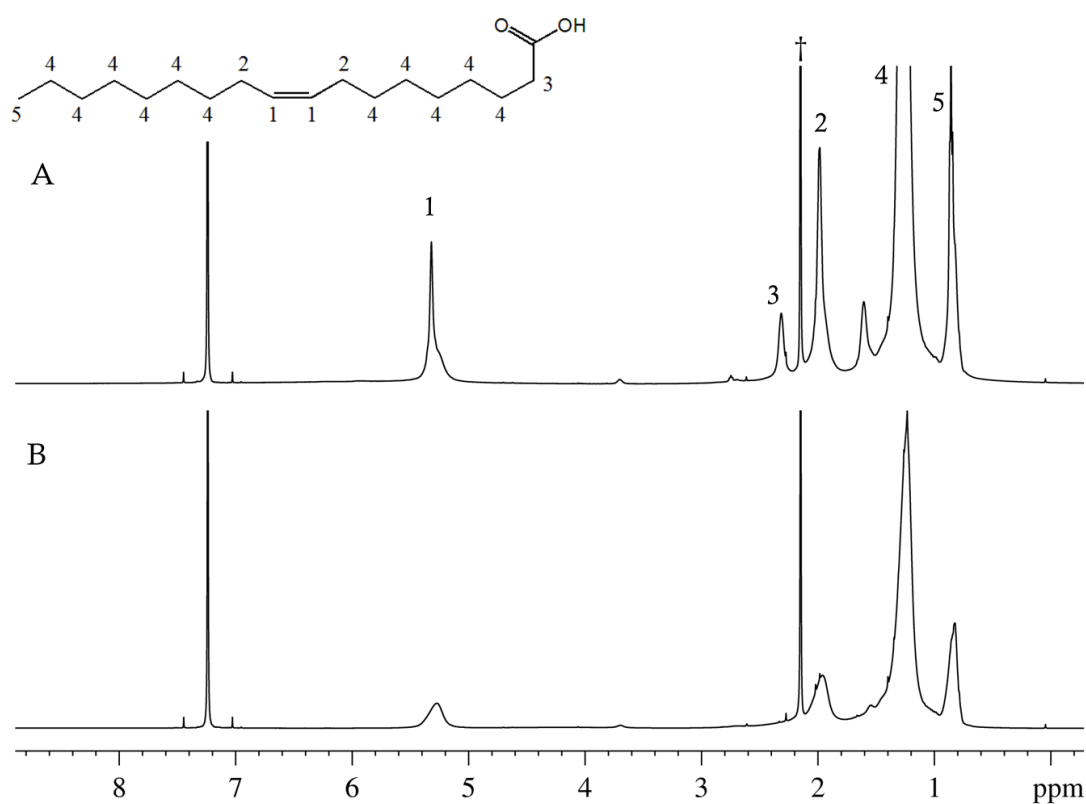


Figure 4.6. 1D ^1H spectrum of OLAc capped HfO_2 NCs in CDCl_3 (B) with an added excess of OLAc (A)

less broadened and slightly shifted towards the chemical shift of free OLAc. This second set of resonances indicates that the added OLAc is not bound on the surface. To gain more information, a 2D NOESY was recorded (figure 4.7). In the 2D NOESY two sets of large negative cross peaks exist, one between the broad and the additional OLAc resonances respectively and in addition mutual intermolecular cross peaks are visible between resonances of both pools. This means that the added OLAc is entangled in NC capping layer. The cross peak observed between the bound and entangled OLAc (figure 4.7 C) can have two origins, as explained in chapter 2. Either it is coming from close spatial proximity, generating a NOE, or it is caused by chemical exchange, due to a swap from bound to entangled and vice versa. To distinguish between both, a 2D off resonance-ROESY was recorded (figure 4.8). In this spectrum, the NOE cross peaks are all positive but exchange peaks will remain negative in sign compared to positively phased diagonal peaks. Looking at the cross peak between the bound and entangled OLAc with 2D ROESY (figure 4.8 B) this is a negative and therefore chemical exchange cross peak. Summing up all the observations, it can be stated that these HfO₂ NCs capped with OLAc exhibit a similar dynamic ligand-surface interaction as found in OLAc capped CdSe NCs synthesized by hot injection methods.¹⁵ This is a two-step dynamic ligand exchange, as explained in chapter 2.1, where the ligands are in fast exchange between the free and entangled mode and in slow exchange between the entangled and bound mode.

Using simple 1D ¹H NMR spectra as such, there is no possibility to tell whether the oleic acid on the HfO₂ surface is bound as a carboxylic acid or as a carboxylate. This is due to the putative carboxylic proton being too close to the surface and therefore being undetectable due to excessive line broadening (cfr. Chapter 2). However, a procedure involving the use of a

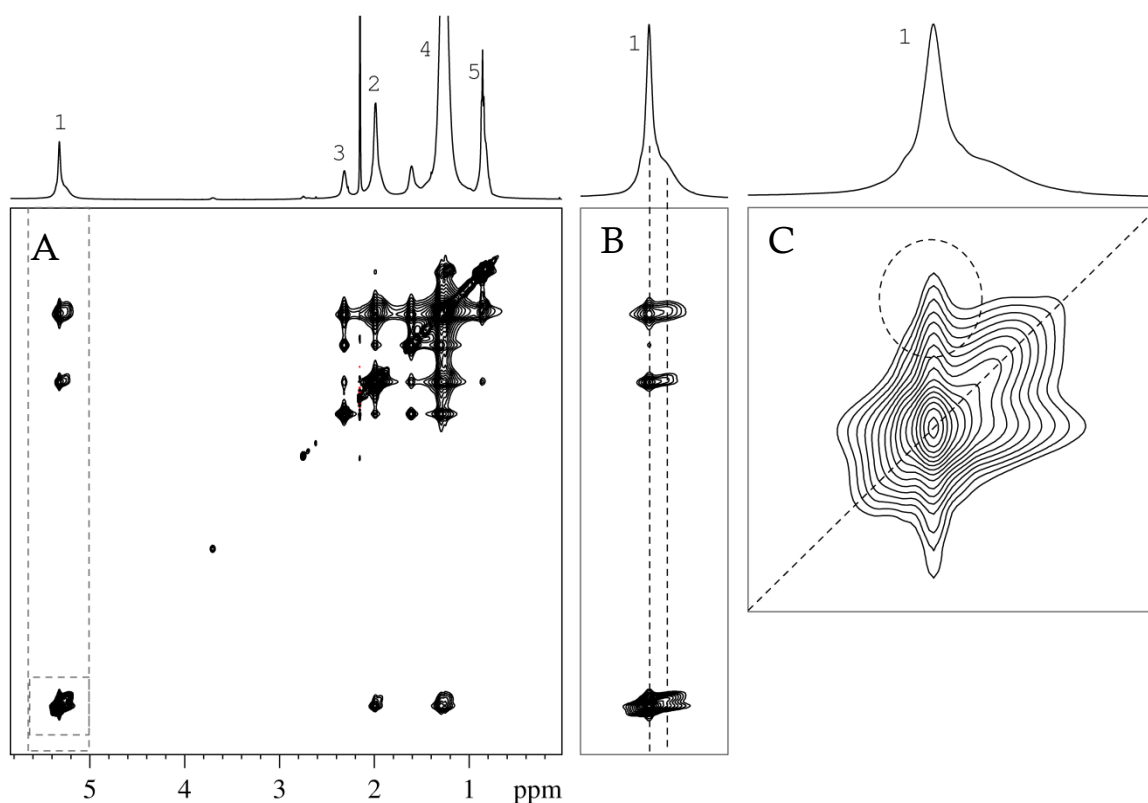


Figure 4.7. 2D NOESY of OLAc capped HfO_2 NCs in CDCl_3 with an excess of OLAc (A), zoom on the NOE cross peaks from the alkene resonances to the alkyl region (B) and zoom on the alkene region with a cross peak between the bound and added OLAc (C)

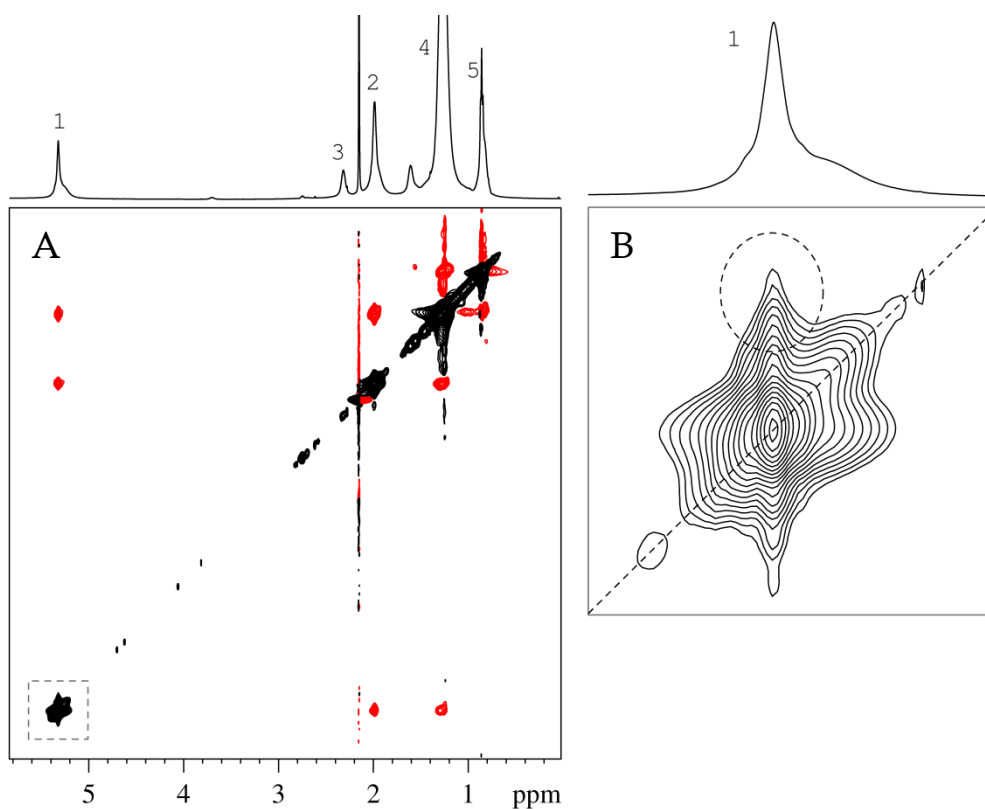


Figure 4.8. 2D off resonance-ROESY of OLAc capped HfO_2 NCs in CDCl_3 with an excess of OLAc (A), zoom on the alkene region with an exchange cross peak between the bound and added OLAc (B)

deuterated carboxylic acid, previously developed within our research groups, can be used to answer this question.¹⁵ First, deuterated OLAc-d₁ was prepared. This is done according to the procedure found in the supporting information of the published article.¹ First, sodium oleate (100 mg, 99% pure) is dissolved in a DCl/D₂O mixture (50 μl DCl (99 atom % D) in 2.0 ml D₂O (99.97 atom% D)), followed by a phase transfer of the formed OLAc-d₁ to cyclohexane-d₁₂ (500 μl – 99.6% atom% D). The organic phase was separated from the aqueous phase in an O₂ and H₂O free glove box. This was considered the OLAc-d₁ stock solution. Considerable efforts were made during these experiments to prevent any water contamination of the NMR tubes or solvents since this would directly impact the experimental results. In order to prevent this, the NMR tubes and the OLAc capped HfO₂ NC suspension were put in the glove box 48 h prior to the experiment. No water resonance was observed in either spectra.

First, 30 μL of d₁-OLAc hexane solution was added to 490 μL CDCl₃. The concentration of OLAc was determined via the ERETIC method to be 12.14 mM in the NMR sample which means the real concentration in the d₁-OLAc stock solution was:

$$c_{OLAc} = \frac{12.14 \text{ mM} \times 520 \text{ } \mu\text{L}}{30 \text{ } \mu\text{L}} = 210 \text{ mM}$$

The degree of deuteration was determined from the residual carboxylic acid signal. When the integration of the alkene resonance was set to 2, the integrated value of the carboxylic acid 1H resonance was 0.0766. Thus 7.66 % of oleic acid molecules still have a proton and consequently 92.34 % is deuterated. This gives an overall concentration of d₁-OLAc in the d₁-OLAc stock solution of 210 x 0.9234 = 194 mM.

Second, 600 μL of the HfO_2 NC stock solution was measured and the concentration of bound OLAc was determined to be 12.87 mM.

In the third and final experiment, 450 μL of NC stock solution was combined with 150 μL of the OLAc- d_1 stock solution. The sample thus contains:

$$450 \mu\text{L} \times 12.87 \text{ mM} = 5.79 \mu\text{mol bound OLAc}$$

$$150 \mu\text{L} \times 210 \text{ mM} = 31.5 \mu\text{mol excess OLAc}$$

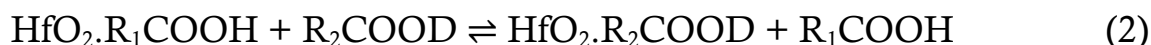
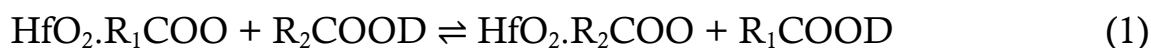
this amounts to 37.29 μmol total OLAc in the sample

$$31.5 \mu\text{mol} \times 0.9234 = 29.09 \mu\text{mol } d_1 - \text{OLAc}$$

$$31.5 \mu\text{mol} - 29.09 \mu\text{mol} = 2.41 \mu\text{mol } h_1 - \text{OLAc}$$

The experimentally observed concentration (derived from the carboxylic acid signal at 12 ppm) of protonated $h_1 - \text{OLAc}$ relative to the total concentration of oleic acid molecules (from the alkene resonance) was $[\text{H}]/[\text{OAc}] = 18.6 \%$.

Theoretically, the expected ratio for the situations when either there are or are no protons on the surface can also be calculated.



If there are no protons on the surface, the only protons that will be visible are the ones from the incomplete deuteration: 2.41 μmol . So the ratio would be

$$\frac{[\text{H}]}{[\text{OLAc}]} = \frac{2.41 \mu\text{mol } H}{37.29 \mu\text{mol total OLAc}} = 6.5 \%$$

If there are as many protons on the surface as there are bound OLAc then the total amount of protons would be: $5.79 + 2.41 = 8.2 \mu\text{mol}$. However, not all these protons will be present in solution, they will be stochastically distributed among all the OLAc molecules, bound (i.e. invisible proton) and not bound (i.e. visible protons). Thus the amount of visible protons will be $8.2 \times \frac{31.5}{37.29} = 6.93$. This results in a ratio:

$$\frac{[H]}{[OLAc]} = \frac{6.93 \mu\text{mol } H}{37.29 \mu\text{mol total } OAc} = 18.57 \%$$

Experimentally, a value of 18.6% is found, which is almost identical to the value calculated for a situation where there are as many protons near the surface as there are bound OLAc. These results are also depicted in figure 4.8 A. Based on this information alone, it would be expected that OLAc is bound as a carboxylic acid $-\text{COOH}$. However, infrared spectroscopy contradicts this. The infrared spectrum of DDAc capped HfO_2 NCs is shown in figure 4.9 B. This lacks any carboxylic acid $\text{C}=\text{O}$ absorption, which is expected at 1710 cm^{-1} . It does contain a carboxylate peak at 1548 cm^{-1} and a broad band around 3388 cm^{-1} , typical for a hydrogen-bonded $\text{O}-\text{H}$ and not a

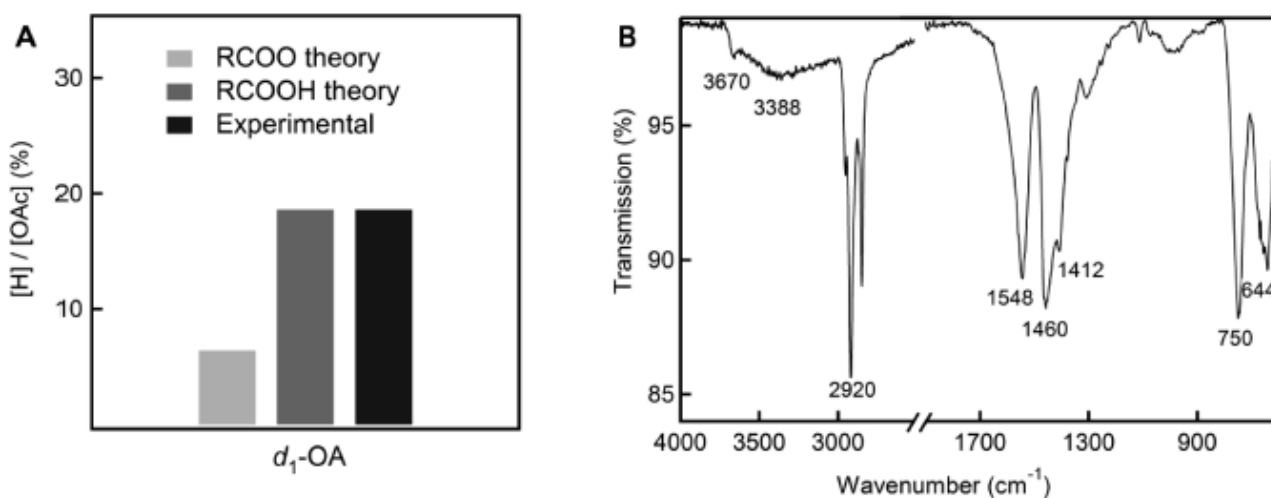


Figure 4.9. Ratio of the proton concentration and the OLAc concentration for the addition of 5 eq of OLAc- d_1 . The experimental and theoretical values that are dependent on the assumption of carboxylate or carboxylic acid on the surface are given. (A) ATR-FTIR spectrum of dried HfO_2 NCs capped with DDAc (B)

COO–H. The small peak at 3670 cm^{-1} is attributed to single hafnol moieties, Hf–O–H. These results lead to the conclusion that hydrogen cations are present on the surface but directly bound to the HfO_2 surface. This information together with the NMR experiments indicates that the carboxylic acid dissociates on the stoichiometric HfO_2 NC surface, leading to the presence of both carboxylates and protons on separate binding sites.

4.4 Role of the amine

Since it was shown that the amine is fully washed away during purification, it is not clear what the role of the amine is in the stabilization. To determine the role of the amine during stabilization, a stabilization procedure was performed *in situ* in the NMR tube using 10-undecenoic acid (UDAc) and oleylamine (OLAm) since they both exhibit well-resolved specific resonances in the ^1H NMR spectrum. Figure 4.10 shows the reference spectra of both UDAc and OLAm in toluene- d_8 . The unstabilized

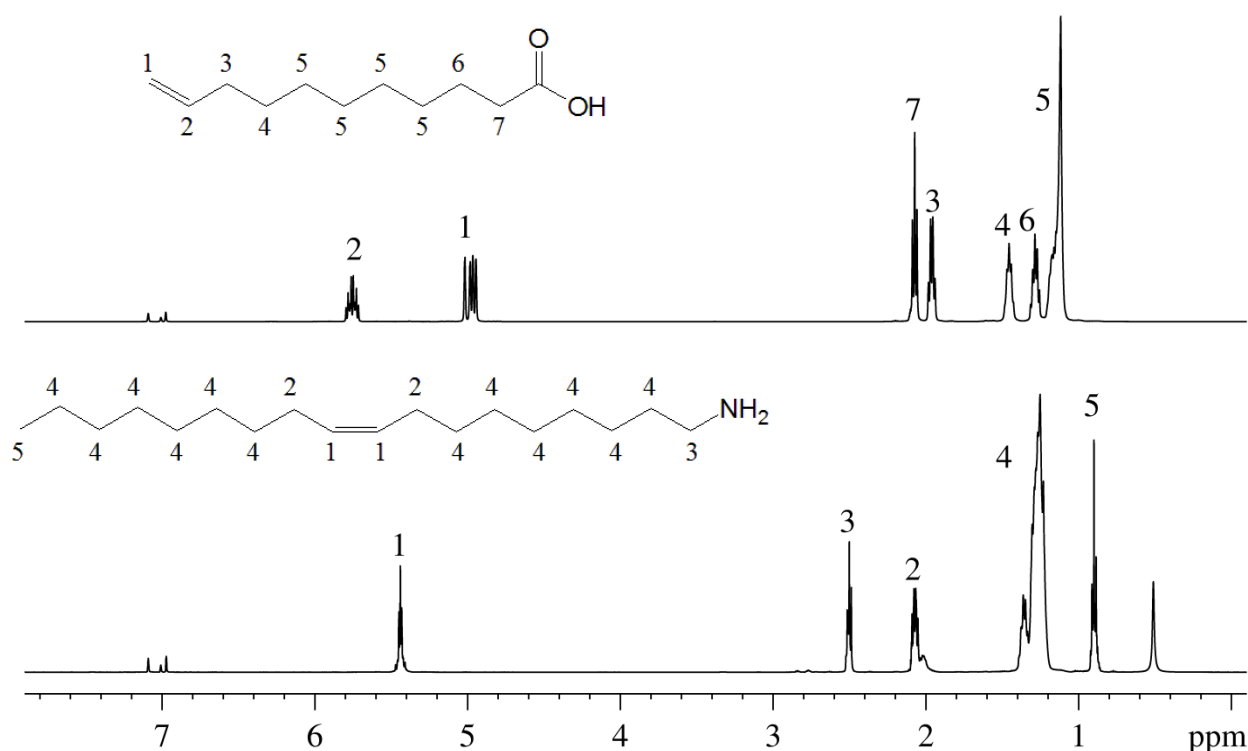


Figure 4.10. Reference spectrum of OLAm (bottom) and UDAc (top) in toluene- d_8 at 298.2 K.

HfO₂ NCs obtained after synthesis in CDCl₃ are put in an NMR tube and, similar to the normal stabilization procedure, first the UDAc is added.

Visually, it is clear that the suspension remains milky and is not stable. Also the 1D ¹H spectrum (figure 4.11 A) and the 2D NOESY (figure 4.12 A) confirm that UDAc is not bound on the HfO₂ surface but is still free in solution. Not only do the UDAc resonances appear sharp in the 1D ¹H, also in the 2D NOESY spectrum no large negative NOEs are observed. On the contrary, only small positive NOEs and ZQC artefacts are present. After addition of 13 mM OLAm (10 mol% with respect to Hf), which visually is not sufficient to fully stabilize the suspension since it remains still a little cloudy, the resonances of OLAm are observed in the 1D ¹H spectrum and all resonances appear a little more broadened (figure 4.11 B). Moreover, large negative NOEs are now observed between all the resonances of the UDAc and OLAm (figure 4.12 B) respectively, indicating that both UDAc

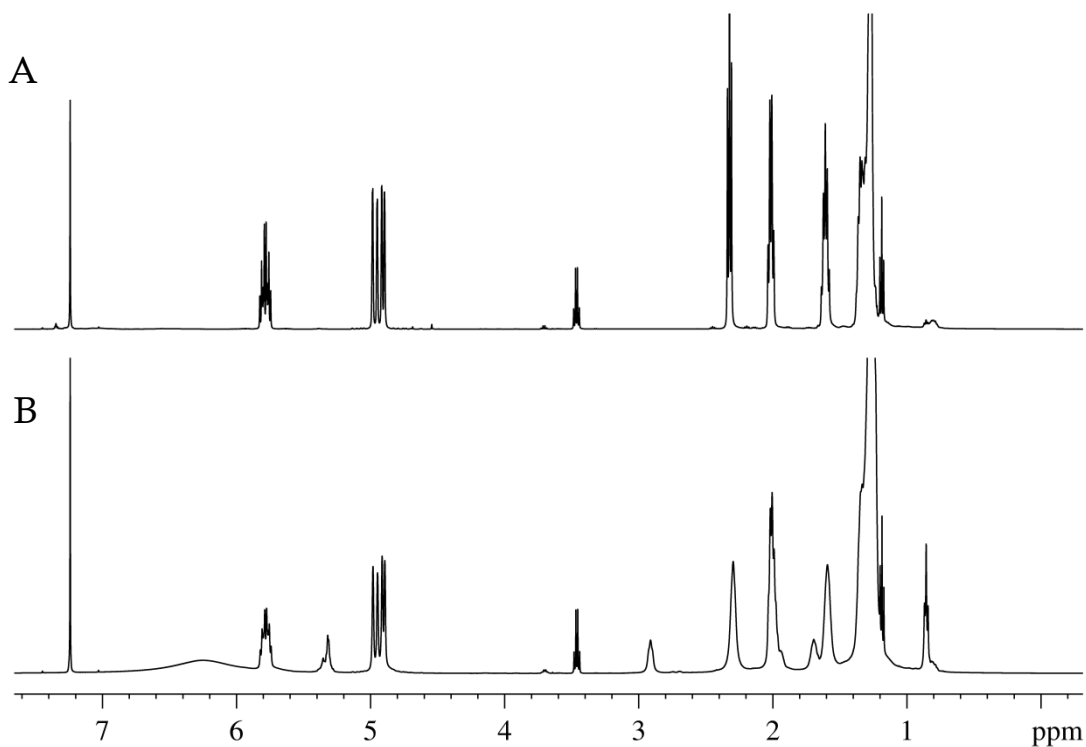


Figure 4.11. 1D ¹H spectrum of HfO₂ NCs in CDCl₃ with UDAc (A) and with UDAc and OLAm (B)

and OLAm interact with the NC surface.

The nature of the interaction becomes clear from the DOSY measurements. The signal intensity decay of the UDAc resonance during the DOSY experiment is bi-exponential (figure 4.13 A), corresponding to the diffusion coefficient of free UDAc ($842 \pm 2 \mu\text{m}^2/\text{s}$) and that of bound UDAc ($96 \pm 6 \mu\text{m}^2/\text{s}$). The signal intensity decay of OLAm also displays a bi-exponential behavior, with fitted diffusion coefficients $767 \pm 61 \mu\text{m}^2/\text{s}$ and $307 \pm 5 \mu\text{m}^2/\text{s}$. Only a very small fraction of the fast diffusing species is present and as a consequence its fitted value is less accurate. Slight deviations between data points and fitted curve seen at higher gradient strength can be attributed to a very small contribution of the tail of the neighboring slow diffusing signal of UDAc. However this will have no significant effect on the fitting. The slow diffusing species is assigned to

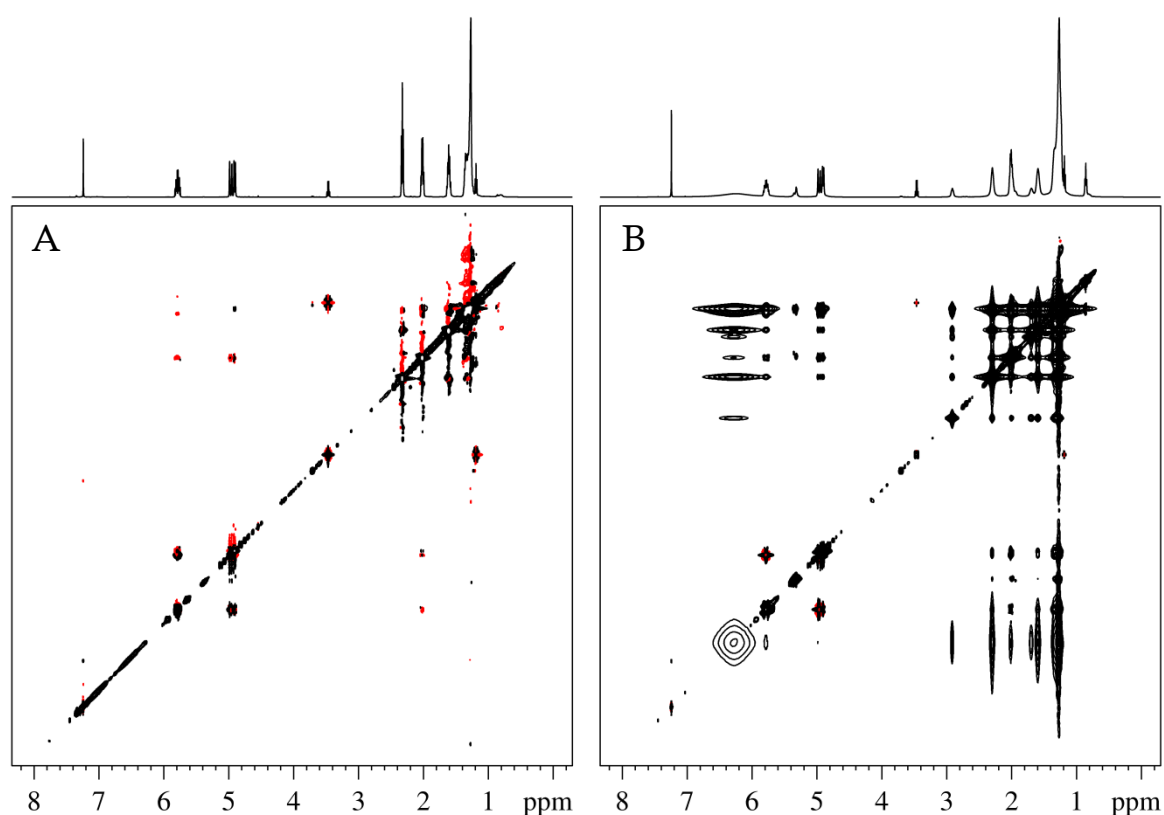


Figure 4.12. 2D NOESY spectrum of HfO_2 NCs in CDCl_3 with UDAc (A) and with UDAc and OLAm (B)

OLAm in fast exchange between the bound and entangled state. Thus UDac is bound to the surface while OLAm is present in the entangled state. It should be noted that UDac is only partially bound since not enough OLAm was added to fully stabilize the particles.

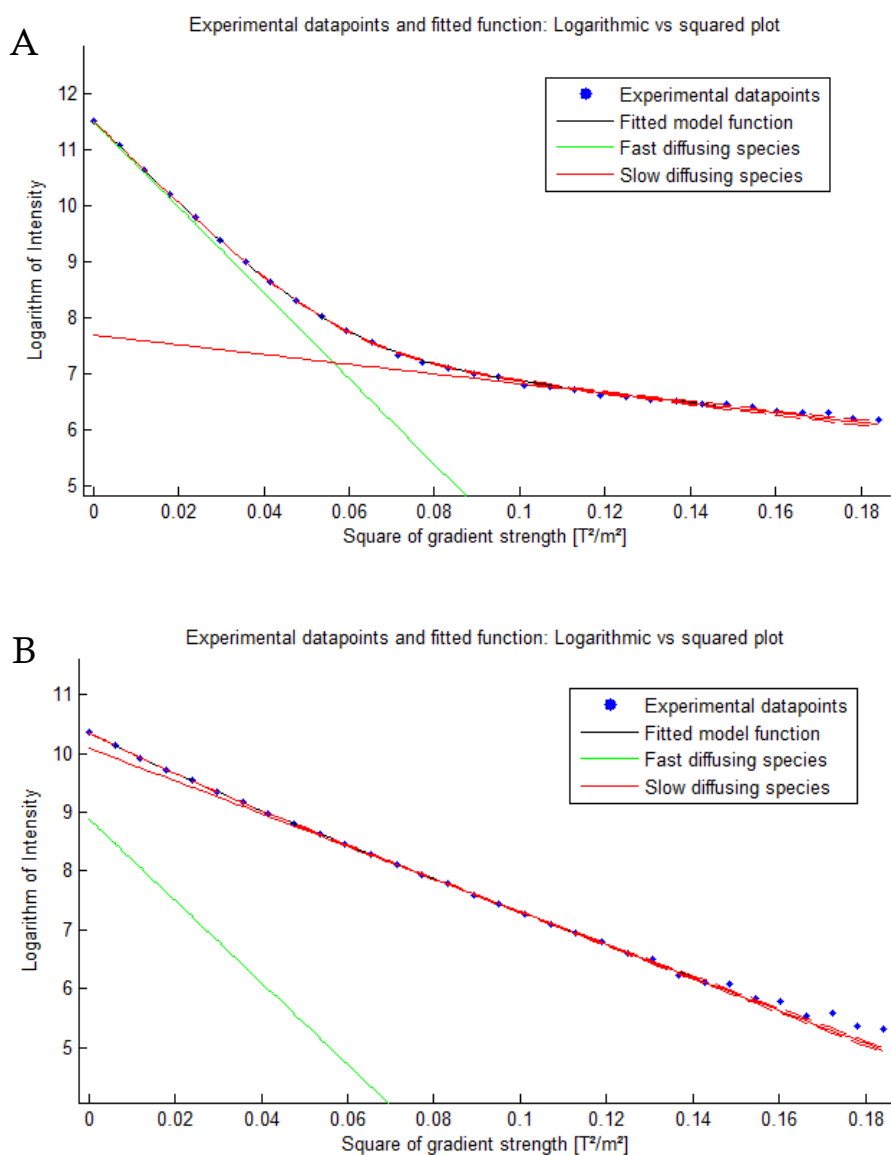


Figure 4.13. Signal intensity decay of UDac, resonance 1, (A) and OLAm, resonance 5, (B) during the DOSY measurement of the HfO₂ NCs with UDac and OLAm in CDCl₃

If we look back at the results of the purification experiments and combine them with these above, some new conclusions can be drawn. First, in figure 4.3 from the purification experiment, the broad resonance present in the less purified sample around 7.5 ppm was tentatively assigned to an oleylammonium ion. Moreover, in the XRF spectrum of this sample chlorine was observed. Combining these results, oleylammoniumchlorine is probably present in the less purified sample. After the purification however, these compounds are no longer present. If we consider this together with the above observation that OLAm is only entangled in the ligand shell and not actually bound to the surface, it makes sense that the oleylammoniumchlorine and OLAm are present in the non-purified sample but get washed away easily during purification.

4.5 Conclusion

Combining the results of all the different experiments, a model of the overall reaction occurring during surface modification is presented in figure 4.14. First, the amine captures a proton from the carboxylic acid. Subsequently, the carboxylate exchanges for the chloride. The chloride is paired with the ammonium compound in the ligand shell. This salt can be washed away when purifying the sample with non-solvents in the second step. The final HfO_2 surface contains a dissociated carboxylic acid.

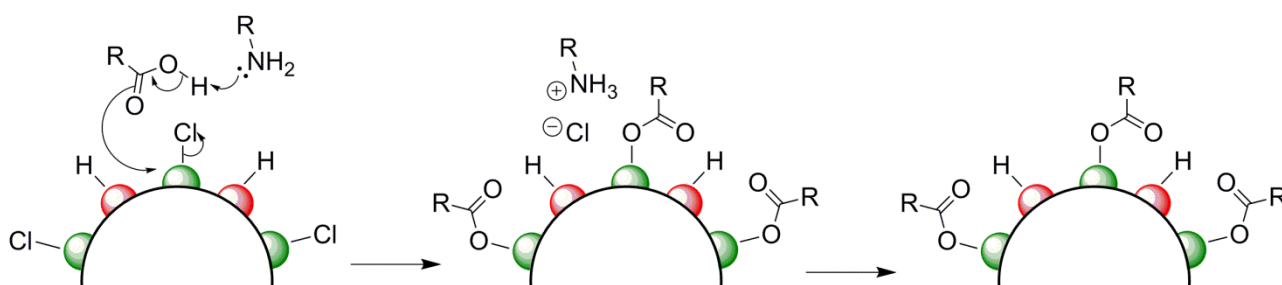


Figure 4.14. model of the overall reaction occurring during surface modification of the HfO_2 NCs using a carboxylic acid and an amine

From this model, it is clear that the amine is merely acting as a base during the stabilization process. In theory, any base would work, but in practice, the options are limited due to solubility and required basicity. This was tested with two other bases. Triethylamine proved to give the same results as oleylamine, pyridine on the other hand did not, most likely because it is too weak a base ($pK_a = 5.2$).

To conclude, using NMR analysis, we have elucidated the surface modification mechanism of HfO_2 NCs synthesized via a surfactant-free non-aqueous method. We showed that the use of both a carboxylic acid and an amine is necessary because of an acid-base reaction occurring at the HfO_2 surface. After stabilization however, the amine can be removed by a simple purification procedure together with the traces of chloride, leaving a clean surface. The carboxylic acids left on the HfO_2 surface feature a similar dynamic behavior in solution as metal chalcogenides NCs stabilized with carboxylates described in chapter 2 and literature.¹⁶⁻¹⁸ However, a crucial difference between both is established since we have observed that the negative charge of the carboxylates on the HfO_2 NCs is not balanced by an excess of cations but by protons that are adsorbed on different adsorption sites on the surface. It is concluded that the carboxylic acids can dissociate on the HfO_2 surface, which is a new and fascinating result. The results can be extended to other MONCs also and were also validated for ZrO_2 NCs by Katrien De Keukeleere, PhD student at the SCRiPTS inorganic chemistry group.¹⁹

4.6 References

- (1) De Roo, J.; Van den Broeck, F.; De Keukeleere, K.; Martins, J. C.; Van Driessche, I.; Hens, Z. *J. Am. Chem. Soc.* **2014**, *136*, 9650.
- (2) Lee, N.; Cho, H. R.; Oh, M. H.; Lee, S. H.; Kim, K.; Kim, B. H.; Shin, K.; Ahn, T.-Y.; Choi, J. W.; Kim, Y.-W.; Choi, S. H.; Hyeon, T. *J. Am. Chem. Soc.* **2012**, *134*, 10309.
- (3) Zou, Z. G.; Ye, J. H.; Sayama, K.; Arakawa, H. *Nature* **2001**, *414*, 625.

- (4) Yamada, Y.; Tsung, C. K.; Huang, W.; Huo, Z. Y.; Habas, S. E.; Soejima, T.; Aliaga, C. E.; Somorjai, G. A.; Yang, P. D. *Nat. Chem.* **2011**, *3*, 372.
- (5) Comini, E.; Faglia, G.; Sberveglieri, G.; Pan, Z. W.; Wang, Z. L. *Applied Physics Letters* **2002**, *81*, 1869.
- (6) Lee, J.; Zhang, S.; Sun, S. H. *Chem. Mat.* **2013**, *25*, 1293.
- (7) Mor, G. K.; Varghese, O. K.; Paulose, M.; Shankar, K.; Grimes, C. A. *Sol. Energy Mater. Sol. Cells* **2006**, *90*, 2011.
- (8) O'Dwyer, C.; Szachowicz, M.; Visimberga, G.; Lavayen, V.; Newcomb, S. B.; Torres, C. M. S. *Nat. Nanotechnol.* **2009**, *4*, 239.
- (9) Poizot, P.; Laruelle, S.; Grugeon, S.; Dupont, L.; Tarascon, J. M. *Nature* **2000**, *407*, 496.
- (10) Sun, Y. K.; Chen, Z. H.; Noh, H. J.; Lee, D. J.; Jung, H. G.; Ren, Y.; Wang, S.; Yoon, C. S.; Myung, S. T.; Amine, K. *Nature Materials* **2012**, *11*, 942.
- (11) Wang, Z. L. *Mater. Sci. Eng. R-Rep.* **2009**, *64*, 33.
- (12) Pinna, N.; Niederberger, M. *Angew. Chem.-Int. Edit.* **2008**, *47*, 5292.
- (13) De Roo, J.; De Keukeleere, K.; Feys, J.; Lommens, P.; Hens, Z.; Van Driessche, I. *J. Nanopart. Res.* **2013**, *15*, 1778.
- (14) Bilecka, I.; Djerdj, I.; Niederberger, M. *Chem. Commun.* **2008**, 886.
- (15) Fritzing, B.; Capek, R. K.; Lambert, K.; Martins, J. C.; Hens, Z. *J. Am. Chem. Soc.* **2010**, *132*, 10195.
- (16) Moreels, I.; Fritzing, B.; Martins, J. C.; Hens, Z. *J. Am. Chem. Soc.* **2008**, *130*, 15081.
- (17) Bernd Fritzing, R. K. C., Karel Lambert, José C. Martins, Zeger Hens.
- (18) Hens, Z.; Martins, J. C. *Chem. Mat.* **2013**, *25*, 1211.
- (19) De Keukeleere, K.; De Roo, J.; Lommens, P.; Martins, J. C.; Van Der Voort, P.; Van Driessche, I. *Inorg. Chem.* **2015**, *54*, 3469.

5

COPPER-INDIUM-SULFIDE NANOCRYSTALS

In this chapter, the NMR toolbox is used to analyze the surface chemistry of CuInS₂ nanocrystals capped with aliphatic amines. By expanding the toolbox with in situ high temperature NMR measurements, a straightforward approach is developed to distinguish L-type from X-type ligands. This careful distinction is important for a rationalized ligand exchange design. This work was published in Chemistry of Materials.¹

5.1 Introduction

Cu(In,Ga)(S,Se)₂ nanocrystals (CIGS) are ternary I-III-VI₂ type NCs. This new type of semiconductor could be an interesting substitute for the binary II-VI and IV-VI types since they are more environmentally friendly. Also, an additional advantage lies in the possibility to tune the band gap both by size, due to quantum confinement, and by increased possibilities to alter the composition. With promising properties for a variation of photovoltaic devices, the study of these types of materials has steadily grown over the last few years²⁻¹², with the main focus on wet-chemical syntheses resulting in colloidal suspensions of CIGS NCs with capping ligands.

In spite of this growing interest, there still exists a lack of information on the surface chemistry of as such synthesized CIGS NCs and the ligand exchange mechanisms involved. The importance of achieving a full understanding of the CIGS surface and dynamic ligand behavior should not be underestimated. In light of further development of post-synthetic processing of CIGS NCs towards applications, this understanding is crucial for devising a well-considered approach. Most characterization studies are based on photoluminescence results^{9,11}, TEM images^{3,10,11} and XRD patterns¹². Ligand exchange has been monitored solely by observation of phase transfer from an apolar to a polar phase¹³ or by indirect IR and TGA analysis¹⁴.

The development and optimization of CIGS synthesis and its future applications are the subject of the PhD thesis of Ruben Dierick, PhD student at the PCN inorganic chemistry research group. Here, we focus on a full NMR characterization of OLAm capped CuInS₂ (CIS) NCs. More specifically, we explored the ligand exchange from long-chain ligands towards different short-chain organic or inorganic ligands, this is required

for the applicability of these NCs. Given the conditions necessary for the exchange to precede required prolonged heating at 130°C, we tried to define the behavior of OLAm using *in situ* high-temperature NMR measurements. Finally, in literature, most synthesis methods make use of technical oleylamine (OLAm).^{3,8,15,16} As the varying and partly unclear composition of this technical OLAm represents a difficult to control variable, we repeated the experiments using high-purity octadecylamine to confirm our hypotheses.

5.2 OLAm capped CIS – basic characterization

Synthesis is conducted as described by Panthani *et al.* in literature and is schematically presented in figure 5.1.³ CIS NCs capped with oleylamine (OLAm) were prepared in by a heating procedure. Cu(acac)₂ (1 mmol), In(acac)₃ (1 mmol) and elemental S (2.05 mmol) are combined in a three-neck flask. 2 ml OLAm (6.06 mmol) and 14 ml 1-octadecene (ODE) are added. Next, the flask is attached to a Schlenk line and flushed with nitrogen over the course of 1 h. The mixture is then heated to 240°C at 80°C/min using an infrared heating device while stirring vigorously. During this period, the precursors dissolve and form CIS NCs as indicated by a change in color from a brown heterogeneous to a clear black mixture. After 1h, the flask is cooled to room temperature using a water bath. Toluene and ethanol

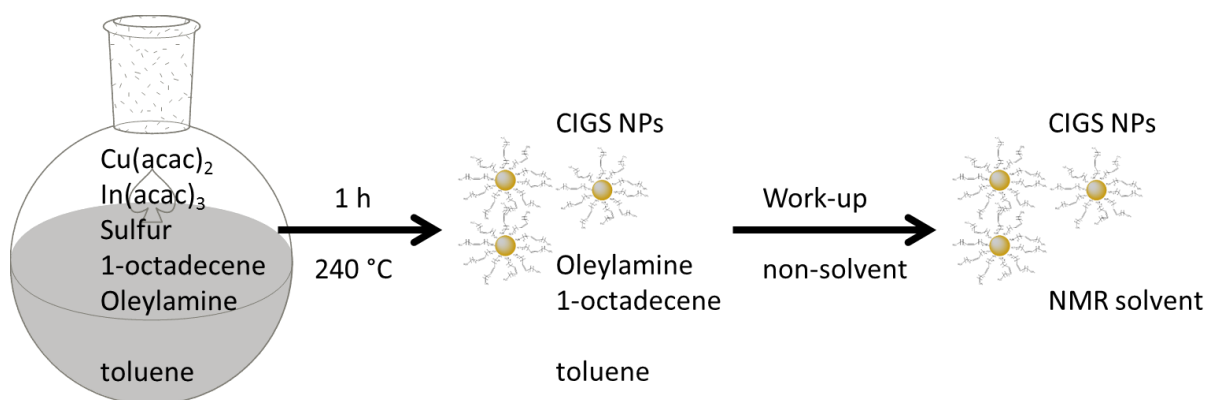


Figure 5.1. Schematic depiction of the synthesis and work-up procedure of CIS NCs.

are added to wash the CIS NCs, which are then separated using a centrifuge. The resulting NC pellet obtained after discarding the supernatant is redissolved in toluene and kept inside a water and oxygen-free glove box as a stock solution. In figure 5.2 a TEM micrograph is shown of the OLAm capped CIS NCs after synthesis. The anisotropic tile-shaped CIS NCs have a hexagonal top surface.

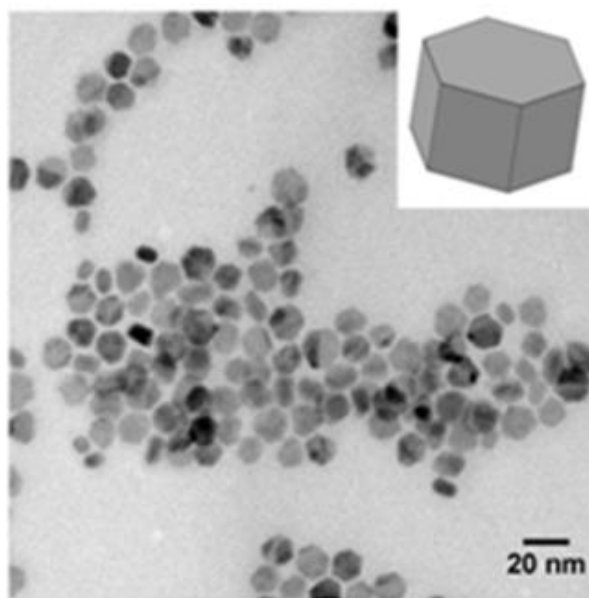


Figure 5.2 TEM micrograph of as-synthesized CIS NCs capped with OLAm

For the NMR measurements, the sample is dried with a nitrogen flow and suspended in deuterated solvent. 20 μl of this suspension is used for UV-VIS determination of the NC concentration and 600 μl is put in an NMR tube.

Given the chemical structure of oleylamine (OLAm), the assignment of the reference spectrum of OLAm in toluene- d_8 and of the OLAm capping ligands on the CIS NC surface is as depicted in figure 5.3. This assignment was carried out using 2D ^1H - ^1H COSY and ^1H - $\{^{13}\text{C}\}$ HSQC. Residual toluene resonances at 7.09, 7.00, 6.98 and 2.09 ppm are observed in the

spectra. The first observations that can be drawn from the spectrum of the OLAm capped CIS suspension are a downfield chemical shift change and a broadening of the resonances. Resonance 3, i.e. the CH₂ protons next to the amine functionality, is broadened so much that it becomes almost invisible. Furthermore, only one set of broad signals of oleylamine is visible, indicating a single species of oleylamine is present that is bound to the CIS NC surface, cfr. chapter 2.

This was further supported by diffusion NMR studies. In figure 5.4 A, the fitting of the data points of the diffusion decay of the alkene protons (resonance 1) to a mono exponential decay is shown. While this is the best resolved resonance for analysis, cfr. chapter 2, the lower signal to noise ratio at high gradient strengths makes the fitting curve deviate from the data

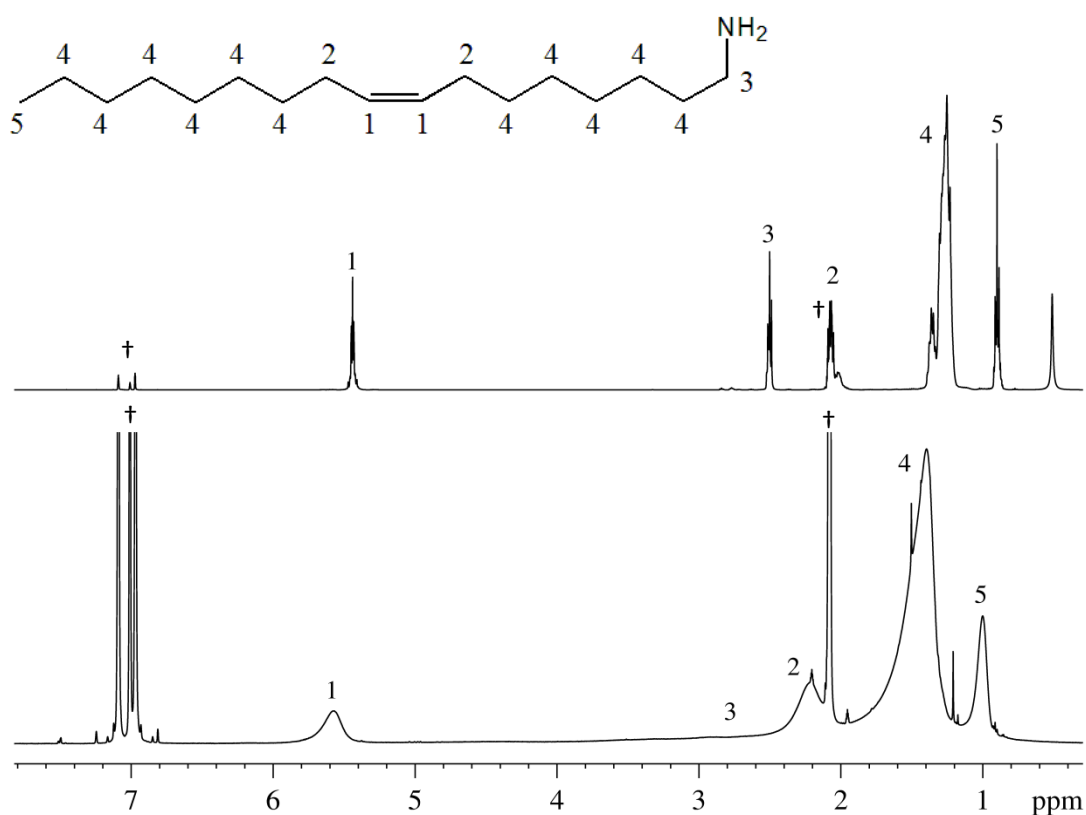


Figure 5.3. Structural formula of oleylamine, 1D ¹H spectrum of a reference sample of oleylamine in toluene-d₈ (top) and of oleylamine capped CIS NCs in toluene-d₈ (bottom)

points and the error on the diffusion coefficient is somewhat increased ($D=61.3 \pm 2.2 \mu\text{m}^2/\text{s}$). Fortunately, the CH_3 signal has a better signal to noise and is well-resolved. Fitting of the decay of this resonance gives a good result (figure 5.4 B): the calculated diffusion coefficient is $59.8 \pm 0.2 \mu\text{m}^2/\text{s}$. Since the shape of the NCs was determined to be anisotropic with a hexagonal top surface, *vide supra*, the Stokes-Einstein equation we use here is

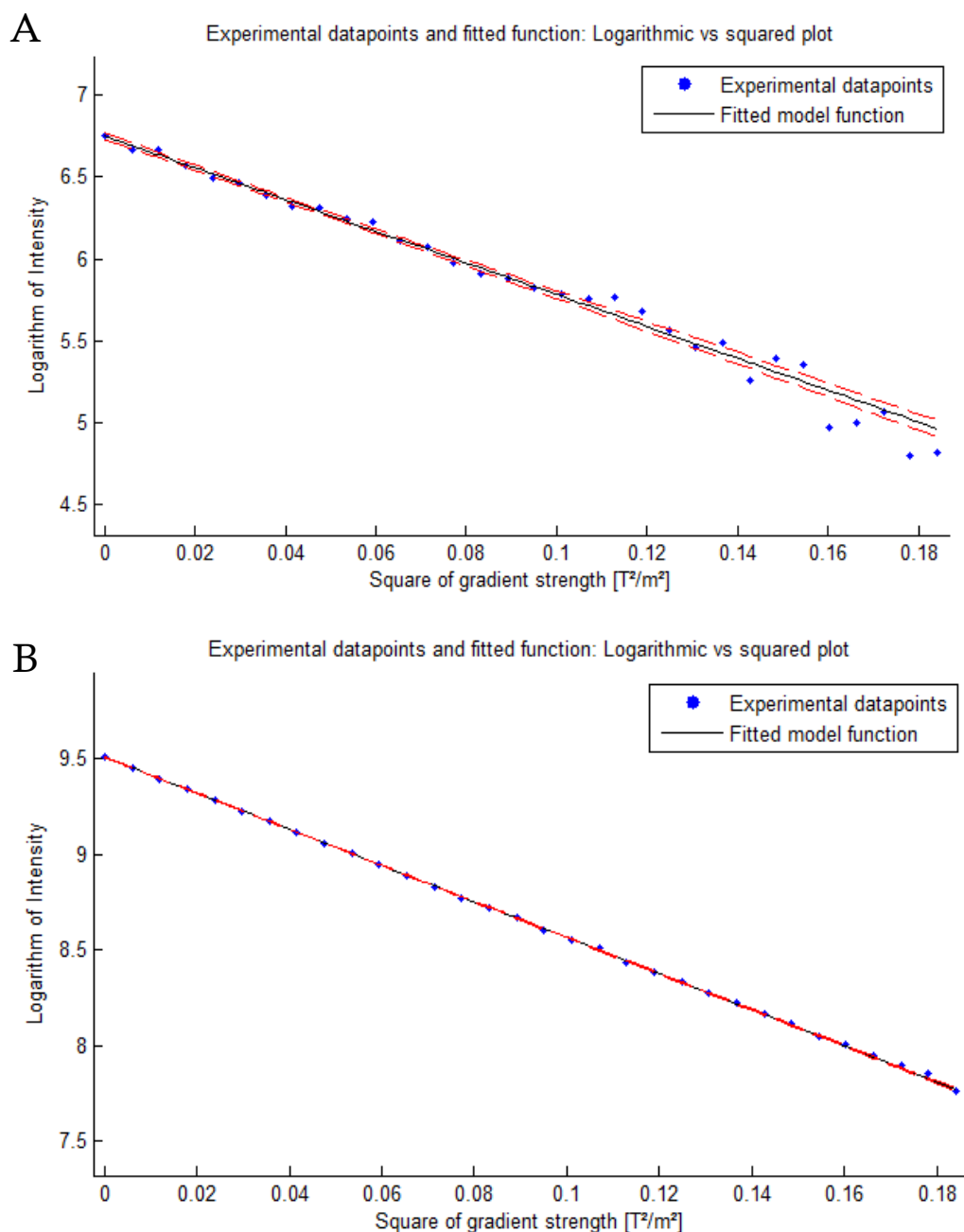


Figure 5.4. Datapoints and mono exponential fitting curve of the decay of the signal intensities of the alkene resonance (A) and the CH_3 resonance (B) of OLAM during the diffusion measurement of the OLAM capped CIS NCs in toluene- d_8 .

that for a disk moving at random (eq 5.1). Calculating the top surface hydrodynamic diameter, a value of 19.4 ± 0.1 nm is obtained. This value closely matches twice the CIS top surface edge (7.6 ± 1.3 nm, calculated from TEM) increased by the thickness of the OLAm capping (≈ 2 nm on each side).

$$r_H = \frac{k_B T}{12\eta D} \quad (\text{eq 5.1})$$

From the result of the diffusion study together with the 1D ^1H spectrum, it can be stated that OLAm is tightly bound to the CIS NC surface. The NOESY spectrum confirms this statement (figure 5.5). Strong negative NOEs are observed between all the resonances of OLAm except for

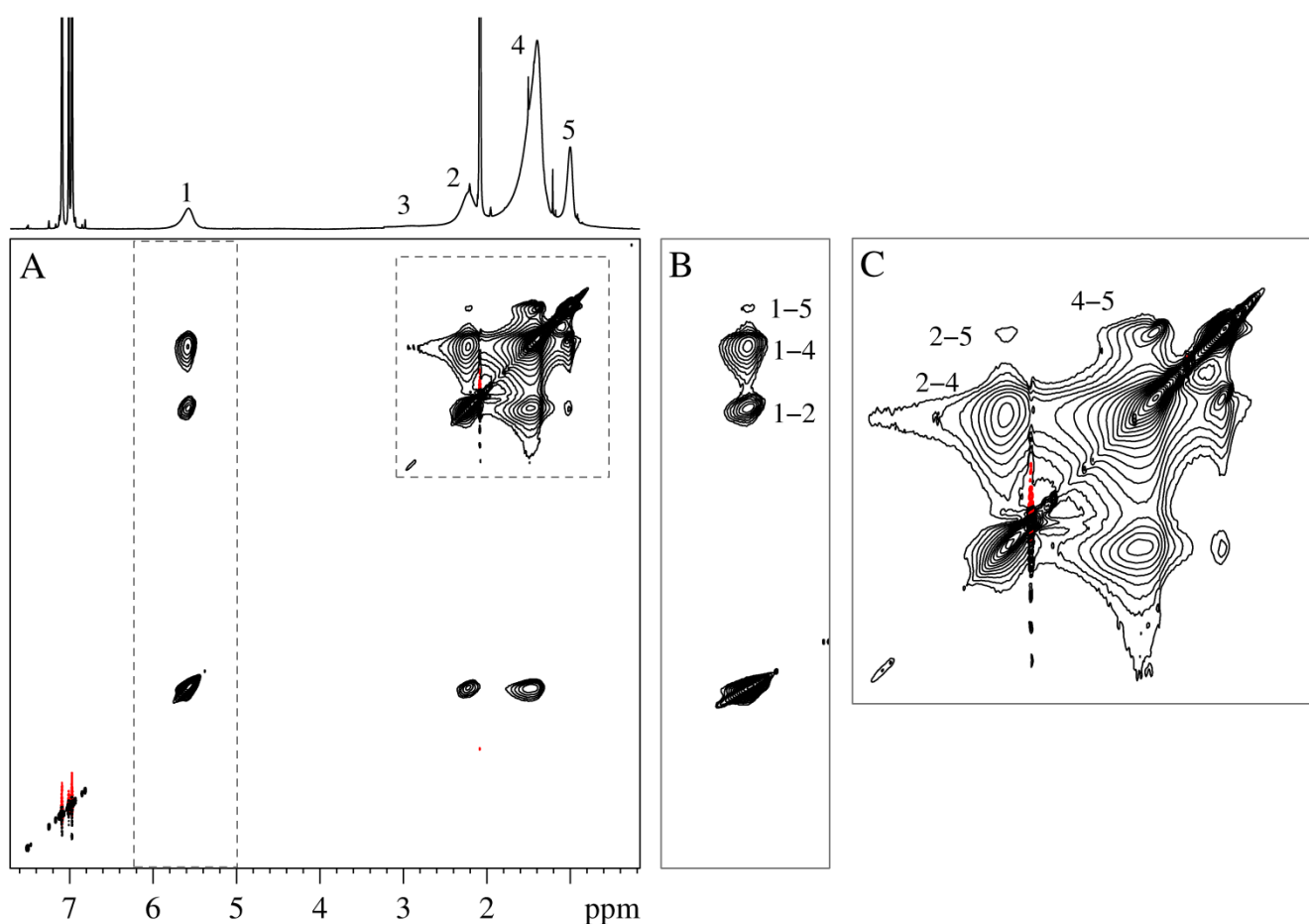


Figure 5.5. 2D NOESY of OLAm capped CIS NCs in toluene- d_8 (A), zoom of the cross peaks from the alkene resonance (B), zoom of the alkyl region (C) recorded at room temperature with a mixing time of 300 ms

resonance 3, the latter due to excessive broadening of this resonance and consequently low intensity. In figure 5.5 B, the NOE cross peaks from resonance 1 to resonance 2, 4 and 5 are indicated. In figure 5.5 C, the NOE cross peaks from resonance 2 to resonance 4 and 5, and from resonance 4 to resonance 5 are indicated.

This initial characterization of the OLAm capped CIS NCs proves that OLAm is tightly bound on the CIS NC surface and experiences no exchange mechanisms, cfr. chapter 2.

5.3 OLAm capped CIS – Ligand behavior

As said before in chapter 1 (1.3 surface chemistry), the various types of ligands binding to NC surfaces have been divided into three categories: X-, L- and Z-types.^{17,18} Previous studies on L-type ligands show that they usually possess a dynamic one-step ligand exchange behavior, cfr. chapter 2. Here however, the OLAm ligands capping the CIS surface were characterized as tightly bound ligands that exhibit no exchange at room temperature, *vide supra*. These amine capping ligands thus do not behave as previously studied L-type ligands that exchange easily at room temperature. Nonetheless, it is not expected that OLAm would behave as X-type ligand either. Given their distinct exchange behavior, it is expected that L-type ligands will self-desorb upon heating while X-type ligands on the other hand will never self-desorb, they will only desorb if a proton donor is present since a charged species would not be released in an apolar solvent. In order to classify the OLAm capping ligands on the CIS surface, a heating experiment was performed and monitored with ¹H NMR *in situ*. When self-desorption occurs at high temperatures, the OLAm can be classified as tightly bound L-type, if not, it is an X-type ligand.

5.3.1 Technical considerations for high temperature measurements

Since the temperature range that we aimed for was up to 150 °C *in situ*, the application of this type of experiments required a series of modifications and considerations for the experimental NMR setup. First, the solvent choice should be altered. Toluene-d8 or chloroform-d1, that are usually used as solvents for NMR measurements of NCs, are not possible since their boiling temperatures are too low (resp. 110 °C and 61 °C). As an alternative 1,2-dichlorobenzene-d4 was chosen, with a boiling point of 181 °C. Second, equipment and probe-head heating should be avoided. To ensure this, a constant stream of air was pushed through the probe and the shim coil temperature was monitored constantly during measurements. This temperature should not exceed 60 °C in order not to damage the coil. Third, accurate temperature calibration is essential to extract relevant information from the experiments. Thus, the probe temperature was calibrated using the method of Findeisen *et al.*²⁴ This method involves the measurement of a standard test sample of 4% methanol in methanol-d4 as “NMR-thermometer” since a known temperature-dependent chemical shift is present between the OH-proton signal and the CH₃-proton signal.

Since the NMR group of DOW Terneuzen already had experience in measuring polymers at temperatures up to 150 °C, the first measurements were executed on the NMR equipment at DOW itself in collaboration with dr. Mieke Lammens. Afterwards, with the obtained expertise, we altered the experimental set-up of one of our own 500 MHz magnets and performed the measurements in-house. The temperatures listed hereafter are those measured by the probe after the probe was externally calibrated according to the method mentioned above.

It is interesting to point out that while for our experiments, 150 °C was sufficient; the temperature range of *in situ* measurements could even be further extended by cooling the shim coils with cold nitrogen gas. Ultimately however, the maximum temperature range is determined by that of the probehead, which typically ranges to 150°C for standard room temperature probes. If higher temperatures are required, one should use a so called high-temperature probe. Importantly, after reaching a higher temperature and before the measurement, the sample is tuned and matched and optimization of the shimming is performed. Also, a new 90° pulse is measured.

5.3.2 High temperature measurements of OLAm capped CIS NCs

First, a CIS NC suspension capped with OLAm ligands was heated to 120 °C in steps of 20 °C. These measurements were initially executed at the facilities of DOW since they already had experience with measuring at high temperature. Figure 5.6 A depicts the full 1D ¹H spectra at 25 °C and 120 °C. Looking closely to the spectra, “shoulders” become visible on top of all the OLAm resonances at 120 °C. This is not the case for the 1,2-dichlorobenzene-d₄ resonances, therefore a shim problem can be ruled out as possible source. Figure 5.6 B depicts a zoom of the alkene region of OLAm in consecutive steps of 25°C to 120 °C in steps of 20°C starting from 40°C. In this overlay picture, it is clearly visible that the shoulder starts to arise around 80 °C and becomes more noticeable as temperature is further increased to 120 °C. This shoulder is attributed to a pool of self-desorbed ligands since it has the typical appearance of entangled ligands in the ligand shell, cfr. chapter 2.

In the first experiment, heating was performed very gradually and the time between starting the measurements at room temperature and reaching 120 °C was app. 7 hours. To see whether time plays a crucial role in this

desorption of OLAm, a new sample was heated in 1 hour to 130 °C and kept at that temperature for 3 hours while recording several 1Ds (figure 5.7) and a 2D NOESY (figure 5.9).

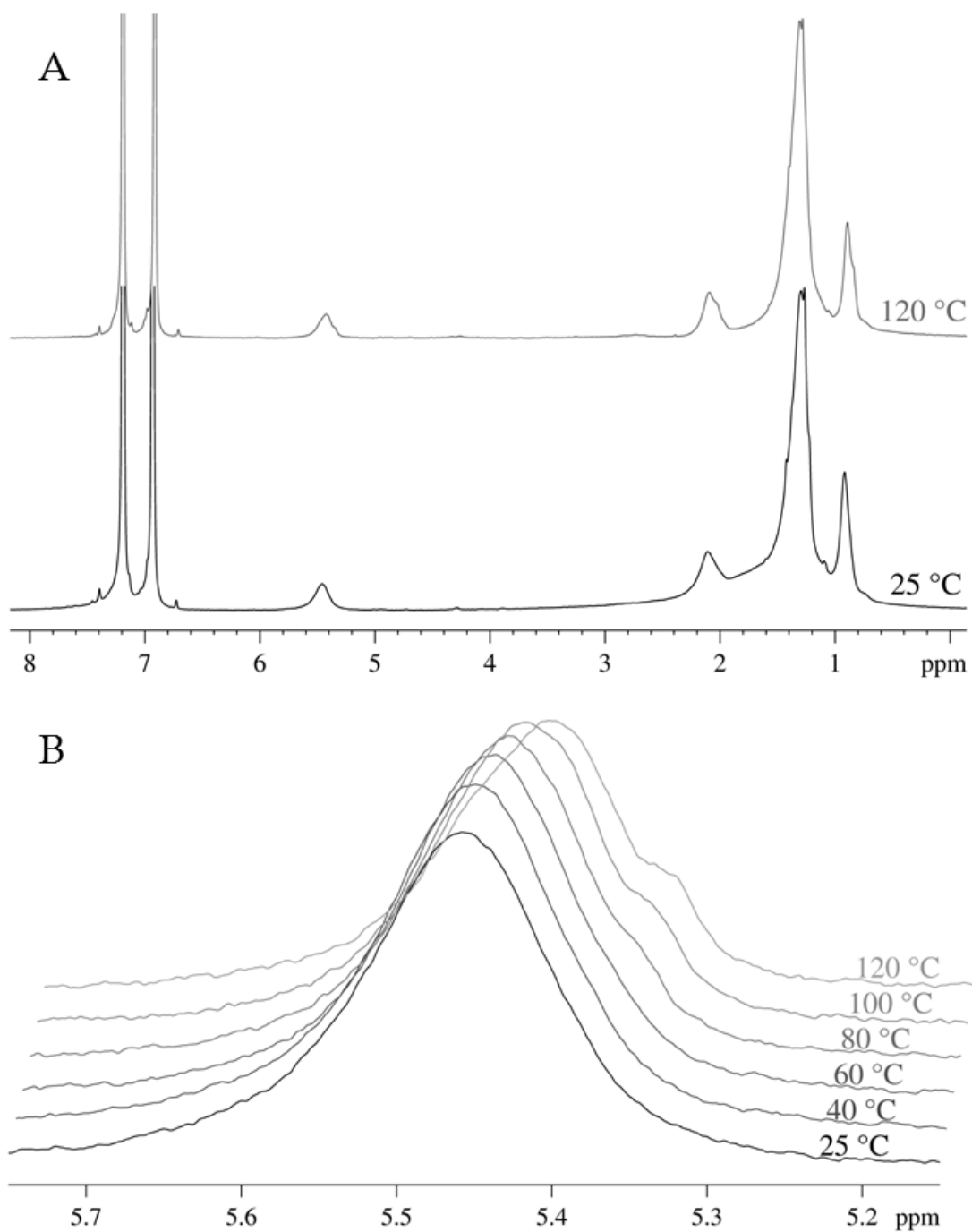


Figure 5.6. Spectra of OLAm capped CIS NCs in 1,2-dichlorobenzene-d₄ at 25 °C and 120 °C (A) and zoom of the alkene region at different temperatures (B)

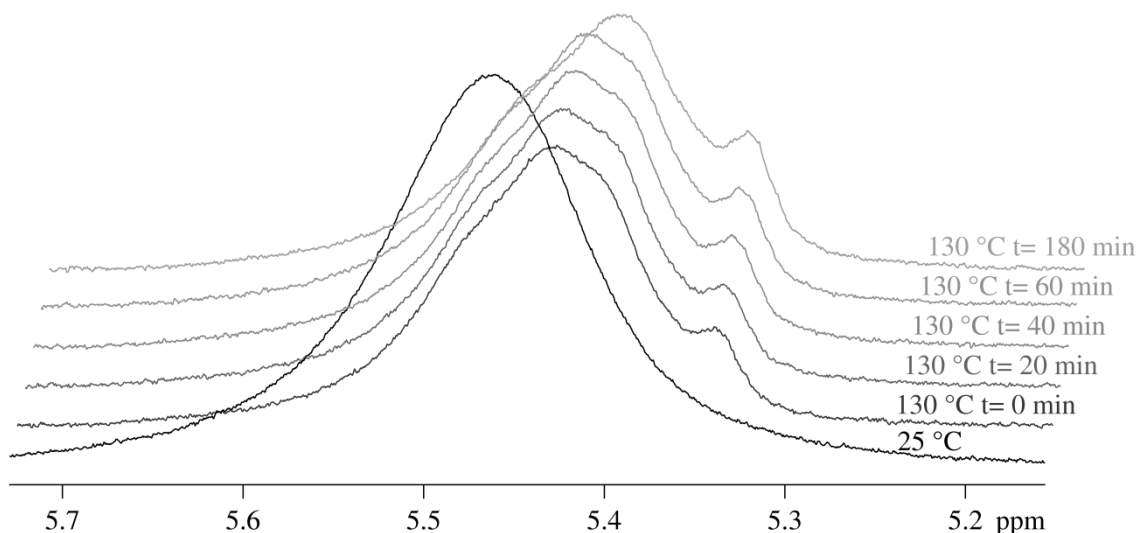


Figure 5.7. Spectra of OLAm capped CIS NCs in 1,2-dichlorobenzene- d_4 at 25 °C and 130 °C at different times.

From the overlay of the different 1D ^1H spectra, several observations can be made. First, it is clear that at 130 °C a shoulder is present from the start, i.e. one hour after starting to heat the sample. After reaching 130°C however, this shoulder still grows steadily during the measurement. Since the recording of consecutive 1D ^1H spectra was interrupted for a 2D NOESY experiment in this experiment, another experiment was performed in which the sample was also heated directly (this took app. 90 min) from 25 °C to 130 °C and kept there for 3h while continuously measuring quantitative 1D ^1H spectra. A scatter plot of the integral value of the shoulder relative to the remaining broad signal of the OLAm alkene resonance is shown in Figure 5.8. Since this shoulder is attributed to self-desorbed OLAm, the obtained percentage can also be said to be the percentage of self-desorbed OLAm relative to the entire pool of OLAm. From this plot, it is clear that at 130 °C OLAm slowly self-desorbs from the CIS surface. Also, within the time frame investigated there is no upper limit percentage detected at which this self-desorption goes to equilibrium.

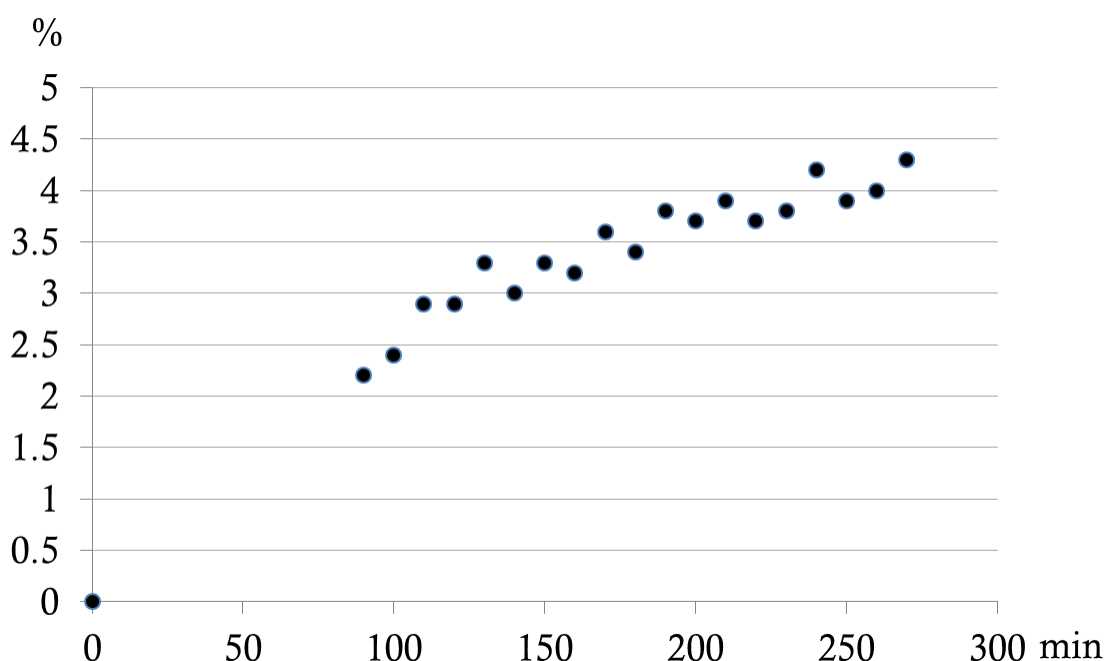


Figure 5.8. Scatter plot of the percentage of OLAm that desorbs from the CIS NC surface in function of time at 130 °C

After the *in situ* heating measurements, a 1D ^1H spectrum of the sample after returning to room temperature is measured (figure 5.10). When comparing this spectrum to the one recorded prior to heating, we observe that the signal has not restored completely. Instead, a small shoulder remains visible that is indicative for free OLAm. This means that not all OLAm that self-desorbed upon heating re-adsorbs on the surface, indicating that both desorption and adsorption are thermally activated.

The 2D NOESY plot that was recorded at 130 °C with a mixing time of 100 ms also contains important information. Clear negative NOEs are visible between the different bound OLAm resonances, as expected. However, no NOEs are observed between the desorbed OLAm resonances, as is evident from viewing the full spectrum A but even more so in the zoom of the alkene resonance in figure B. Furthermore, no exchange or NOE crosspeak is observed between the alkene resonance of bound OLAm and the desorbed OLAm. This means that the two molecules are not in mutual

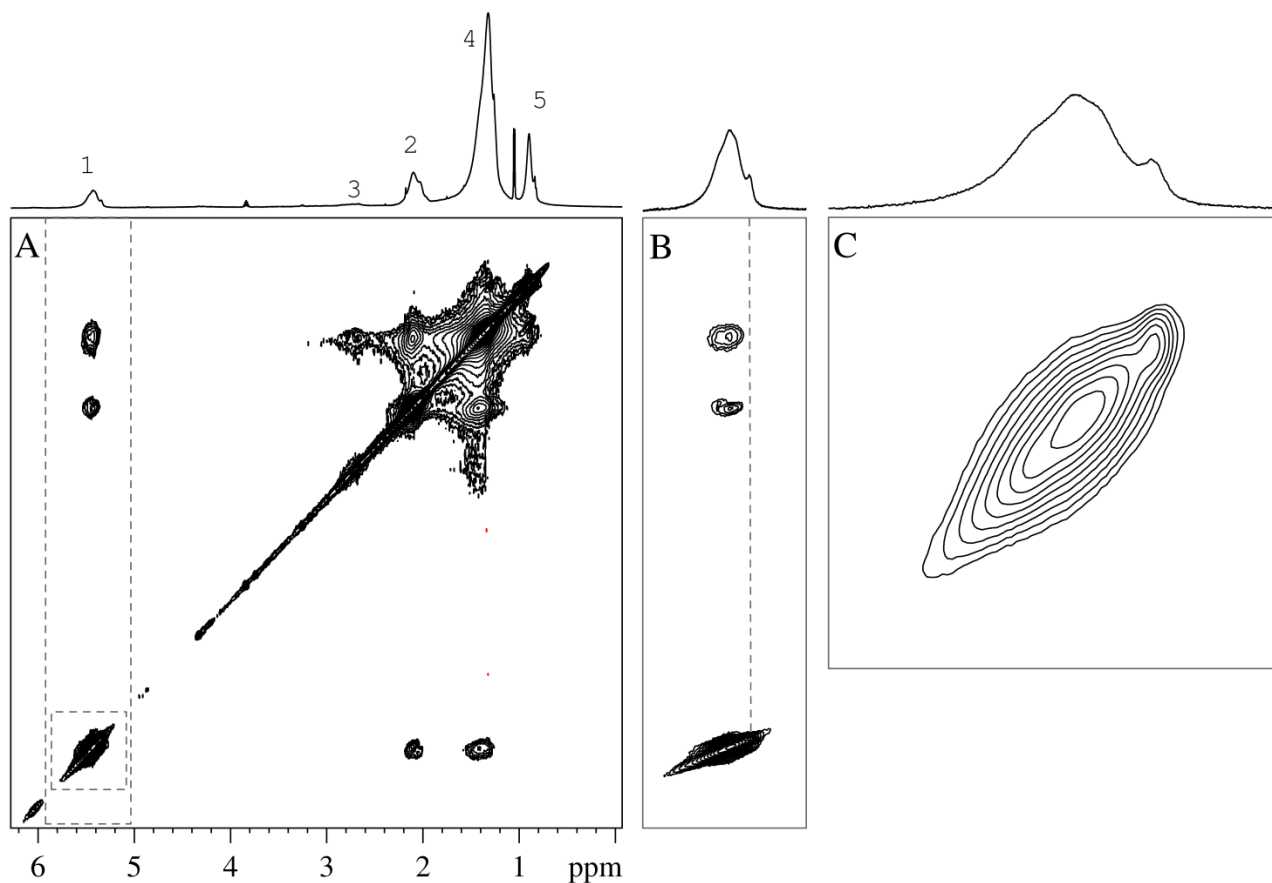


Figure 5.9. 2D NOESY of OLAm capped CIS NCs in 1,2-dichlorobenzene at 130 °C (A), detail of the alkene NOEs to the alkyl region(B) and the alkene region (C)

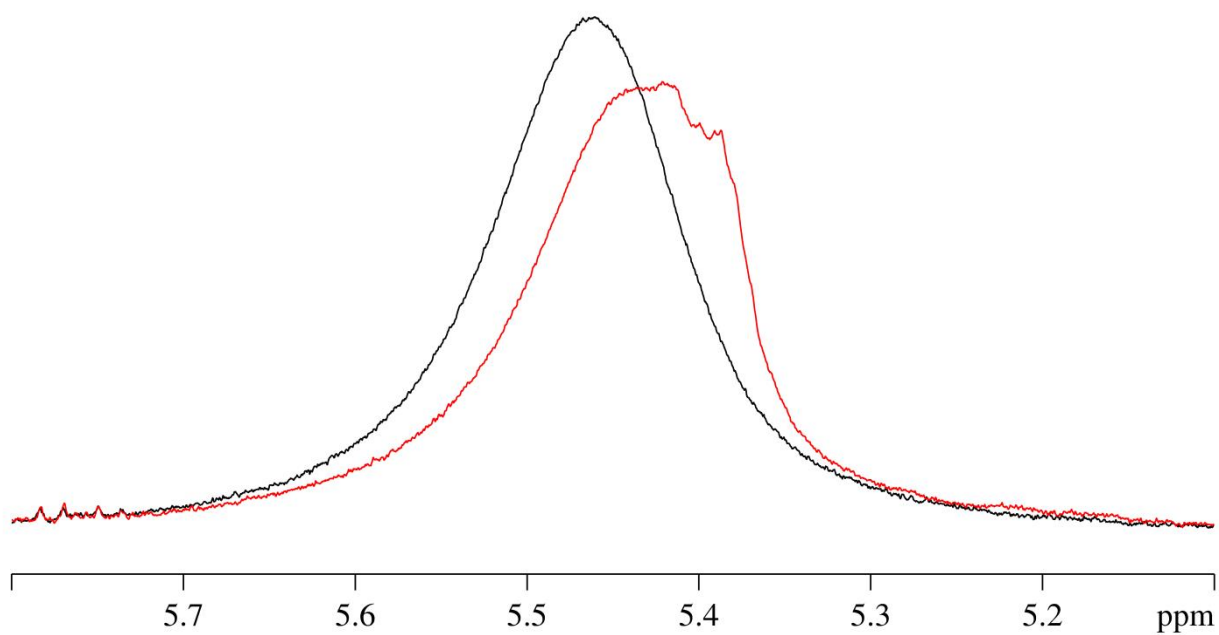


Figure 5.10. Spectra of OLAm capped CIS NCs in 1,2-dichlorobenzene-d₄ at 25 °C before (black spectrum) and after (red spectrum) heating

proximity and that mutual chemical exchange, if present occurs on a timeframe considerably longer than 100 ms.

With these high-temperature measurements, OLAm capping ligands on CIS NCs can be said to be L-type ligands that are tightly bound to the CIS NC surface. They do not exhibit a dynamic adsorption/desorption behavior at room temperature but desorb at higher temperatures without addition of other proton donors. This is in contrast to the L-type ligands that were characterized so far in literature.²⁵

5.4 ODPAc capped CdSe – Ligand behavior

As stated above, the desorption of OLAm at high temperature from the CIS NC surface made us conclude that OLAm is an L-type ligand because X-type ligands would not desorb upon heating only. To further substantiate this proposal, a well-known X-type ligand was tested, octadecylphosphonic acid (ODPAc) and used to cap CdSe NCs.²⁶ This sample was purified and

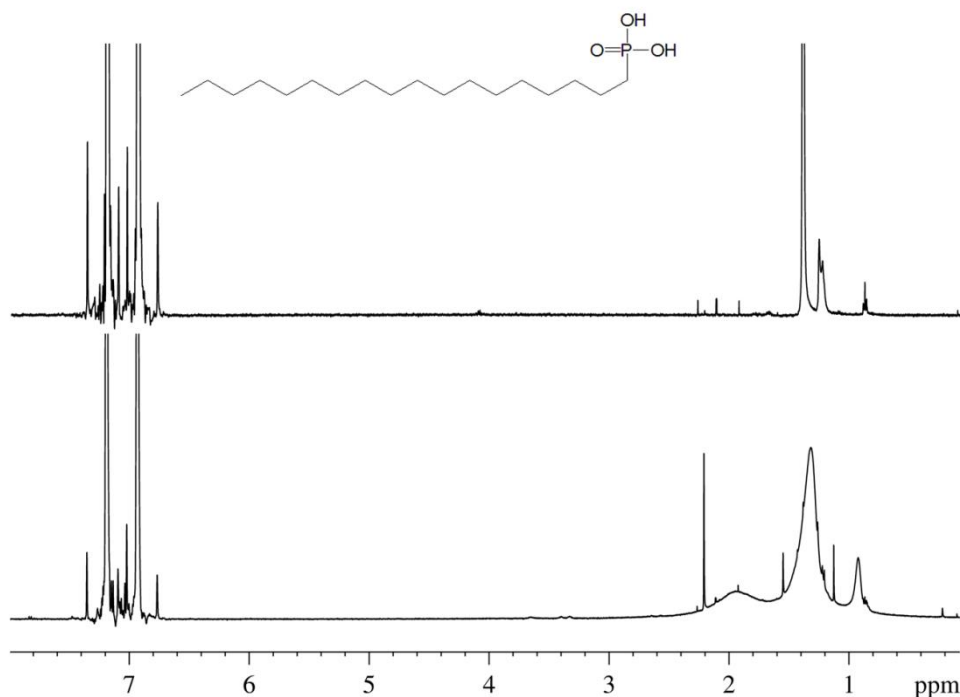


Figure 5.11. Structural formula of ODPAc, 1D ^1H spectrum of a reference sample of ODPAc (top) and of ODPAc capped CIS NCs (bottom) in 1,2-dichlorobenzene

suspended in 1,2-dichlorobenzene-d₄ for the *in situ* temperature measurement. The 1D ¹H spectrum of an ODPAc reference sample and of the ODPAc capped CdSe NCs in 1,2-dichlorobenzene is shown in figure 5.11. Figure 5.12 gives an overlay of the alkyl region during the *in situ* heating to 130 °C in steps of 20 °C. As stated before, this X-type ligand should not desorb during this experiment. Indeed, if we look at the CH₃ resonance at 0.9 ppm in particular, it is clear that there is no release of ODPAc from the surface since there is almost no change in the peak position and shape, while no additional signal appears on top of it. This clearly contrasts with the observations for the OLAm capped CIS NCs.

To conclude, a method was developed that provides the ability to distinguish between X- and L-type ligands. These high temperature measurements therefore provide a very useful addition to the existing NMR toolbox.

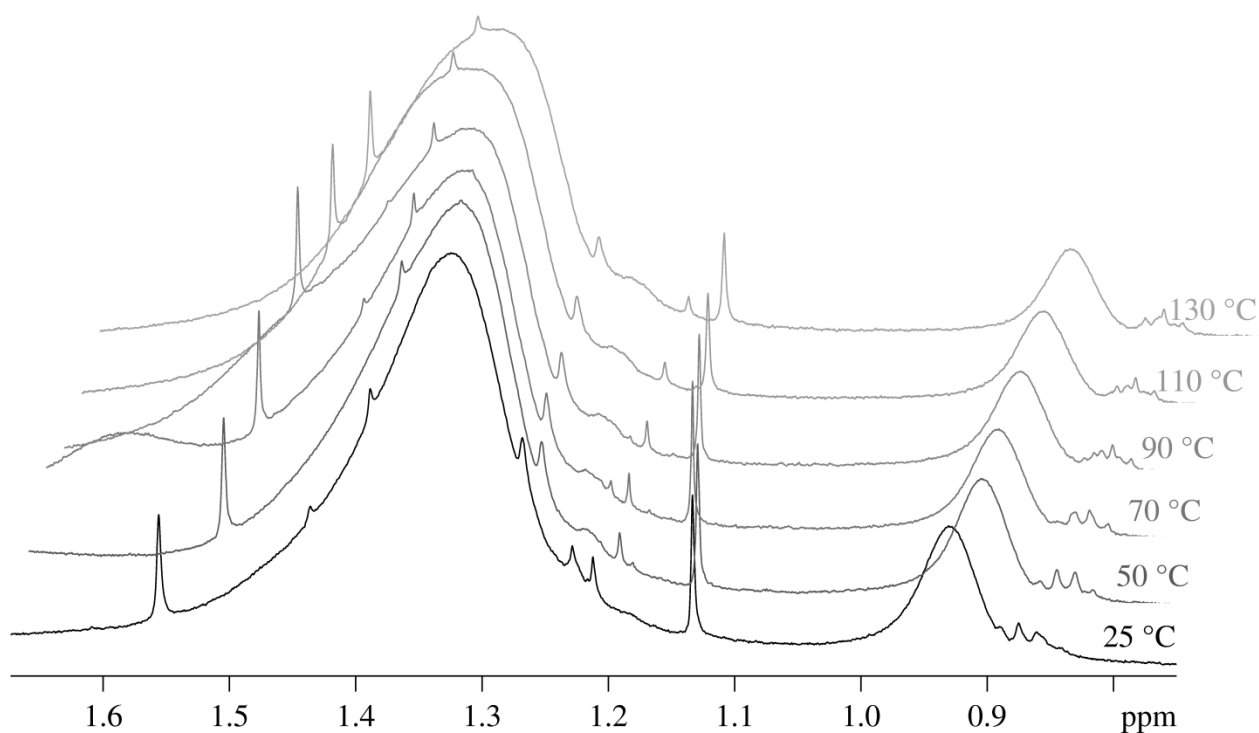


Figure 5.12. Stacked plot of the alkyl region of ODPAc capped CdSe NCs in 1,2-dichlorobenzene-d₄ during the *in situ* heating experiment from 25 °C to 130 °C

5.5 OLAm capped CIS – Ligand exchange

With the information obtained on OLAm binding on the CIS NC surface, ligand exchange design can now be performed. First, it is clear that exchanging OLAm with other ligands will require relatively high temperatures and successive exchange steps. Also, exchange will only be possible towards other L-type ligands.

Exchange procedures were performed with dodecanethiol (DDT), an L-type ligand and nonanoic acid (NAC), an X-type ligand. These molecules are selected for their lack of alkene resonances, allowing to distinguish and monitor the OLAm species by 1D ^1H NMR. This is shown in figure 5.13

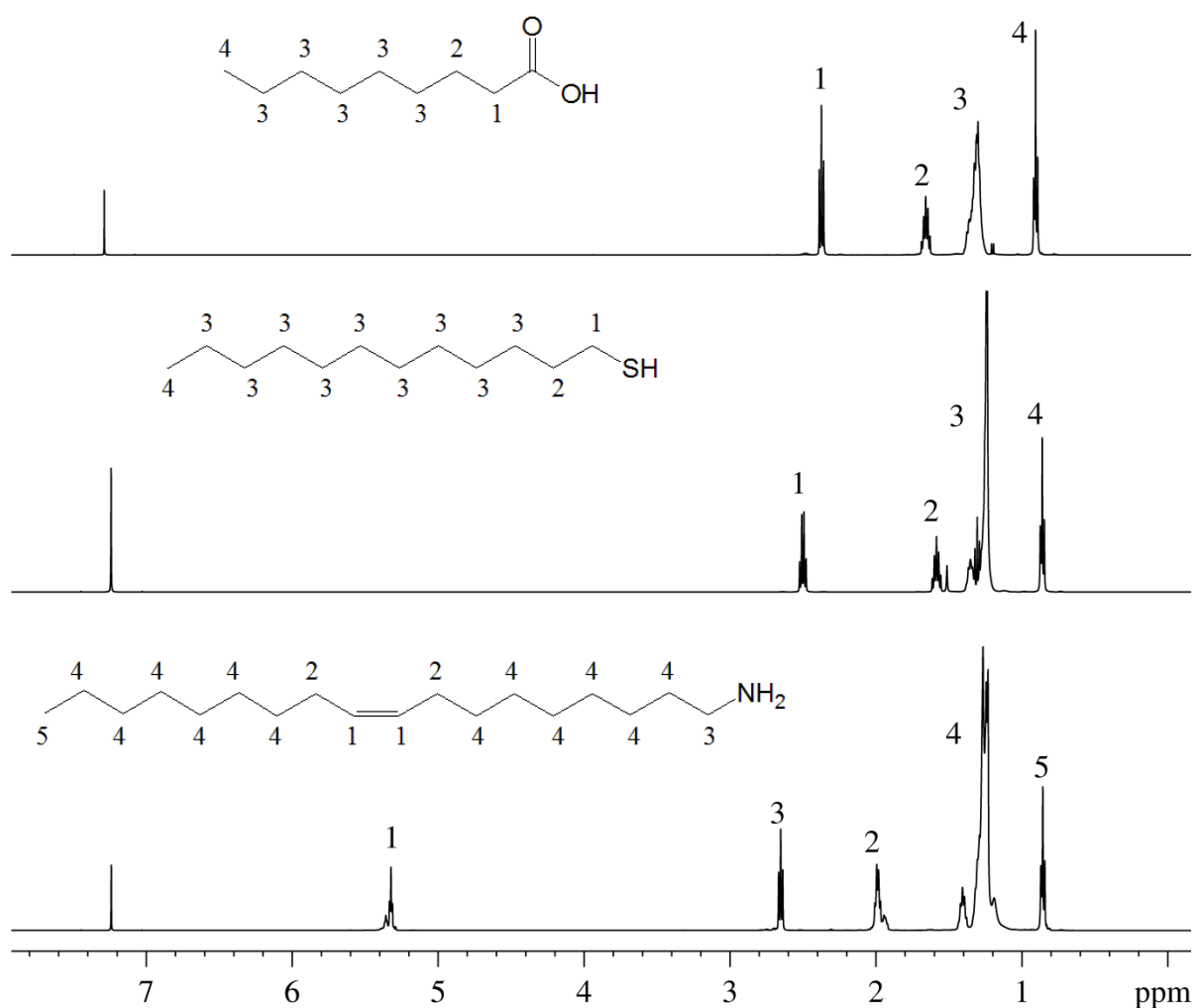


Figure 5.13. Reference spectrum of OLAm (bottom), DDT (middle) and NAc (top) in CDCl_3 at 298.2 K

where the 1D ^1H spectrum of reference solutions of DDT, NAc and OLAm in CDCl_3 are depicted. For quantitation, the alkene resonance of OLAm is used as a measure for the OLAm quantity and the CH_3 signal is used as a measure for the sum of OLAm and DDT or NAc respectively. From the difference between both, the amount of DDT or NAc can be derived.

As stated previously, the exchange procedure requires an excess of new ligand, relatively high temperature and has to be repeated several times for a good result. The procedure followed in our research is shown in figure 5.14, and this cycle is repeated three times.

The results of these exchange tests are summarized in figure 5.15. The original ligand density of OLAm on the CIS NC is 5.1 /nm^2 ; this was determined with a standard ERETIC measurement, i.e. a 1D ^1H with 16 scans, 4 dummy scans, a receiver gain set to 64 and a d1-delay of 30 sec. For better comparison, this value is normalized to 1 in the graph. After

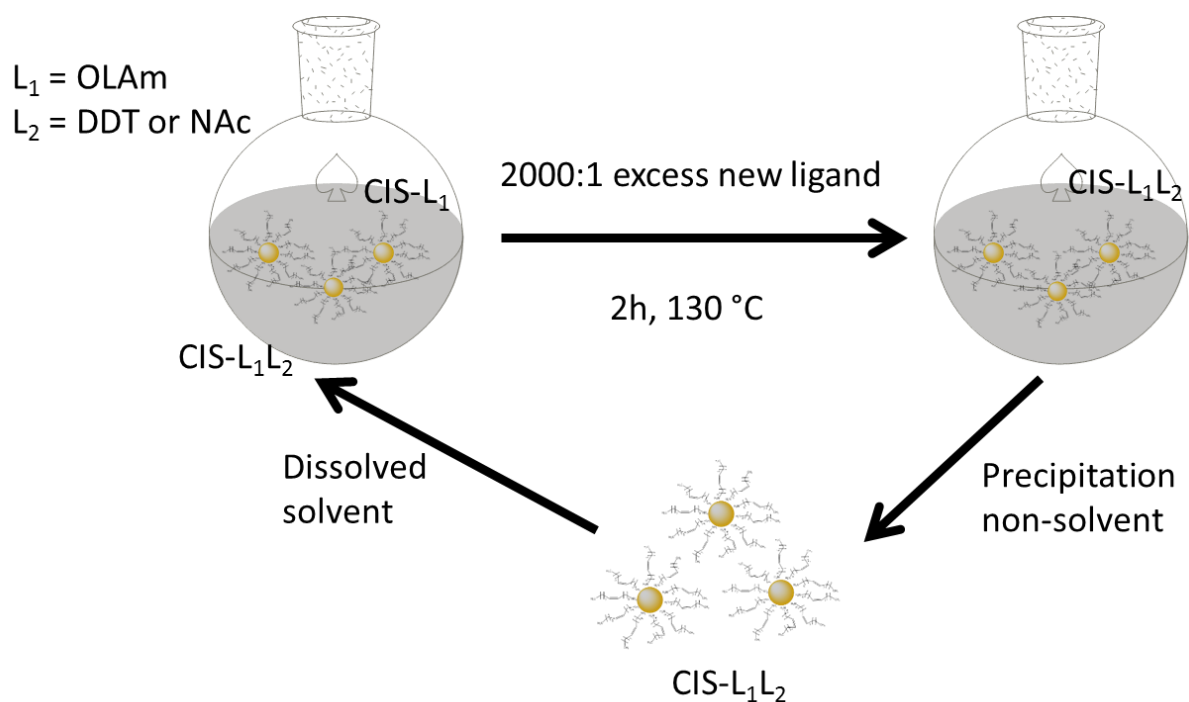


Figure 5.14. Depiction of exchange procedure followed, the cycle is repeated 3 times.

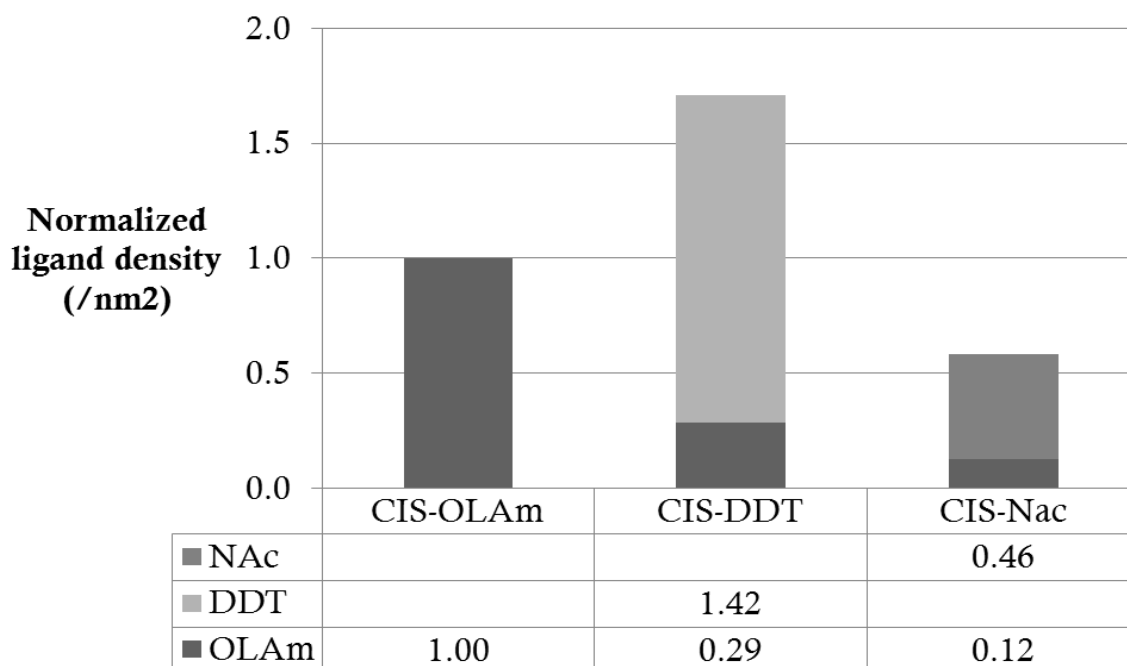


Figure 5.15. Plot of the normalized ligand densities of CIS-OLAm and after the consecutive exchange to DDT and NAc

completing the exchange procedure to DDT, most of the OLAm is lost but surprisingly, the total ligand density derived from the integral of the methyl resonance increases to 8.72 /nm^2 . This equals an increase of more than 60 % of the original surface coverage value. Thus more DDT is bound than OLAm is desorbed. Subsequent exposure to NAc further reduces the amount of OLAm and also brings down the total ligand density to 2.98 /nm^2 , which is about 60 % of the original ligand density. As mentioned before, these observations were somewhat unexpected since we did not expect the ligand density to increase when exchanging L- to L-type ligand. Moreover, L- to X-type exchange is something impossible and it was not expected that NAc would get exchanged at all.

In order to understand the source of this unexpected exchange behavior, the Cu:In and S:In ratios were estimated based on a Rutherford Backscattering Spectroscopy (RBS) measurement. The Cu:In ratio was found to be 1.00 ± 0.04 and the S:In ratio was found to be 1.54 ± 0.12 .

From these results, it can be concluded that OLAm capped CIS NCs are cation rich with a net ratio of the formal cation to anion charge of 1.30 ± 0.10 . However, this net formal charge should be balanced to zero, meaning that X-type moieties are probably also present on the surface. Since they do not have any observable resonances in the 1D ^1H spectrum, these are most likely small moieties, such as OH^- or acetylacetonate that was used during the synthesis, *vide supra*. Their resonances will not be visible due to severe broadening caused by their close proximity to the surface.

For additional confirmation of the initial presence of X-type moieties on the OLAm capped CIS, an exchange to undecenoic acid (UDAc) was also executed. UDAc has two distinct alkene resonances that do not coincide with the alkene resonance of OLAm. In addition, it does not contribute an end methylgroup, as this position is taken by the alkene group. Both features allow better monitoring of the individual ligand's behavior. In figure 5.16

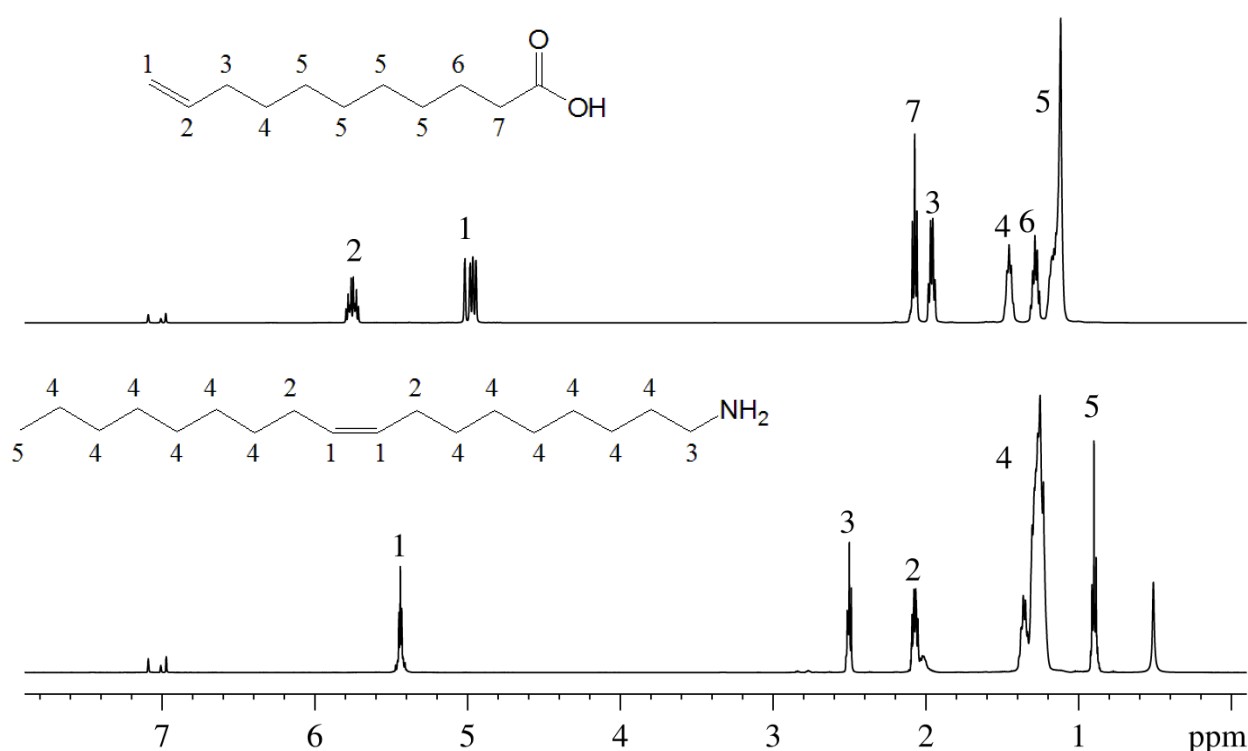


Figure 5.16. Reference spectrum of OLAm (bottom) and UDAc (top) in toluene- d_8 at 298.2 K.

the reference 1D ^1H spectra of OLAm and UDAc in toluene are shown for comparison.

In figure 5.17 the spectrum of OLAm capped CIS NCs before and after exchange to UDAc is shown. In the 1D ^1H spectrum after exchange, additional resonances from UDAc are present and they are also broadened, suggesting that UDAc is indeed also bound to the NC surface. This is confirmed with a DOSY measurement. The decay of resonance 1 of UDAc that is relatively well resolved at 5.1 ppm shows a bi-exponential behavior, with a small diffusion coefficient of $38.7 \pm 2.1 \mu\text{m}^2/\text{s}$ (figure 5.18 A). This is more or less the same value as for the slow diffusing component in the bi-exponential decay of the OLAm CH_3 resonance which is $35.6 \pm 0.1 \mu\text{m}^2/\text{s}$ (figure 5.18 B).

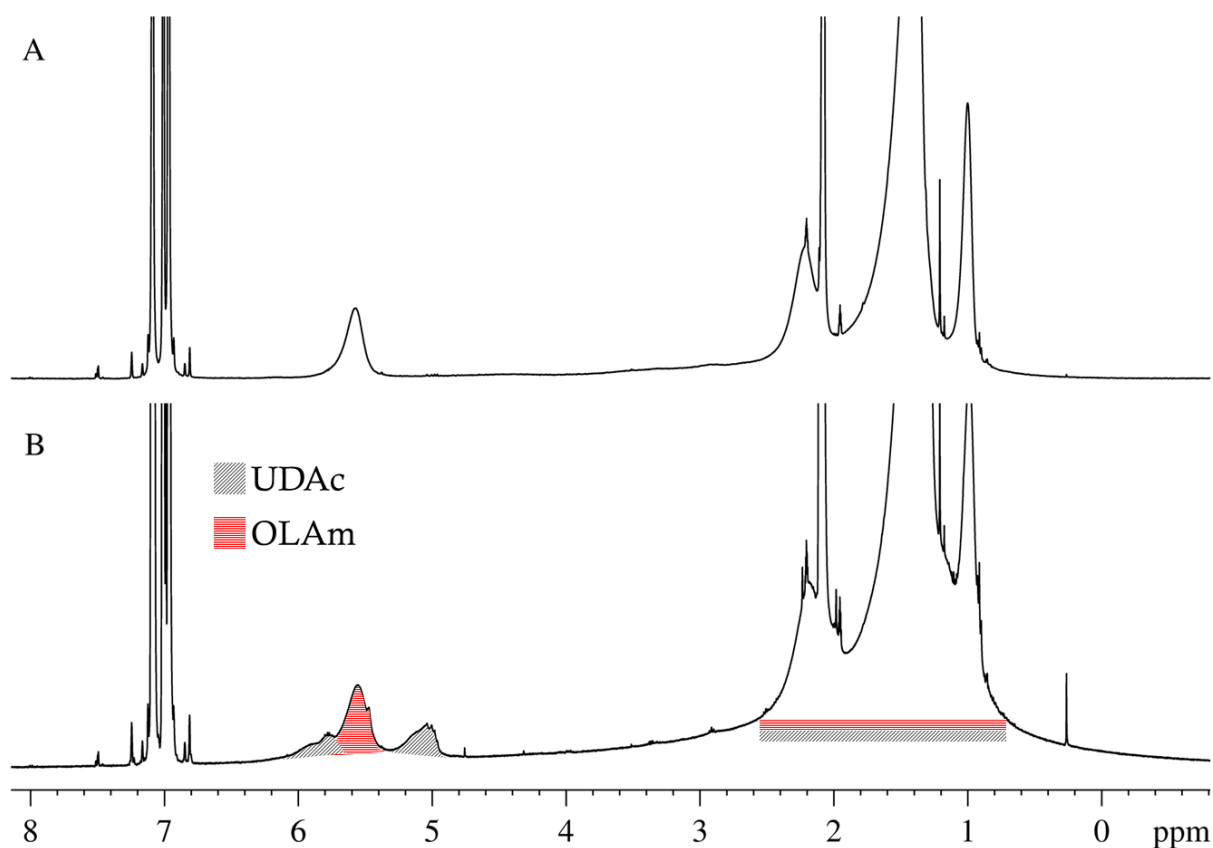


Figure 5.17. Spectrum of OLAm capped CIS NCs in toluene- d_8 before (top) and after exchange to UDAc (bottom)

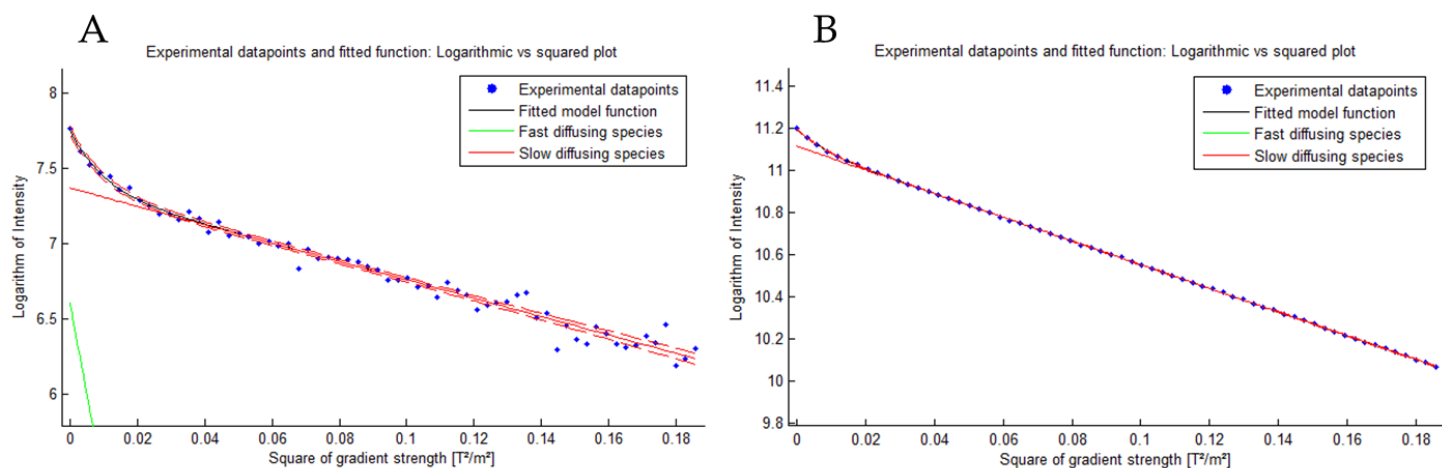


Figure 5.18. Datapoints and bi exponential fitting of the diffusion decay of the UDAc resonance 1 at 5.1 ppm (A) and the OLAm CH₃ resonance (B)

5.6 ODAm capped CIS – Ligand behavior

The OLAm used in the standard synthesis is technical grade OLAm, which is probably the cause of the appearance of additional X-type moieties. To prove that the amine ligands bound on CIS NCs are tightly bound L-type ligands, synthesis was adjusted and pure grade 1-octadecylamine (ODAm) was used. In figure 5.19 a reference spectrum of ODAm and ODAm capped CIS NCs in 1,2-dichlorobenzene-d₄ is shown. From these 1D ¹H spectra, it is already clear that 1-octadecylamine is also bound to the CIS NCs surface. Additional confirmation of this binding is obtained by recording both 2D NOESY and 2D DOSY spectra. With a calculated disk top hydrodynamic diameter of 19.4 ± 0.1 nm, this is in good agreement with previous results for OLAm capped CIS NCs (see 5.2).

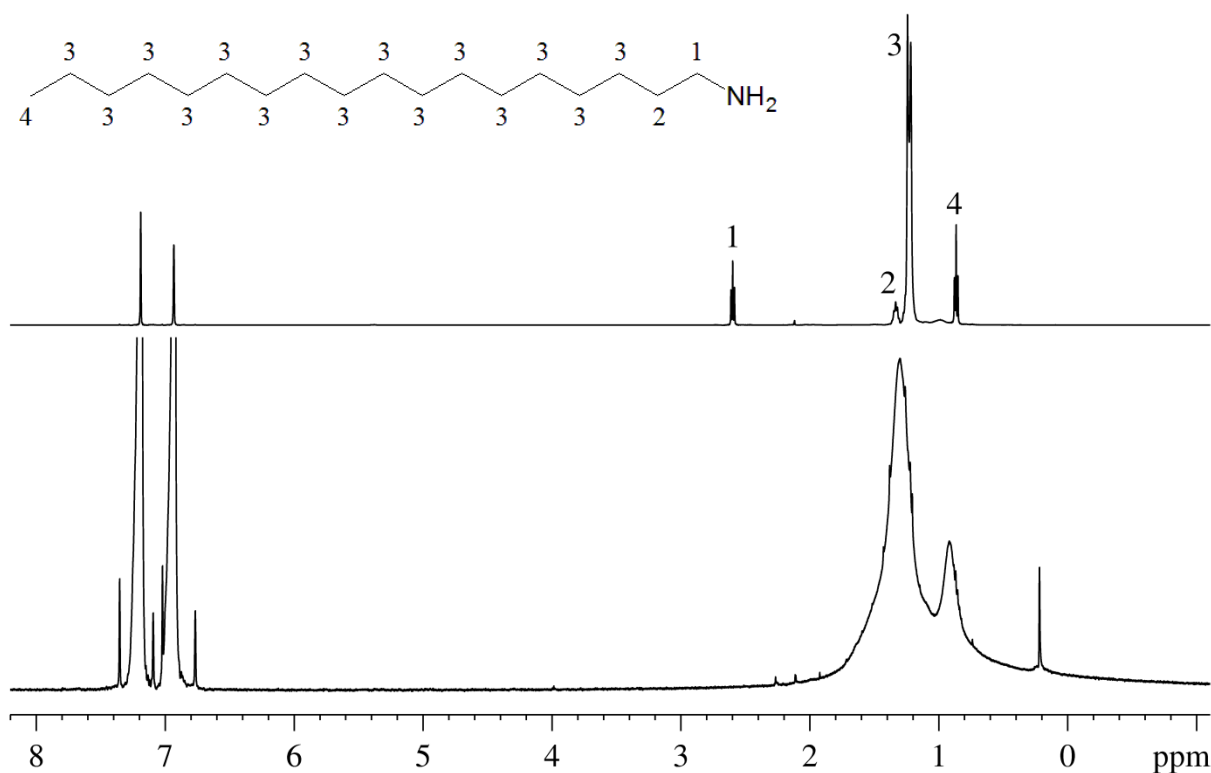


Figure 5.19. Structural formula of 1-octadecylamine, 1D ^1H spectrum of a reference sample of 1-octadecylamine in 1,2-dichlorobenzene- d_4 (top) and of ODAm capped CIS NCs in 1,2-dichlorobenzene- d_4 (bottom)

Next, a heating experiment with the ODAm capped CIS NCs (figure 5.20) was performed. The sample was gradually heated *in situ* from room temperature to 130 °C. Looking closely at the spectra, it is observed that for both the CH_2 and CH_3 resonances, a shoulder arises upfield from the bound resonance upon heating. This shoulder is attributed to a part of the bound ODAm that is released upon heating. This result confirms that ODAm is also acting as a tightly bound L-type ligand that only releases upon heating.

Since the purity of the analytical grade ODAm is much better than the technical grade OLA_m used before, no X-type moieties are expected to be present on the surface. To check this assumption, an exchange procedure as shown in figure 5.14 for OLA_m capped NCs was now also attempted with ODAm capped NCs towards both a thiol, L-type ligand, and a carboxylic acid, X-type ligand. The exchange towards a thiol is expected to work fine since this is an L-to-L type exchange, *vide supra*. For this exchange, 2-

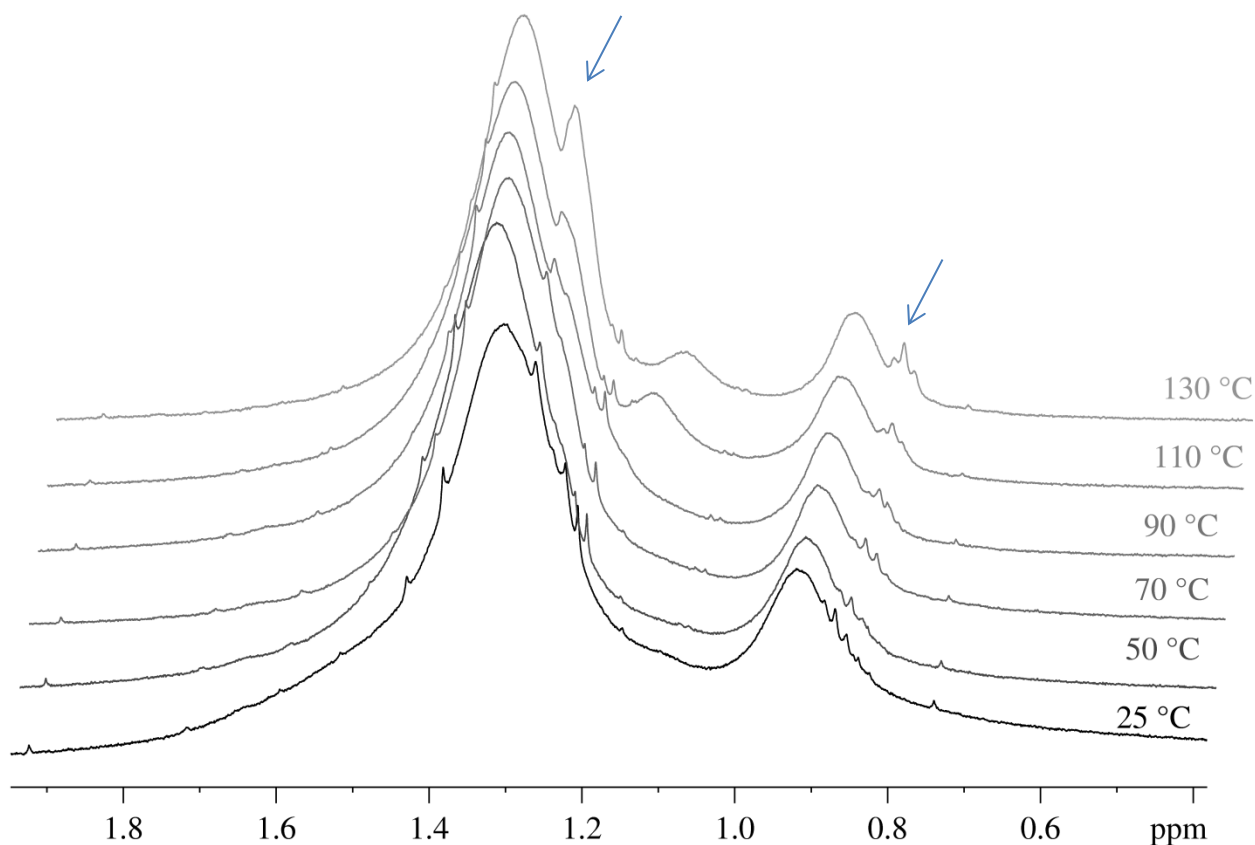


Figure 5.20. Zoom on the alkyl region of ODAm capped CIS NCs in 1,2-dichlorobenzene- d_4 during the *in situ* heating experiment from 25 °C to 130 °C

phenylethanethiol (PET) was chosen as thiol because it exhibits aromatic resonances and can thus be monitored and quantified in the spectrum next to the original ODAm that only has alkyl resonances. Looking at the spectrum measured after the exchange towards PET (figure 5.21), the PET resonances are indeed broadened, meaning that PET is also bound on the CIS NCs and exchange is successful. Next to the broad resonances, also free PET is observed in the spectrum. This is due to minor work-up after the exchange.

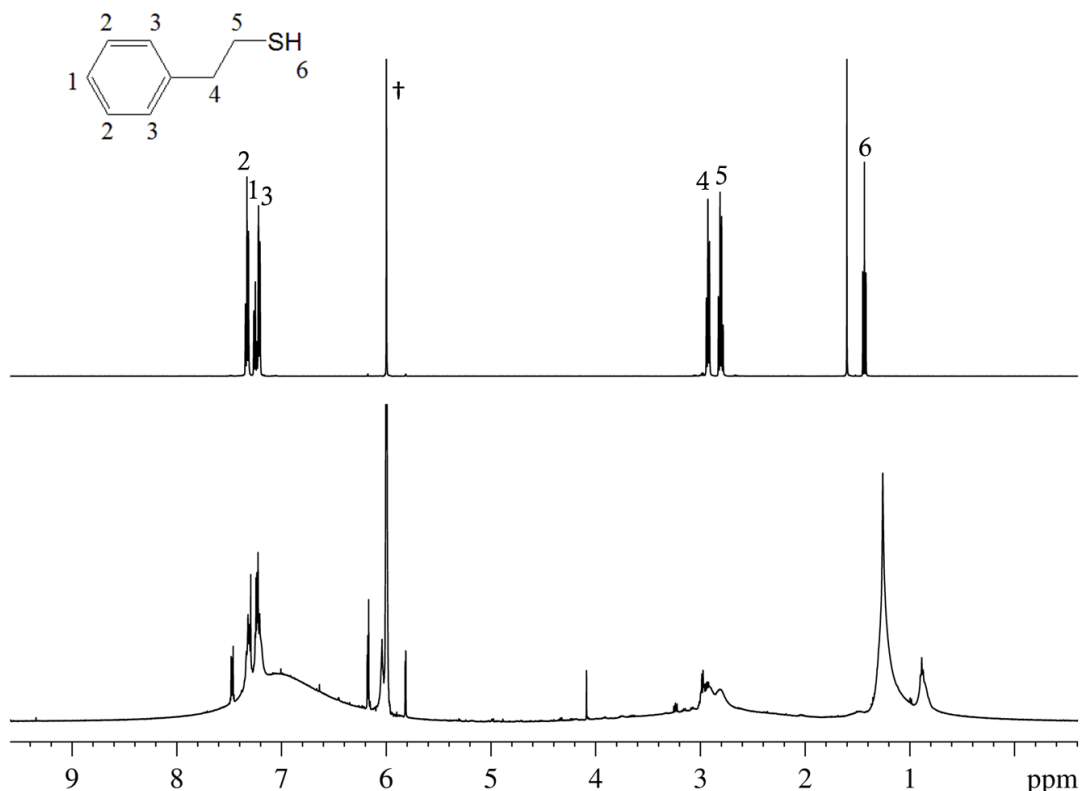


Figure 5.21. Structural formula of 2-phenylethanethiol, 1D ^1H spectrum of a reference sample of 2-phenylethanethiol (top) and of PET capped CIS NCs after exchange (bottom) in 1,1,2,2-tetrachloroethane- d_2

In order to test whether X-type moieties are also present on the surface of these ODAm capped CIS NCs; an attempt was made to perform an exchange towards oleic acid (OLAc), an X-type ligand. The spectrum after ligand exchange does not show any bound nor free resonances of OLAc (figure 5.22). This indicates that the X-type OLAc cannot exchange the L-type ODAm and as a result, it is fully washed away during work-up procedure. This is in good agreement with the theory of ligand exchange (figure 5.6) and shows that the amines bound on CIS NCs are indeed L-type ligands and that no X-type moieties are present on the surface of these ODAm capped CIS NCs. Thus, to avoid the former, analytical grade amines are preferred over technical grade ones.

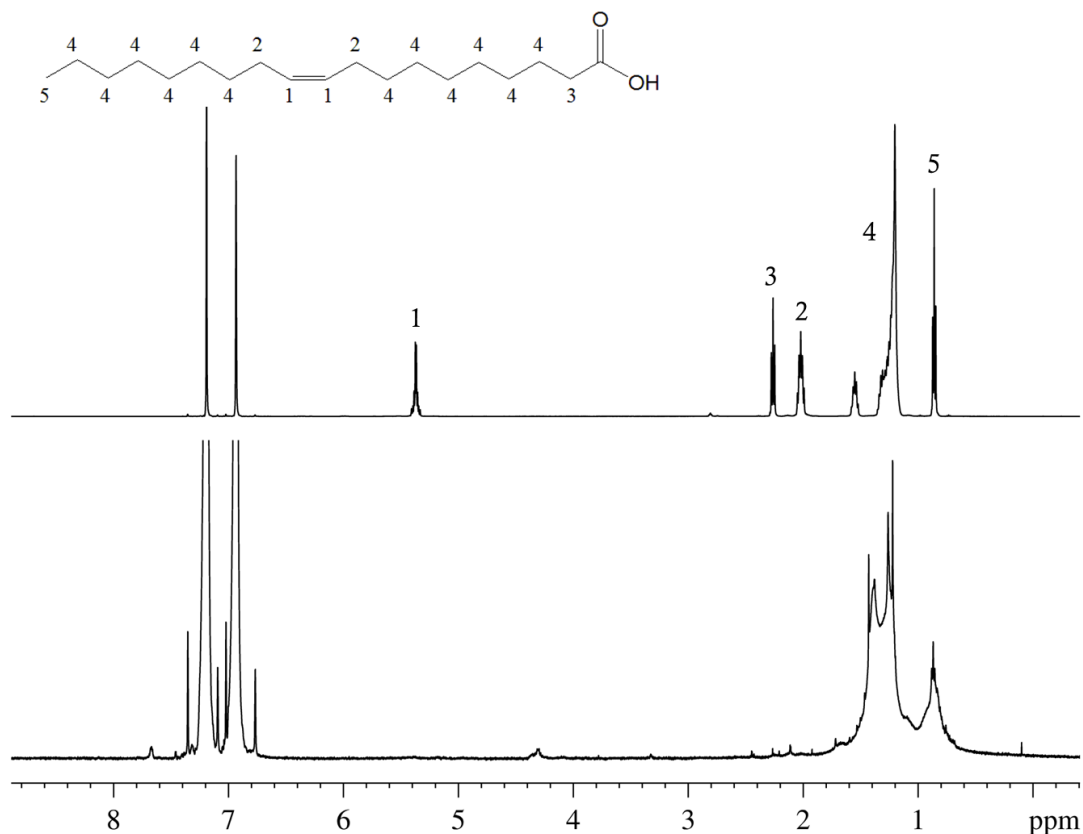


Figure 5.22. Structural formula of oleic acid, 1D ^1H spectrum of a reference sample of OLAc (top) and of ODAm capped CIS NCs after exchange procedure towards OLAc (bottom) in 1,2-dichlorobenzene- d_4 at 298 K.

5.7 Conclusion

In this chapter, the surface chemistry of CIS NCs synthesized using amines was analyzed and possible ligand exchange strategies were explored. Using the NMR toolbox for nanocrystals (see chapter 2) and expanding this toolbox with *in situ* heating experiments, we concluded that the surface of as-synthesized CIS NCs consists of L-type, tightly bound amines. Importantly, these *in situ* heating NMR measurements provide a new straightforward approach to distinguish L-type from X-type binding ligands. Desorption of an L-type ligand becomes apparent by the apparition of additional resonances while for X-type ligands no change is apparent in the spectra, indicating the absence of desorption. For technical grade OLAm that is typically used during CIS synthesis, we showed that this leads to non-

stoichiometric NCs capped with a combination of L-type OLAm and X-type impurities. This is an important result since it demonstrates the importance of a careful surface analysis prior to ligand exchange. For the synthesis with analytical grade ODAm, tight L-type binding was illustrated. This was demonstrated by performing ligand exchange reactions towards acids (X-type) and thiols (L-type), where only the thiols could be found on the surface after several ligand exchange steps.

5.8 References

- (1) Dierick, R.; Van den Broeck, F.; De Nolf, K.; Zhao, Q.; Vantomme, A.; Martins, J. C.; Hens, Z. *Chem. Mat.* **2014**, *26*, 5950.
- (2) Kolny-Olesiak, J.; Weller, H. *ACS Applied Materials & Interfaces* **2013**, *5*, 12221.
- (3) Panthani, M. G.; Akhavan, V.; Goodfellow, B.; Schmidtke, J. P.; Dunn, L.; Dodabalapur, A.; Barbara, P. F.; Korgel, B. A. *J. Am. Chem. Soc.* **2008**, *130*, 16770.
- (4) Li, L.; Daou, T. J.; Texier, I.; Kim Chi, T. T.; Liem, N. Q.; Reiss, P. *Chem. Mat.* **2009**, *21*, 2422.
- (5) Xie, R.; Rutherford, M.; Peng, X. *J. Am. Chem. Soc.* **2009**, *131*, 5691.
- (6) Aldakov, D.; Lefrancois, A.; Reiss, P. *Journal of Materials Chemistry C* **2013**, *1*, 3756.
- (7) Witt, E.; Kolny-Olesiak, J. *Chemistry – A European Journal* **2013**, *19*, 9746.
- (8) Guo, Q.; Kim, S. J.; Kar, M.; Shafarman, W. N.; Birkmire, R. W.; Stach, E. A.; Agrawal, R.; Hillhouse, H. W. *Nano Lett.* **2008**, *8*, 2982.
- (9) Zhong, H. Z.; Bai, Z. L.; Zou, B. S. *Journal of Physical Chemistry Letters* **2012**, *3*, 3167.
- (10) Fan, F. J.; Wu, L.; Yu, S. H. *Energy & Environmental Science* **2014**, *7*, 190.
- (11) Zhong, H. Z.; Zhou, Y.; Ye, M. F.; He, Y. J.; Ye, J. P.; He, C.; Yang, C. H.; Li, Y. F. *Chem. Mat.* **2008**, *20*, 6434.
- (12) Chen, B. K.; Zhong, H. Z.; Zhang, W. Q.; Tan, Z. A.; Li, Y. F.; Yu, C. R.; Zhai, T. Y.; Bando, Y. S.; Yang, S. Y.; Zou, B. S. *Advanced Functional Materials* **2012**, *22*, 2081.
- (13) Yao, R.-Y.; Zhou, Z.-J.; Hou, Z.-L.; Wang, X.; Zhou, W.-H.; Wu, S.-X. *ACS Applied Materials & Interfaces* **2013**, *5*, 3143.
- (14) Lauth, J.; Marbach, J.; Meyer, A.; Dogan, S.; Klinke, C.; Kornowski, A.; Weller, H. *Advanced Functional Materials* **2014**, *24*, 1081.
- (15) Tang, J.; Hinds, S.; Kelley, S. O.; Sargent, E. H. *Chem. Mat.* **2008**, *20*, 6906.
- (16) Kruszynska, M.; Borchert, H.; Parisi, J.; Kolny-Olesiak, J. *J. Am. Chem. Soc.* **2010**, *132*, 15976.
- (17) Hens, Z.; Martins, J. C. *Chem. Mat.* **2013**, *25*, 1211.
- (18) Anderson, N. C.; Hendricks, M. P.; Choi, J. J.; Owen, J. S. *J. Am. Chem. Soc.* **2013**, *135*, 18536.
- (19) Moreels, I.; Fritzing, B.; Martins, J. C.; Hens, Z. *J. Am. Chem. Soc.* **2008**, *130*, 15081.
- (20) Fritzing, B.; Capek, R. K.; Lambert, K.; Martins, J. C.; Hens, Z. *J. Am. Chem. Soc.* **2010**, *132*, 10195.
- (21) Hassinen, A.; Moreels, I.; De Nolf, K.; Smet, P. F.; Martins, J. C.; Hens, Z. *J. Am. Chem. Soc.* **2012**, *134*, 20705.
- (22) Moreels, I.; Martins, J. C.; Hens, Z. *ChemPhysChem* **2006**, *7*, 1028.
- (23) Moreels, I.; Justo, Y.; De Geyter, B.; Haustraete, K.; Martins, J. C.; Hens, Z. *ACS Nano* **2011**, *5*, 2004.
- (24) Findeisen, M.; Brand, T.; Berger, S. *Magnetic Resonance in Chemistry* **2007**, *45*, 175.

Chapter 5

- (25) Fritzinger, B.; Moreels, I.; Lommens, P.; Koole, R.; Hens, Z.; Martins, J. C. *J. Am. Chem. Soc.* **2009**, *131*, 3024.
- (26) Gomes, R.; Hassinen, A.; Szczygiel, A.; Zhao, Q.; Vantomme, A.; Martins, J. C.; Hens, Z. *The Journal of Physical Chemistry Letters* **2011**, *2*, 145.

6

HYDROXYAPATITE MICROPARTICLES

In this chapter, hydroxyapatite microparticles that are stabilized using amino acids are studied using NMR. For our research interests, this new kind of much larger particles provided an ideal opportunity to test and expand the NMR toolbox for micro-sized systems. Also, Saturation Transfer Difference measurements that were so far not used in this type of research were included. This work was published in Chemistry, A European Journal.¹

6.1 Introduction

Over the last few decades, the development of devices for controlled oral delivery of proteins and different drugs has attracted considerable interest because of the ease of administration and the reduced risks compared to parental administration.²⁻⁵ However, there are still several challenges to surmount for delivering proteins or other vaccines orally. One such challenge is that proteins or peptides administered as is are poorly bio-available. Various strategies have been proposed that should enhance the bio-availability of these drugs.^{6,7} When a protein is administered along with a microparticulate carrier for example, the antibody-mediated immune response could be enhanced.^{8,9}

Different carrier systems such as viral, recombinant protein, inorganic and polymeric carriers have been tested extensively over the past decades. Inorganic microparticulate carriers are interesting due to their biocompatibility, functionality, easier production and low cost. One example of such a material is HydroxyApatite (HA). The loading of bovine serum albumin (BSA, selected as model antigen) on HA powder was the topic of this study. Enhancement of the adsorption capacity of HA powder can be achieved by functionalizing the HA powder with linker molecules in order to increase the electrostatic or other kind of interactions with BSA. The HA surface has neutral or slightly negative charge in aqueous suspensions at neutral pH, while BSA is negatively charged under these conditions. Two amino acid linker molecules (L-Arginine and L-Lysine) were selected in order to change the BSA loading. In each case, the carboxyl group is expected to react with the Ca^{2+} ions present on the HA surface¹⁰ which leaves the amino group available and positively charged at physiological pH for further reactions with BSA. In addition to the

quantification problem, little information was available regarding the interaction between HA and the amino acid molecules, posing a new interesting opportunity to test and expand the application of the NMR toolbox to larger microparticles. Indeed, up until now, the NMR toolbox was tested extensively and applied for a very wide range of nanomaterials in the 1 to 20 nm scale.¹¹ This work was performed in collaboration with Vinayaraj Ozhukil Kollath, a PhD student at the University of Liège and also in collaboration with Steven Mullens, researcher at VITO. The results were published in Chemistry, A European Journal.¹

6.2 Materials

The HA powder (complexometric assay > 90%, Merck, Germany) used in this study was not modified and has a specific surface area of 63 m²/g. The diameter of the particles varies from 50 to 200 nm but also agglomerates are formed. In figure 6.1 on the right, a Scanning Electron Microscope image of the powder is shown. On the left, a scheme of the unit cell of HA¹² is shown. The OH⁻ groups in this crystal structure are ordered along the c-axis. These hydroxyl protons give rise to a resonance at 0 ppm when studied with solid-state NMR.¹³

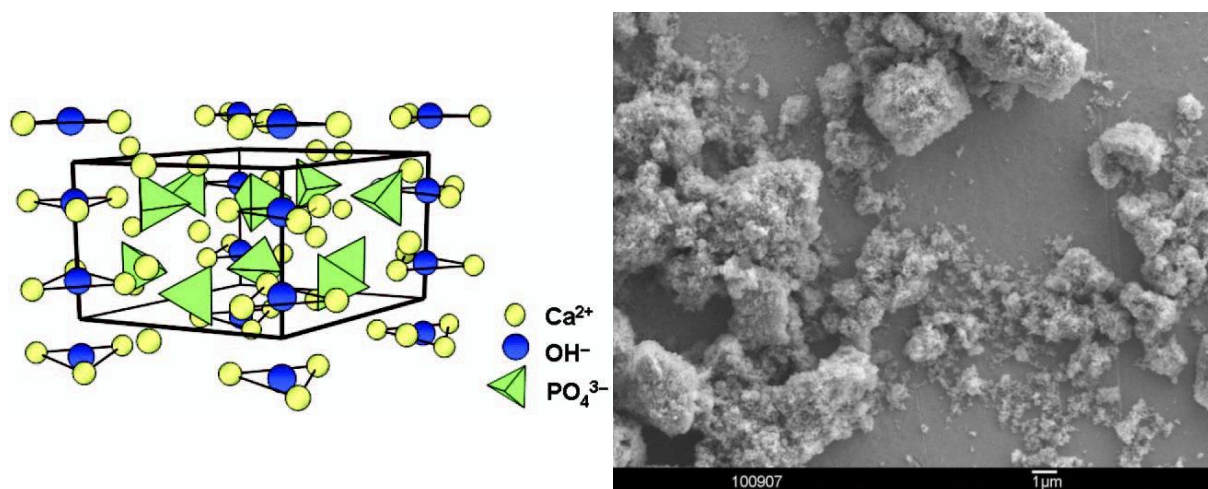
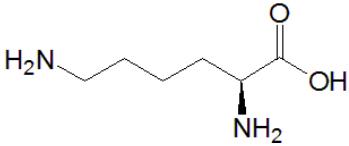
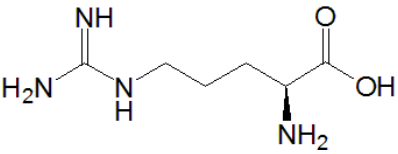


Figure 6.1. left: scheme of unit cell of HA (from ref 12), right: SEM image of the HA powder

The linker molecules used and their chemical structures are shown in table 6.1. Samples were always prepared as follows. First a 38 mM solution of L-amino acid in D₂O was prepared and put in a vial with a magnetic stirrer. Then, 0.1 g HA powder per 1 ml of D₂O was added. The resulting suspension was stirred during 2.5 h. Subsequently, 500 µl of the suspension was transferred to an NMR tube for measurement. This milky suspension remained stable for over 24h, and thus also during the NMR experiments. As L-amino acids were used at all times, the stereochemistry will no longer be explicitly mentioned hereafter.

Table 6.1. Chemical structures of the linker molecules used in this study, dissociation constants (pKa values) of ionisable groups on the linker molecules and calculated isoelectric points (IEP).

	pKa ₁ (C _α -COOH)	pKa ₂ (α-C-NH ₃ ⁺)	pKa ₃ (NH ₃ ⁺)	IEP
L-lysine (lys) 	2.2	9.2	10.7	9.7
L-Arginine (arg) 	2.0	9.0	12.1	10.8

6.3 NMR study of L-lysine with hydroxyapatite in suspension

The 1D ¹H reference spectrum of L-lysine in D₂O is shown in figure 6.2. In this reference spectrum, 5 distinct resonances are observed that can be assigned to the different non-exchangeable protons. While these 5

resonances appear at identical positions in the NMR spectrum of the lysine-HA suspension (figure 6.3), they are all broadened and devoid of fine

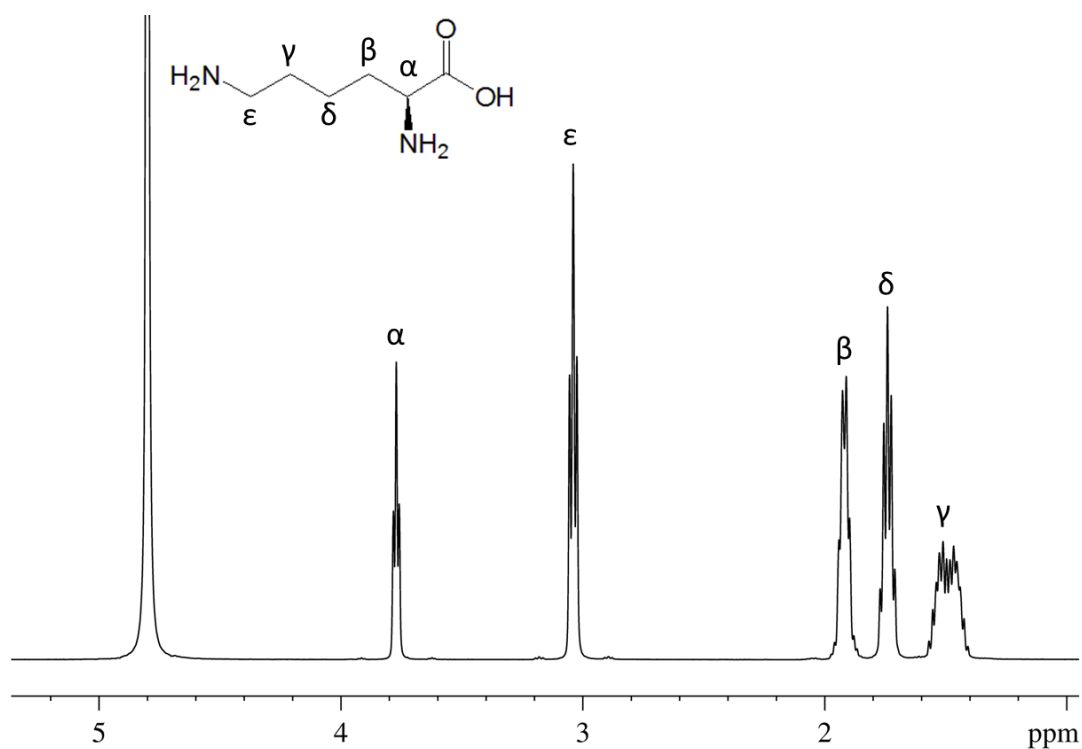


Figure 6.2. 1D ^1H spectrum of a reference sample of L-lysine in D_2O at 298.2 K

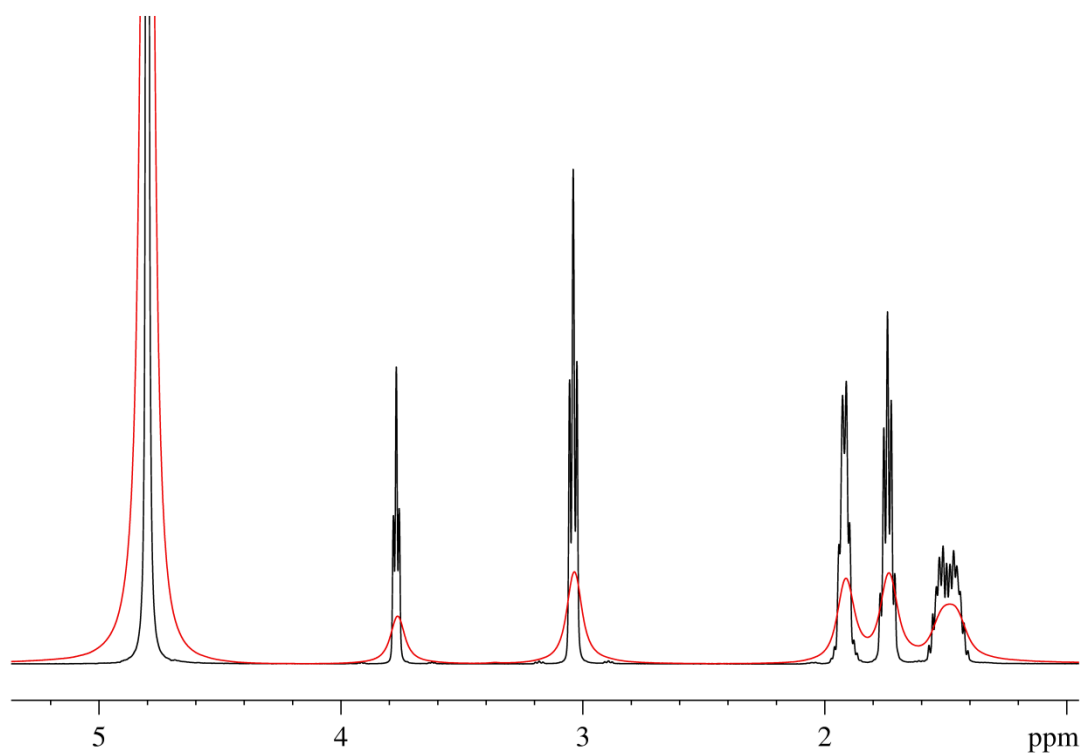


Figure 6.3. Comparison of the 1D ^1H spectra of the hydroxyapatite suspension stirred with lysine for 2.5 h (red) and of the lysine reference sample (black)

structure. It is known that this broadening can be a result of slow tumbling of a bound ligand, resulting in a fast T_2 relaxation (cfr. chapter 2). But in this sample however, the presence of much larger, micrometer sized HA particles in the solution causing variations in magnetic susceptibility across the sample should also be considered as a possible source of line-broadening (vide infra, 6.4).¹⁴

One means to establish whether broadening is due to a surface interaction or due to magnetic susceptibility effects is to assess the line broadening of resonances of a non-interacting ‘control’ species. Here, tetraethyl ammonium chloride (TEACl) was added to the dispersion. In the 1D ^1H spectrum (figure 6.4) it is visible that all resonances are broadened, including those of the control species. Therefore, broadening cannot by itself be seen as a proof of interaction with the surface but must at least be partially due to magnetic susceptibility effects. In this case, an alternative

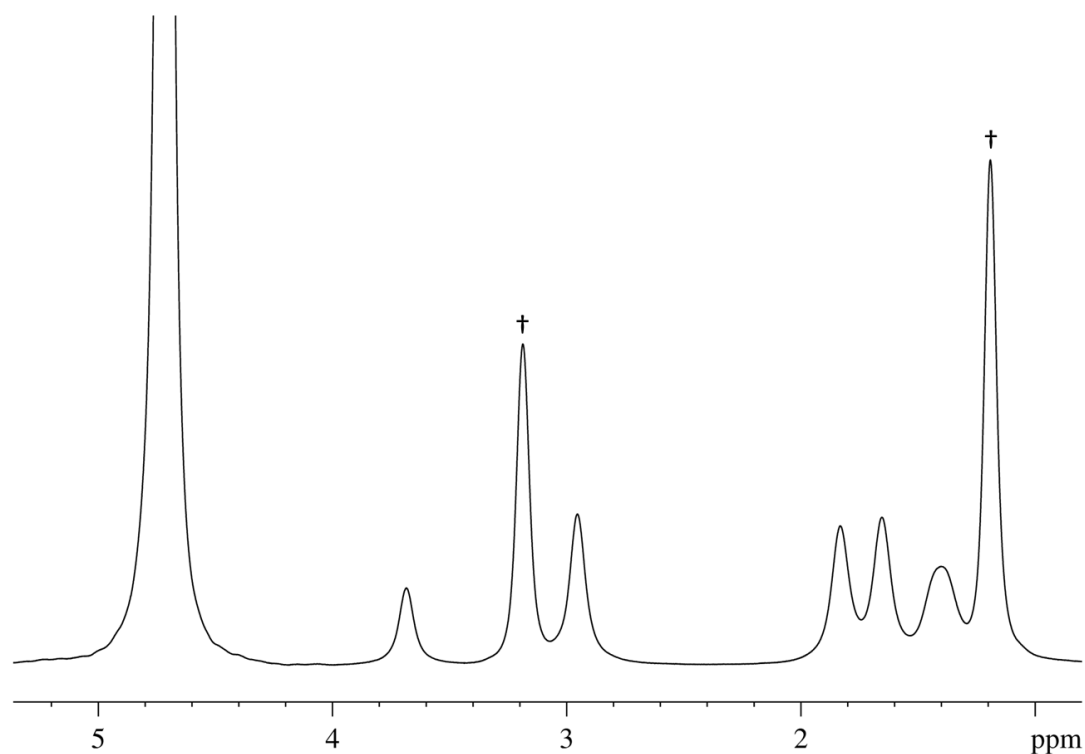


Figure 6.2. 1D ^1H spectrum of the hydroxyapatite suspension stirred with lysine for 18h with TEACl (resonances marked with †) added afterwards as control species

approach to offer proof of interaction is afforded by recording a 2D NOESY spectrum (figure 6.5). In the 2D NOESY spectrum, cross-like cross peaks are observed between the CH₂ and CH₃ resonances of TEACl that come from the superimposition of weak positive NOEs typical for small molecules and ZQC artefacts (Chapter 2.2). This confirms the fact that TEACl is not interacting with the HA powder but is free in solution. The different lysine resonances however, are connected by large negative NOEs. In addition, they are of rather uniform intensity, indicating the action of spin diffusion as can be expected to be occurring from large particle dynamics. Both observations indicate that lysine interacts with the hydroxyapatite surface, which is an independent confirmation of what was reported previously from IR studies that are not discussed further here.¹

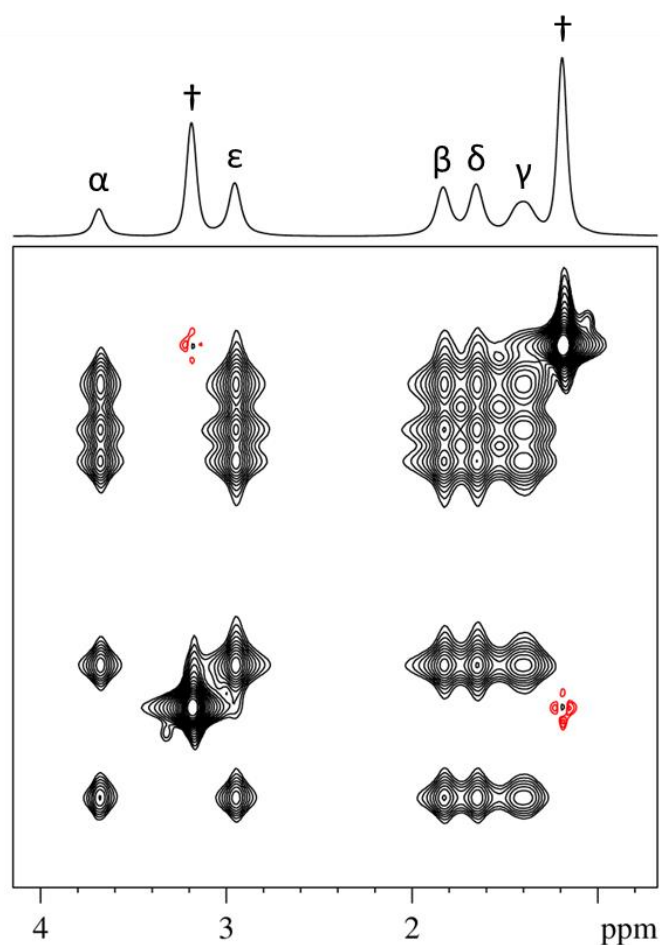


Figure 6.3. 2D NOESY spectrum of a suspension of L-lysine-hydroxyapatite with TEACl added as a control species

By consecutively precipitating and suspending the lysine-hydroxyapatite suspension several times, excess lysine was removed but a stable solution was still obtained. This solution was then used to determine an upper limit of the amount of lysine that is actually interacting with the hydroxyapatite surface by recording an ERETIC measurement. The amount of lysine adsorbed on the HA surface was subsequently calculated as being $1.5 \cdot 10^{-5}$ mol/g, which is very similar to the value obtained in a thermogravimetric analysis ($1.4 \cdot 10^{-5}$ mol/g).

6.4 high resolution- Magic Angle Spinning (hr-MAS)

As mentioned before, a variation of the magnetic susceptibility in a sample with large solid particles can lead to significant line broadening. The principle of this can be explained as follows.

When a sample in solution is placed in a homogeneous magnetic field H_0 , it acquires a magnetization M that is:

$$M = \chi H_0$$

With χ the magnetic susceptibility which is uniform across the sample. The magnetic induction B_0 that is felt within the sample is therefore given by:

$$B_0 = \mu_0 H_0 + \mu_0 M = \mu_0 (1 + \chi) H_0$$

With μ_0 the permeability of free space.

In the case of a sample with large solid particles in it however, the magnetic susceptibility is not necessarily uniform across the sample and the B_0 field might no longer be homogeneous:

$$B_0^{solid} = (1 + \chi^{solid}) H_0$$

$$B_0^{liquid} = (1 + \chi^{liquid})H_0$$

This inhomogeneity will in his turn lead to significant broadening of the NMR signals as observed in the above results. This line broadening can be treated as a dipolar interaction between a sphere of magnetization M and the magnetic moment m of the spins in its surrounding at a distance r which can be represented by:¹⁵

$$E(r) = \frac{\mu_0}{4\pi} \frac{Mm}{r} (1 - 3\cos^2\theta)$$

Importantly, the geometric factor $(1 - 3\cos^2\theta)$ is zero when θ is 54.7° , i.e. at the magic angle. At this angle, the dipolar interaction vanishes. However, the spins in a liquid sample will all have a different θ value which is time-dependant due to the rotational dynamics of the molecules in

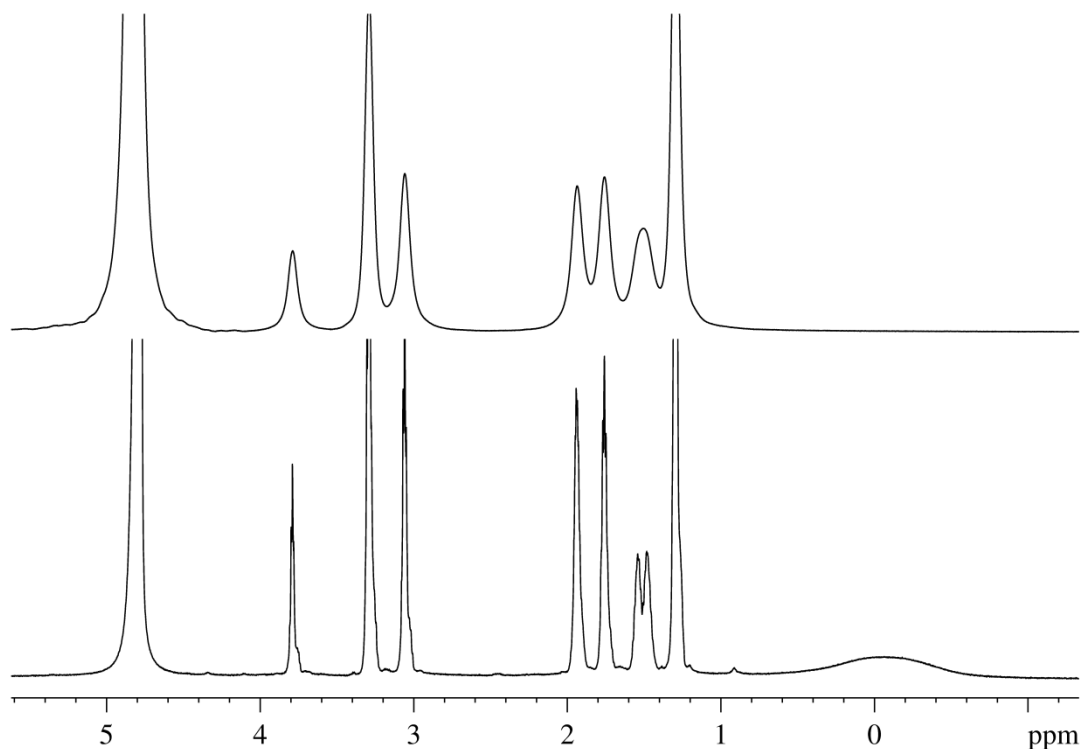


Figure 6.4. 1D ^1H spectrum of a suspension of lysine-hydroxyapatite with TEACl as ‘control’ species, in a 5 mm normal acquisition at 500 MHz (top) and in a rotor spinning at 6000 Hz over the magic angle at 700 MHz (bottom)

solution. By rotating the sample around an axis oriented at 54.7° with respect to the B_0 field any vector joining M and a particular magnetic moment m can be decomposed in two orthogonal contributions. One lies along the magic angle spinning axis and is invariant towards the sample spinning, while the other will be spinning in a plane perpendicular to this axis. On average, the latter will average to zero as it rapidly samples 360° . Therefore the only remaining contribution will behave, on average as if it were along the magic angle, where the geometric factor is zero. As such, hr-MAS is a suitable technique to remove the effect of magnetic susceptibility inhomogeneities.

Practically, we put 70 μl of the suspension in a rotor and measured the hr-MAS measurements at 700 MHz in a 4mm high-resolution magic angle spinning probe. When comparing the spectrum that was recorded while rotating the sample along the magic angle at 6000 Hz with the regular spectrum (figure 6.5), all the resonances are clearly sharpened. It is not clear whether there is broadening left that can be said to be from interaction but since this was already shown by 2D NOESY, this is not so important to establish. Interestingly however, a very broad resonance appears around 0 ppm in the hr-MAS spectrum. This resonance is probably the OH-resonance from the hydroxyapatite powder¹³ that is at the surface of this powder and becomes visible at this high spinning rate. To confirm that this resonance indeed belongs to the hydroxyapatite powder, a reference hr-MAS spectrum was recorded from a 'suspension' of only HA powder. HA does not stay in suspension but given the small volume needed in the rotor is fully enclosed by the detection coil and the fact that we would be spinning the sample anyway, we just made sure that enough powder was put inside the rotor to be able to observe the OH resonance. The resulting spectrum is shown in figure 6.7.

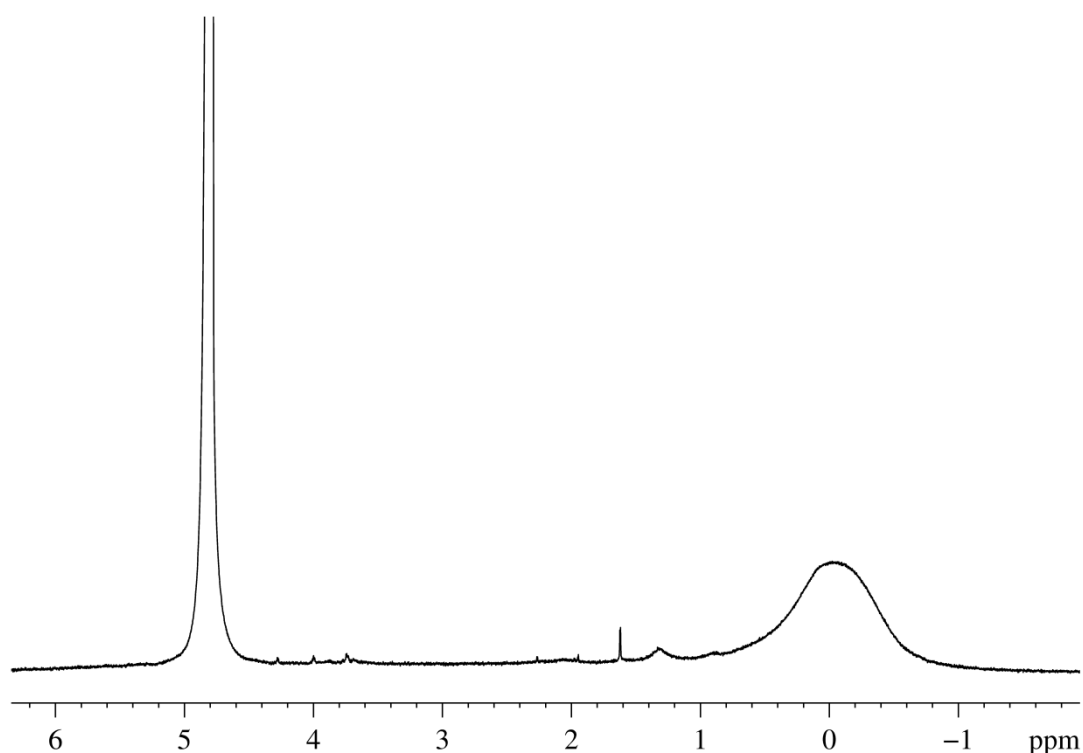


Figure 6.5. hr-MAS spectrum at a spinning rate of 6000 Hz of a reference sample of the hydroxyapatite powder in D₂O

Indeed, in the hr-MAS spectrum of the hydroxyapatite powder as such, the same resonance appears around 0 ppm, confirming the assignment of this resonance to the OH of hydroxyapatite in our lysine-hydroxyapatite-TEACl sample. The observation of this OH resonance brings along interesting possibilities to further investigate the interaction of lysine with the surface, which is explored in the next paragraphs.

6.5 Saturation Transfer Difference (STD) NMR spectroscopy

STD NMR spectroscopy has been used over the last few decades to study ligand binding to bio macromolecules, such as proteins.^{16,17} It can be used to study ligands that exchange between the bound and free state. The experiment involves the selective saturation of a resonance from one or more protons of the protein. This saturation will spread through the entire protein via spin diffusion eventually also reaching the ligand present in the

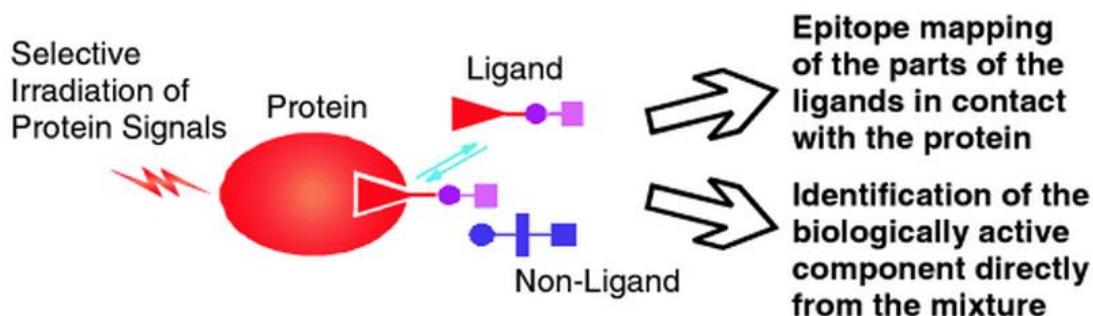


Figure 6.6. Representation of the STD experiment (adapted from ref 16).

binding site (figure 6.8). The rate at which the saturation is transferred to the ligand is determined by the dissociation rate k_{off} and the protein-ligand complexation constant K_d . Even though the ligand may not be observable when bound, the fast exchange dynamics causes a release of the ligand and an exchange averaging of the various spectral properties such as chemical shift and line-width. By using an excess of free ligand the ligand becomes observable since the spectral properties become weighted towards those of the free state. Due to the saturation transfer however, the ligand resonance intensity will have been decreased in this so-called ‘on-resonance’ experiment to an intensity $I_{\text{sat,on}}$. Using an ‘off-resonance’ experiment, where the saturation is applied outside the frequency range of protein and ligand resonances alike, a reference spectrum with intensities $I_{\text{sat,off}}$, is obtained. The difference spectrum of both will show non-zero intensities only for resonances of the protein itself and of binding ligands, $I_{\text{STD}} = (I_{\text{sat,off}} - I_{\text{sat,on}})$. Also, as is clearly shown in figure 6.8, protons in close contact with the protein will receive more saturation than protons that are more distant. As such, the relative I_{STD} values can provide information on how a ligand is bound to a protein surface.

In our case, the presence of the OH^- resonance of hydroxyapatite in the hr-MAS experiment provided an ideal opportunity to explore possibilities to map the interaction of lysine with the hydroxyapatite via an STD measurement. For the on-resonance experiment, a selective irradiation was applied at 0 ppm, which corresponds with the position of the OH resonance. The off-resonance irradiation was applied at -50 ppm, a value that is far from the frequency range of our resonances. The final STD experiments under hr-MAS conditions are shown in figure 6.9. First, a reference hr-MAS spectrum of the lysine-hydroxyapatite-TEACl suspension is shown in figure 6.9A. Then, two STD measurements are shown, one experiment performed on a reference sample of lysine and TEACl but without hydroxyapatite powder (figure 6.9 B) to check whether the chosen irradiation frequency is

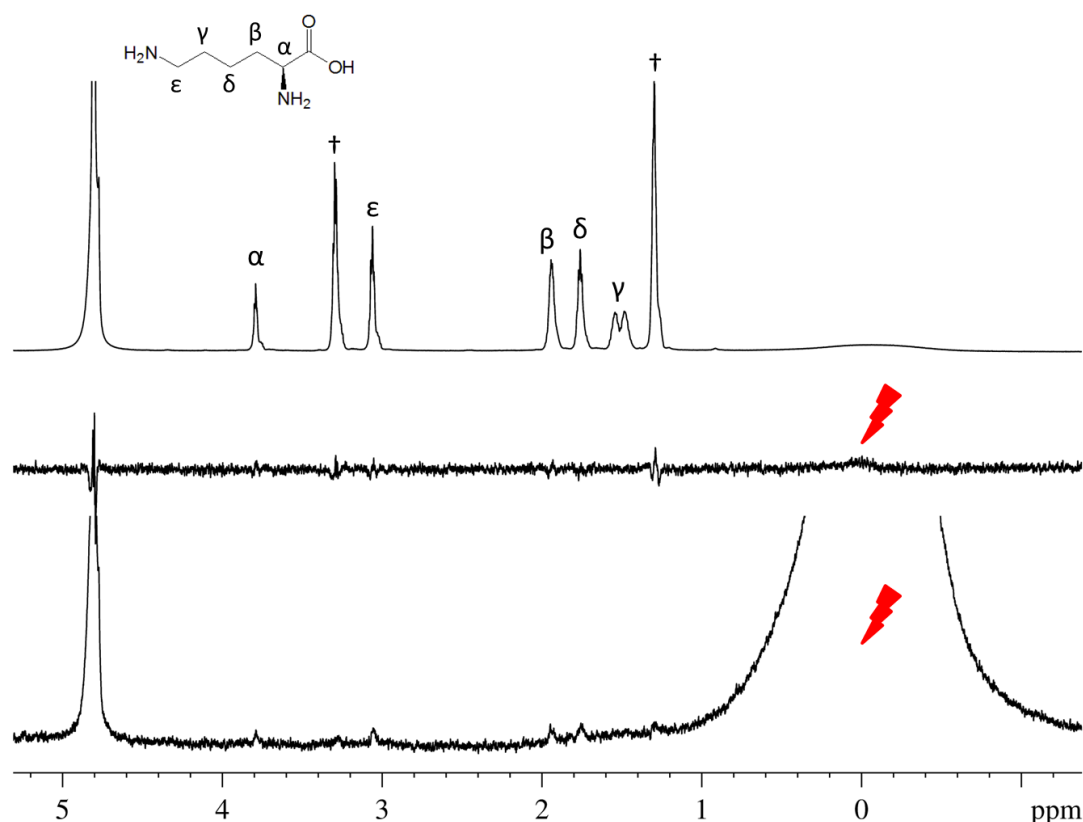


Figure 6.7. 1D ^1H spectrum of a suspension of lysine-hydroxyapatite with TEACl as ‘control’ species, in a rotor spinning at 6000 Hz over the magic angle at 700 MHz (A) STD spectrum of the same sample under the same hr-MAS conditions (C) STD spectrum of a lysine and TEACl reference suspension void of HA powder under the same hr-MAS conditions (B)

selective. This spectrum should not show any signals from the lysine and the TEACl since no resonance is present at 0 ppm. Indeed, in the spectrum, no signals are observed, only minor subtraction artefacts, indicating that the experimental set-up is adequate. Finally, the same STD experiment was performed on the lysine-hydroxyapatite-TEACl suspension (figure 6.9 C). In this spectrum, small but nevertheless clear signals are visible from the different lysine resonances, which means that these signals have interactions with the –OH protons of hydroxyapatite. It should be noted that some very weak signals are also visible from the TEACl resonances. However, it was difficult to establish if these were real or rather subtraction artefacts. As they are, in comparison, much weaker than those of the lysine and we did not expect any signal since it is known that TEACl does not interact with the hydroxyapatite (*vide supra*), we believe these should not be seen as indicative of a significant interaction. Also, given the very weak signal intensities, it was not possible to map the binding direction of lysine on the HA surface. More optimization of the STD experiment could provide even more insight but this was unfortunately beyond the time-frame of this PhD.

6.6 Conclusions

The NMR toolbox developed for nanocrystals was successfully implemented and expanded for the study of HA microparticles stabilized by short amino-acid linker molecules. The interaction of L-lysine with the hydroxyapatite was demonstrated using 2D NOESY NMR and the amount of interacting lysine was calculated. For samples using L-Arginine instead of L-lysine to establish the stabilization of the hydroxyapatite powder, the same set of measurements was performed and the behaviour and main results were found to be identical (data not show).

Furthermore, the possibility of performing hr-MAS measurements on this type of suspensions was illustrated and broadening of the signals could in part be attributed to magnetic susceptibility effects. First steps were made towards the implementation of STD measurements on these dynamically stabilized microparticles. Promising results were obtained and further investigation should provide more insight.

6.7 References

- (1) Ozhukil Kollath, V.; Van den Broeck, F.; Fehér, K.; Martins, J. C.; Luyten, J.; Traina, K.; Mullens, S.; Cloots, R. *Chemistry – A European Journal* **2015**, *21*, 10497.
- (2) Grenha, A. *Journal of Pharmacy And Bioallied Sciences* **2012**, *4*, 95.
- (3) Giudice, E. L.; Campbell, J. D. *Advanced Drug Delivery Reviews* **2006**, *58*, 68.
- (4) Lee, H. J. *Arch. Pharm. Res.* **2002**, *25*, 572.
- (5) des Rieux, A.; Fievez, V.; Garinot, M.; Schneider, Y.-J.; Préat, V. *Journal of Controlled Release* **2006**, *116*, 1.
- (6) Renukuntla, J.; Vadlapudi, A. D.; Patel, A.; Boddu, S. H. S.; Mitra, A. K. *Int. J. Pharm.* **2013**, *447*, 75.
- (7) Thanki, K.; Gangwal, R. P.; Sangamwar, A. T.; Jain, S. *Journal of Controlled Release* **2013**, *170*, 15.
- (8) Kovacsovicbankowski, M.; Clark, K.; Benacerraf, B.; Rock, K. L. *Proc. Natl. Acad. Sci. U. S. A.* **1993**, *90*, 4942.
- (9) Houde, M.; Bertholet, S.; Gagnon, E.; Brunet, S.; Goyette, G.; Laplante, A.; Princiotta, M. F.; Thibault, P.; Sacks, D.; Desjardins, M. *Nature* **2003**, *425*, 402.
- (10) Wassell, D. T. H.; Hall, R. C.; Embery, G. *Biomaterials* **1995**, *16*, 697.
- (11) Hens, Z.; Martins, J. C. *Chem. Mat.* **2013**, *25*, 1211.
- (12) Vallet-Regi, M.; Arcos, D. *J. Mater. Chem.* **2005**, *15*, 1509.
- (13) Jäger, C.; Welzel, T.; Meyer-Zaika, W.; Epple, M. *Magnetic Resonance in Chemistry* **2006**, *44*, 573.
- (14) Hyanes, W. M. *CRC Handbook of Chemistry and Physics, 91st edition*; CRC Press: Boca Raton, FL, 2010.
- (15) Ippens, G.; Bourdonneau, M.; Dhalluin, C.; Warrass, R.; Richert, T.; Seetharaman, C.; Boutillon, C.; Piotto, M. *Current Organic Chemistry* **1999**, *3*, 147.
- (16) Meyer, B.; Peters, T. *Angewandte Chemie International Edition* **2003**, *42*, 864.
- (17) Szczygiel, A.; Timmermans, L.; Fritzing, B.; Martins, J. C. *J. Am. Chem. Soc.* **2009**, *131*, 17756.

GENERAL CONCLUSIONS

For this PhD research, the starting point was the existing NMR toolbox that was developed for the study of nanoparticles by the PCN and NMR research group.¹ Using this toolbox, some specific research questions were investigated and solved. At the same time, these presented opportunities to extend the NMR toolbox itself.

As shown in chapter 3, the investigation into the stabilization procedure of Aluminium doped Zinc Oxide (AZO) nanocrystals was a first research question that we were confronted with. Here, both oleic acid and oleylamine are added during synthesis to provide colloidal stability to the NCs. However, it was not clear why both a fatty acid and an amine were needed and whether they both ended up in the NC's ligand layer or not. Since the spectral fingerprint of oleic acid (OLAc) and oleylamine (OLAm) on the NC surface cannot be distinguished using solely 1D ¹H NMR, stearic acid was used as an alternative fatty acid. From this experiment, it could be concluded that the amine is washed away during work-up, while the fatty acid stabilizes the AZO NP by forming a ligand layer. Also, the dynamic behavior of the OLAc on the surface was studied. It was concluded that OLAc is tightly bound to the surface and exhibits a two-step exchange process with free OLAc when additional OLAc is added to the dispersion. This work was published in RSC Advances.²

In chapter 4, a study of Copper Indium Sulfide NPs is reported. This project was conducted throughout the four years of my PhD, which gives an idea on the difficulties involved in obtaining a complete characterization. The CIS NPs are stabilized with oleylamine ligands, but preferably, these ligands should be exchanged to others afterwards. However, in order to design a proper exchange experiment, the dynamic behavior of the OLAm ligands on the CIS surface had to be understood. From a first characterization, we concluded that OLAm is tightly bound to the surface

and does not exchange at room temperature. This was quite unexpected since OLAm is usually referred to as an L-type ligand that has a dynamic ligand behavior. By monitoring the dispersions *in-situ* with NMR at high temperatures the dynamic behavior of OLAm could be revealed. Since temperatures above 100°C were required but never applied before in house, the possibilities and limitations of for achieving these temperatures and obtaining useful data on the NMR spectrometers were first explored. The first measurements were therefor conducted at the NMR facilities of DOW Terneuzen, where high temperature measurements are already more routine. After gaining more expertise, one of the 500 MHz spectrometers at UGent (Nestor) was set-up for high-temperature measurements up to 150°C. Applied to the system of interest, it was concluded that OLAm capping ligands on CIS NPs are L-type ligands that are tightly bound to the CIS NP surface. They do not exhibit a dynamic adsorption/desorption behavior at room temperature but desorb at higher temperatures without the involvement of other proton donors. In order to further confirm this conclusion, also a known X-type ligand was studied, namely octadecylphosphonic acid (ODPAc) capping ligands on CdSe NPs. Since this is an X-type ligand, we proposed that the difference with our L-type ligand should be that ODPAc will not desorb at higher temperature when no proton donors are available. Indeed, no desorption was observed at temperatures up to 130°C. Importantly, with these experiments, we established a new way to distinguish X- and L-type ligands, which represents an extension of the NMR Toolbox and could be helpful for future research.

After establishing the dynamic behavior of OLAm at the CIS surface, an exchange procedure to replace this L-type ligand was set-up and tested. This exchange with dodecylthiol proved succesful. However, exchange with nonanoic acid and undecenoic acid, both X-type ligands was also

demonstrated. This was unexpected since L- to X-type exchange is in principle not possible. By combining the NMR data with those from Rutherford backscattering spectroscopy we could conclude that this exchange does not involve OLAm but is due to the presence of X-type species on the CIS NP surface, such as OH⁻ or acetylacetonate that are used during synthesis but too small to be detected by NMR when tightly bound to the surface. The presence of these contaminants on the surface, we believed, should be avoidable by using pure grade octadecylamine instead of the technical grade oleylamine. Thus, the synthesis was repeated with ODAm and after a basic characterization and heating experiment that showed that ODAm is also bound to the CIS NP surface as an L-type ligand, two new exchange experiments were set-up. Indeed, the exchange to phenylethanethiol, an L-type ligand, was successful while this time the exchange to oleic acid, an X-type ligand, was not. This proved that the amine bound to the CIS NP surface is a tightly bound L-type ligand and exchange is only possible to other L-type ligands. Simultaneously it indicates that when X-type ligand exchange can be observed, the involvement of X-type species at the NC surface should be considered. In this respect, the use of technical grade OLAm should be avoided since this results in the presence of other small and therefore undetectable X-type species on the surface that are not desirable and result in a different exchange behavior. This work was published in *Chemistry of Materials*.³

In chapter 5, the study of Hafnium Oxide NCs capped with oleic acid ligands was presented. This study was conducted at the end of my PhD and while similar to the research on AZO NPs at the start of my PhD (chapter 3) since here also, metal oxides are studied that are synthesized using an amine and fatty acid. However, additional emphasis was placed on elucidating the molecular events involved in bringing about the stabilization, allowing a

much more in depth view of the processes involved that was enabled by the experience gained in studying such systems over the period of my PhD research. Thus, we focussed on why the amine is needed for the stabilization procedure when it can clearly be washed away afterwards. First, the HfO₂ NCs stabilized using dodecanoic acid and oleylamine were fully characterized after one and five consecutive purification steps. The latter confirmed that the amine is fully washed away after purification. After this confirmation of our previous findings on AZO systems presented in chapter 3, the binding mode of the fatty acid on the HfO₂ surface was further investigated. Therefore, the synthesis was repeated using oleylamine and oleic acid as capping ligands since the latter is more conveniently followed using 1D ¹H NMR. First, it was concluded that OLAc is tightly bound to the HfO₂ surface and exhibits a two-step exchange mechanism when additional ligand is added. However, we were also interested in telling whether the OLAc was bound as a carboxylic acid or as a carboxylate. To determine this, a procedure was followed that was already used before in our research group, using deuterated oleic acid-d1.⁴ When this OLAc-d1 is added to a water-free OLAc capped HfO₂ NC dispersion, the ratio of carboxylic protons versus the other resonances of OLAc is different for both cases. If OLAc is bound as a carboxylate, it will be desorbed after exchanging a deuterium and almost no carboxylic protons will be present. If however OLAc is bound as a carboxylic acid, it will be desorbed with its own carboxylic proton on it, resulting in a higher [COOH]/[OLAc] resonance ratio. After comparing the experimentally obtained ratio to the theoretically calculated possibilities for both binding modes, we concluded that there are as many protons present on the surface as bound OLAc. However, the IR data contained a carboxylate absorption and no carboxylic acid absorption, indicating that the oleic acid is bound as a carboxylate. Combining these results, we concluded that oleic acid dissociates at the NC surface,

effectively binding the carboxylate form and H^+ at the surface. The question remained why the amine that is washed away after stabilization is needed during synthesis. To answer this question, an experiment was set-up where the stabilization procedure of the HfO_2 NPs was monitored *in-situ* with NMR using 10-undecenoic acid (UDAc) and oleylamine. Use of the latter generates a distinct alkene 1H fingerprint that is resolved from that of OLAm, allowing both species to be monitored. First, the UDAc was added and it was shown that the UDAc was now free in suspension and did not bind to the HfO_2 surface. After adding OLAm however, the spectra showed that UDAc was now bound to the NP surface and OLAm was entangled in the ligand shell. The amine can be easily washed away afterwards. In conclusion, this research revealed some fascinating new insight in the mechanisms that take place at the HfO_2 surface. First, the amine merely acts as a base that captures a proton from the carboxylic acid. The resulting carboxylate replaces a Cl^- at the surface that is then captured by the ammonium compound and washed away. This leaves a HfO_2 surface that is covered with H^+ and carboxylate ligands. These results were published in the Journal of the American Society⁵ and are proposed to be applicable to other metal oxide NPs, such as for instance the AZO NPs in chapter 3.

Finally, in chapter 6, the possibilities to extend the application range of the NMR toolbox – beyond semi-conductor or metaloxide nanocrystals was explored. Here, sub- μm -sized hydroxyapatite powder used as an inorganic carrier for antigens in the body was involved. Previous study showed an improvement of the antigen loading when the HA powder was first covered with amino acid linker molecules, such as lysine and arginine. No characterization of this capping of amino acids on the HA powder was however present and we aimed at providing insight in this matter by applying and modifying the existing NMR experiments. First, with a basic

characterization, it was shown that the amino acid was indeed bound to the HA surface. Then, using hr-MAS, a technique that was not considered for this type of research before, it was possible to reveal the ^1H resonance from the OH^- groups present inside the HA lattice. With this OH resonance present, a Saturation Transfer Difference experiment appeared an interesting NMR technique to attempt here. STD experiments are used when studying the ligand binding on large bio macromolecules but were never yet applied on interactions between ligands and inorganic particles. In our first attempts, the STD experiments were positive for interaction of lysine with the HA surface, however no information could be obtained about the orientation of the binding or ligand. Having been performed at the end of the PhD project, more optimization of the technique is required. We could however conclude that lysine is present on the HA surface, while introducing new extensions of the NMR toolbox for the research of sub- μm particles. Part of this work was published in Chemistry, A European Journal.⁶

As a final conclusion, it can be said that during this PhD work, we did not only assist in the understanding and characterization of different NC-ligand interactions but in doing so, we did also expand the existing NMR toolbox with new types of experiments. The heating experiments that are shown in chapter 4, are now conducted more regularly to distinguish different types of ligands. Also, the hr-MAS and STD-experiments shown in chapter 6, provide new possibilities in studying both nano- and micro-sized particles.

References

- (1) Hens, Z.; Martins, J. C. *Chem. Mat.* **2013**, *25*, 1211.
- (2) Damm, H.; Kelchtermans, A.; Bertha, A.; Van den Broeck, F.; Elen, K.; Martins, J. C.; Carleer, R.; D'Haen, J.; De Dobbelaere, C.; Hadermann, J.; Hardy, A.; Van Bael, M. K. *RSC Advances* **2013**, *3*, 23745.

General conclusions

- (3) Dierick, R.; Van den Broeck, F.; De Nolf, K.; Zhao, Q.; Vantomme, A.; Martins, J. C.; Hens, Z. *Chem. Mat.* **2014**, *26*, 5950.
- (4) Fritzinger, B.; Capek, R. K.; Lambert, K.; Martins, J. C.; Hens, Z. *J. Am. Chem. Soc.* **2010**, *132*, 10195.
- (5) De Roo, J.; Van den Broeck, F.; De Keukeleere, K.; Martins, J. C.; Van Driessche, I.; Hens, Z. *J. Am. Chem. Soc.* **2014**, *136*, 9650.
- (6) Ozhukil Kollath, V.; Van den Broeck, F.; Fehér, K.; Martins, J. C.; Luyten, J.; Traina, K.; Mullens, S.; Cloots, R. *Chemistry – A European Journal* **2015**, *21*, 10497.
- (7) De Roo, J.; Justo, Y.; De Keukeleere, K.; Van den Broeck, F.; Martins, J. C.; Van Driessche, I.; Hens, Z. *Angewandte Chemie International Edition* **2015**, *54*, 6488.

***NEDERLANDSTALIGE
SAMENVATTING***

Het uitgangspunt van het doctoraatsonderzoek gepresenteerd in deze thesis is de bestaande NMR *toolbox* die ontwikkeld werd voor de studie van nanodeeltjes door de PCN and NMR onderzoeksgroepen. Met deze *toolbox* als startpunt zijn er enkele specifieke onderzoeksvragen beantwoord. Deze onderzoeksvragen stelden terzelfdertijd ook nieuwe uitdagingen en mogelijkheden om de NMR *toolbox* verder uit te breiden.

In hoofdstuk 3 worden de resultaten van het onderzoek naar de stabilisatie van Aluminium gedopeerde Zink Oxide (AZO) nanokristallen gepresenteerd. Bij de synthese van deze nanokristallen worden namelijk zowel oleïnezuur als oleylamine toegevoegd om een stabiele suspensie te verkrijgen. Het was echter niet duidelijk waarom zowel een vetzuur als een amine nodig waren en ofdat beide dan finaal ook in de ligandschil eindigden. Na verschillende experimenten werd geconcludeerd dat enkel het oleïnezuur eindigt in de ligandschil terwijl het amine weggewassen wordt tijdens de opzuivering. Verder werd ook het dynamische gedrag van het oleïnezuur aan het AZO oppervlak in kaart gebracht.

In hoofdstuk 4 worden de resultaten van het onderzoek naar Koper Indium Sulfide (CIS) nanokristallen gepresenteerd. Deze worden tijdens de synthese gestabiliseerd met oleylamine liganden dewelke dan nadien uitgewisseld moeten worden voor andere, kortere liganden. Het ontwerpen van een goede uitwisselingsprocedure vereist echter een complete kennis van het dynamische gedrag van de oleylamine liganden aan het CIS oppervlak. Om dit gedrag in kaart te brengen werd een nieuw type experiment aan de NMR *toolbox* toegevoegd, namelijk het *in-situ* opwarmen tot 150°C van de dispersie in de magneet. Uit deze hoge temperatuur metingen kon besloten worden dat het oleylamine aan het CIS oppervlak een sterk gebonden L-type ligand is. Het vertoont namelijk geen adsorptie en desorptie bij kamertemperatuur maar desorbeert wel bij hogere temperaturen zonder de

aanwezigheid van een protondonor. Ook het gedrag van een gekend X-type ligand werd nagegaan, namelijk octadecylfosfonaatzuur liganden gebonden aan een Cadmium Selenide nanokristal. Deze X-type liganden desorbeerden inderdaad niet bij hogere temperaturen als er geen protondonoren aanwezig waren. Dit nieuwe type van experiment is dus van groot belang aangezien het een manier biedt om X- en L-type liganden van elkaar te onderscheiden.

Met het dynamische gedrag van oleylamine aan het CIS oppervlak in gedachte werd een uitwisselingsprocedure uitgedacht en getest. Zoals verwacht was de uitwisseling naar een ander L-type ligand, dodecylthiol, succesvol. Maar verrassend genoeg was ook de uitwisseling naar X-type liganden mogelijk. In principe is een L- naar X-type uitwisseling echter niet mogelijk. Na extra onderzoek en in combinatie met resultaten van Rutherford Backscattering Spectroscopie kon besloten worden dat er naast oleylamine ook kleine X-type groepen aanwezig zijn aan het CIS oppervlak, zoals bijvoorbeeld OH^- of acetylacetaat, die gebruikt worden tijdens de synthese. Deze kunnen echter niet door NMR gevisualiseerd worden wegens te dicht en sterk gebonden aan het oppervlak. Aangezien deze onzuiverheden ongewenst zijn en de zuivere uitwisselingsprocedures verstoren werd een nieuwe synthese uitgevoerd met zuivere octadecylamine in plaats van de oleylamine die slechts beschikbaar is in technische kwaliteit. Octadecylamine vertoonde hetzelfde gedrag bij de hoge temperatuur metingen en is dus ook een sterk gebonden L-type ligand. En bovendien gaven de uitwisselingsexperimenten nu ook de verwachte resultaten, namelijk een L- naar L-type uitwisseling en geen L-naar X-type. Het gebruik van oleylamine van technische kwaliteit zou dus beter vermeden worden bij de synthese van nanokristallen.

In hoofdstuk 5 worden de resultaten van het onderzoek naar Hafnium Oxide nanokristallen met oleïnezuur liganden gepresenteerd. Deze metaaloxide nanokristallen worden net als de Aluminium Zink Oxide nanokristallen gesynthetiseerd met zowel oleïnezuur als oleylamine. Voor dit onderzoek werd de nadruk echter gelegd op de oppervlakte chemie en de moleculaire interacties die samen gaan met de stabilisatie, dit om zo een veel diepgaandere kijk te bieden op de betrokken processen. Na een standaard karakterisatie en bevestiging van het wegwassen van het amine na stabilisatie werd de rol van het vetzuur verder onderzocht. Om te onderzoeken of het oleïnezuur gebonden is als een carbonzuur of als een carboxylaat werd er een procedure gevolgd met gedeutereerd oleïnezuur-d1. Als dit oleïnezuur-d1 wordt toegevoegd aan een water-vrije dispersie van HfO₂ nanokristallen gestabiliseerd met oleïnezuur kan men het verschil tussen beide bindingsvormen afleiden uit de verhouding van de carbonzure protonen en de andere oleïnezuur resonanties. Beide bindingsmodes zullen hier namelijk een verschillend resultaat geven. Uit de resultaten kon besloten worden dat er evenveel protonen gebonden zijn aan het oppervlak als dat er oleïnezuur moleculen gebonden zijn. Uit de IR data bleek echter dat er een carboxylaat op het oppervlak gebonden is. Met de combinatie van deze experimenten kan dus besloten worden dat er zowel een carboxylaat als een proton bindt aan het oppervlak maar wel op aparte bindingsplaatsen. Nu restte nog de rol van het amine te onderzoeken. Hiervoor werd er een experiment uitgedacht waarbij de stabilisatie van de HfO₂ nanokristallen *in-situ* gevolgd werd. Voor dit experiment werden oleylamine en 10-undecenaatzuur gebruikt omdat beide duidelijk onderscheidbare alkeen ¹H resonanties hebben en dus apart kunnen onderzocht worden. Uit dit experiment kon duidelijk worden afgeleid dat het vetzuur pas aan het oppervlak bindt na toevoegen van het amine. Uit al deze resultaten werd besloten dat het amine zich gedraagt als een base die een proton van het

vetzuur afsplitst. Daarna bindt het gevormde carboxylaat aan het oppervlak en vervangt daar een Cl^- dat wordt opgevangen door het ammonium en tesamen wordt weggewassen. Hierdoor blijft er dus een oppervlak over met gebonden carboxylaat liganden en protonen.

In hoofdstuk 6 worden de mogelijkheden onderzocht om de toepasbaarheid van de NMR *toolbox* verder uit te breiden. In dit onderzoek werd hydroxyapatiet poeder in de sub-micrometer grootteorde onderzocht. Dit poeder wordt ingezet als inorganische drager voor antigenen in het lichaam. Eerdere studies toonden aan dat er een hogere antigenen lading mogelijk werd als het hydroxyapatiet eerst werd gebonden met aminozuren, zoals lysine of arginine. Deze stabilisatie kon tot dusver echter niet gekarakteriseerd worden en dit onderzoek trachtte dan ook om hier nieuwe inzichten te bieden. Eerst werd een standaard karakterisatie uitgevoerd waarmee kon worden aangetoond dat het aminozuur gebonden was aan het hydroxyapatiet oppervlak. Daarna werd met behulp van hr-MAS de ^1H resonantie van de OH^- groepen aanwezig in het hydroxyapatiet kristalrooster aangetoond. De aanwezigheid van deze resonantie is interessant om een nieuwe, “oude” techniek uit te proberen, namelijk de *Saturation Transfer Difference (STD)* techniek. Deze wordt meestal gebruikt bij liganden gebonden aan grote bio macromoleculen maar was nooit eerder getest op liganden gebonden aan inorganische deeltjes. Uit de resultaten bleek dat er wel degelijk een interactie is tussen lysine en het hydroxyapatiet oppervlak. Uit deze eerste experimenten kon echter geen informatie bekomen worden over de bindingsoriëntatie, hiervoor zou meer optimalisatie van de experimenten vereist zijn.

Als besluit kan gezegd worden dat tijdens dit doctoraatsonderzoek niet enkel verschillende onderzoeksvragen opgelost werden en verschillende

ligand-nanokristal interacties onderzocht, maar dat er ook nieuwe types experimenten aan de bestaande NMR *toolbox* werden toegevoegd.

LIST OF PUBLICATIONS

1. Damm, H.; Kelchtermans, A.; Bertha, A.; Van den Broeck, F.; Elen, K.; Martins, J. C.; Carleer, R.; D'Haen, J.; De Dobbelaere, C.; Hadermann, J.; Hardy, A.; Van Bael, M. K., Thermal decomposition synthesis of Al-doped ZnO nanoparticles: an in-depth study. *RSC Advances* **2013**, *3* (45), 23745-23754.
2. Risseeuw, M. D. P.; De Clercq, D. J. H.; Lievens, S.; Hillaert, U.; Sinnaeve, D.; Van den Broeck, F.; Martins, J. C.; Tavernier, J.; Van Calenbergh, S., A "Clickable" MTX Reagent as a Practical Tool for Profiling Small-Molecule–Intracellular Target Interactions via MASPIT. *ChemMedChem* **2013**, *8* (3), 521-526.
3. Vernieuwe, K.; Lommens, P.; Martins, J.; Van Den Broeck, F.; Van Driessche, I.; De Buysser, K., Aqueous ZrO₂ and YSZ Colloidal Systems through Microwave Assisted Hydrothermal Synthesis. *Materials* **2013**, *6* (9), 4082.
4. Dierick, R.; Van den Broeck, F.; De Nolf, K.; Zhao, Q.; Vantomme, A.; Martins, J. C.; Hens, Z., Surface Chemistry of CuInS₂ Colloidal Nanocrystals, Tight Binding of L-Type Ligands. *Chem. Mat.* **2014**, *26* (20), 5950-5957.
5. De Roo, J.; Van den Broeck, F.; De Keukeleere, K.; Martins, J. C.; Van Driessche, I.; Hens, Z., Unravelling the Surface Chemistry of Metal Oxide Nanocrystals, the Role of Acids and Bases. *J. Am. Chem. Soc.* **2014**, *136* (27), 9650-9657.
6. Toti, K. S.; Derudas, M.; Pertusati, F.; Sinnaeve, D.; Van den Broeck, F.; Margamuljana, L.; Martins, J. C.; Herdewijn, P.; Balzarini, J.; McGuigan, C.; Van Calenbergh, S., Synthesis of an Apionucleoside Family and Discovery of a Prodrug with Anti-HIV Activity. *The Journal of Organic Chemistry* **2014**, *79* (11), 5097-5112.
7. Ozhukil Kollath, V.; Van den Broeck, F.; Fehér, K.; Martins, J. C.; Luyten, J.; Traina, K.; Mullens, S.; Cloots, R., A Modular Approach To Study Protein Adsorption on Surface Modified Hydroxyapatite. *Chemistry – A European Journal* **2015**, *21* (29), 10497-10505.
8. De Roo, J.; Justo, Y.; De Keukeleere, K.; Van den Broeck, F.; Martins, J. C.; Van Driessche, I.; Hens, Z., Carboxylic-Acid-Passivated Metal Oxide Nanocrystals: Ligand Exchange Characteristics of a New Binding Motif. *Angewandte Chemie International Edition* **2015**, *54* (22), 6488-6491.
9. Geltmeyer, J.; De Roo, J.; Van den Broeck, F.; Martins, J.; De Buysser, K.; De Clerck, K., The influence of tetraethoxysilane sol preparation on the electrospinning of silica nanofibers. *Journal of Sol-Gel Science and Technology* **2015**, 1-10.

APPENDIX A
PUBLISHED PAPERS

Thermal decomposition synthesis of Al-doped ZnO nanoparticles: an in-depth study†

Cite this: DOI: 10.1039/c3ra43328e

Hanne Damm,^{abc} Anke Keldtermans,^{ab} Anne Bertha,^{cd} Freya Van den Broeck,^{ce} Ken Elen,^{abc} José C. Martins,^{ce} Robert Carleer,^f Jan D'Haen,^{bg} Christopher De Dobbelaere,^{ab} Joke Hadermann,^{cd} An Hardy^{abc} and Marlies K. Van Bael^{*abc}

Al-doped ZnO nanoparticles are synthesized by means of a heating up solution based thermal decomposition method. The synthesis involves a reaction of zinc acetylacetonate hydrate, aluminium acetylacetonate and 1,2-hexadecanediol in the presence of oleic acid and oleyl amine. A proposed reaction mechanism from reagents to monomers is corroborated by analysis of the evolving gases using headspace GC-MS analysis. The Al-doped ZnO nanoparticles synthesized are dynamically stabilized by adsorbed oleate ions, after deprotonation of oleic acid by oleyl amine, as was found by NOESY proton NMR and complementary FTIR spectroscopy. Precession electron diffraction shows a simultaneous increase in lattice parameters with Al concentration. This, together with HAADF-STEM and EDX maps, indicates the incorporation of Al into the ZnO nanoparticles. By the combination of complementary characterization methods during all stages of the synthesis, it is concluded that Al is incorporated into the ZnO wurtzite lattice as a dopant.

Received 1st July 2013

Accepted 27th September 2013

DOI: 10.1039/c3ra43328e

www.rsc.org/advances

Introduction

Zinc oxide has been the subject of extensive research, not only as a material for transparent conductor applications, but also for blue/UV optoelectronics including light emitting diodes,¹ laser diodes,² solar cells,³ transistors,⁴ sensors⁵ and spintronic devices doped with Co, Mn, Fe,...⁶ ZnO is an n-type semiconductor with a band gap around 3.4 eV, a large exciton binding energy of 60 meV and an excellent thermal stability.⁷ The typical charge carrier density of undoped ZnO is in the range of 10^{17} cm⁻³, which can be further increased by trivalent element doping of e.g. Al, Ga or In.^{8,9}

As a result, aluminium-doped ZnO (ZnO:Al) has demonstrated conductivities up to 10^4 S cm⁻¹ combined with a transparency of 90%.¹⁰ These properties, together with the abundant availability of its constituent elements render ZnO:Al

attractive as a transparent conductive oxide (TCO) material to replace indium tin oxide (ITO; 90% In₂O₃ and 10% SnO₂), currently the most commercialized TCO material. Although ITO has a superior conductivity and transparency,¹¹ the high price of In¹² necessitates the search for alternatives.

A further cost reduction for mass production favors the use of solution based methods instead of vacuum based physical routes.^{13–16} Solution deposition starting from suspensions of ZnO:Al nanoparticles (NPs) enables deposition on temperature sensitive substrates, since the crystallization is separated from the deposition step.¹⁸ Methods such as coprecipitation,¹⁷ hydrothermal synthesis¹⁸ and microwave assisted polyol routes¹⁹ have been reported for the synthesis of Al-doped ZnO NPs. Besides these, recently a thermal decomposition route has been used for the fabrication of ZnO:Al NPs.²⁰ The biggest asset of this thermal decomposition route is that it results in highly monodisperse NPs with a high colloidal stability, made possible by the separation of nucleation and growth in function of temperature and the use of surfactants. There are two approaches for conducting thermal decomposition synthesis: the hot-injection method and the heating-up method.²¹

Hot-injection induces a nucleation burst through the fast injection of the reagents into a hot precursor solution, whereas the starting solution of the heating-up route is prepared at room temperature and is gradually heated. During this heating-up stage the reagents are progressively decomposed which induces a more gradual nucleation of NPs. However, there is still debate about the mechanism of nanoparticle formation in the heating up method. Also, to our knowledge, no work has been reported

^aInorganic and Physical Chemistry, Institute for Materials Research, Hasselt University, Agoralaan building D, B-3590 Diepenbeek, Belgium. E-mail: marlies.vanbael@uhasselt.be; Tel: +32 11263107

^bIMEC Division IMOMEC, Agoralaan building D, B-3590 Diepenbeek, Belgium

^cSIM (Flemish Strategic Initiative on Materials), SOPPON program, Belgium

^dEMAT, University of Antwerp, Groenenborgerlaan 171, B-2020 Antwerp, Belgium

^eNMR and Structure Analysis Unit, Ghent University, Krijgslaan 281 S4, B-9000 Ghent, Belgium

^fApplied and Analytical Chemistry, Institute for Materials Research, Hasselt University, Agoralaan building D, B-3590 Diepenbeek, Belgium

^gMaterials Physics, Institute for Materials Research, Hasselt University, Wetenschapspark 1, B-3590 Diepenbeek, Belgium

† Electronic supplementary information (ESI) available. See DOI: 10.1039/c3ra43328e

DOI: 10.1002/cmdc.201200493

A “Clickable” MTX Reagent as a Practical Tool for Profiling Small-Molecule–Intracellular Target Interactions via MASPIT

Martijn D. P. Risseuw,^[a] Dries J. H. De Clercq,^[a] Sam Lievens,^[b] Ulrik Hillaert,^[a] Davy Sinnaeve,^[c] Freya Van den Broeck,^[c] José C. Martins,^[c] Jan Tavernier,^{*,[b]} and Serge Van Calenbergh^{*,[a]}

We present a scalable synthesis of a versatile MTX reagent with an azide ligation handle that allows rapid γ -selective conjugation to yield MTX fusion compounds (MFCs) appropriate for MASPIT, a three-hybrid system that enables the identification of mammalian cytosolic proteins that interact with a small molecule of interest. We selected three structurally diverse pharmacologically active compounds (tamoxifen, reversine, and FK506) as model baits. After acetylene functionalization of these baits, MFCs were synthesized via a CuAAC reaction, demonstrating the general applicability of the MTX reagent. In analytical mode, MASPIT was able to give concentration-dependent reporter signals for the established target proteins. Fur-

thermore, we demonstrate that the sensitivity obtained with the new MTX reagent was significantly stronger than that of a previously used non-regiomer conjugate mixture. Finally, the FK506 MFC was explored in a cellular array screen for targets of FK506. Out of a pilot collection of nearly 2000 full-length human ORF preys, FKBP12, the established target of FK506, emerged as the prey protein that gave the highest increase in luciferase activity. This indicates that our newly developed synthetic strategy for the straightforward generation of MFCs is a promising asset to uncover new intracellular targets using MASPIT cellular array screening.

Introduction

As we move toward systems biology and personalized medicine, it will become increasingly important to profile small molecule–target interactions and to map this information with metabolic and signaling pathways. Indeed, many clinically used drugs have been found to be more promiscuous than originally thought. However, modulation of multiple targets can also cause harmful side effects, and another considerable challenge is to uncover the mechanisms of toxicities that are not directly related to the desired pharmacological effects of drugs (“off-target pharmacology”). As classical *in vitro* target

profiling requires time- and budget-consuming expression, purification, and assay setup for each individual target, it usually involves testing of a compound against a limited panel of related targets and is thus not comprehensive.

The number of “tried-and-true” drug targets is quite small.^[1,2] The emergence of molecular biology and the completion of the human genome project have hitherto failed to produce the expected flood of compounds aimed at new targets. Unbiased, phenotype-based screens represent a promising approach to uncover drugs with a novel mechanism of action. For small molecules discovered in such screens, identifying the biological targets remains largely an ad hoc affair. Traditional approaches using affinity pull-down reagents^[3] have been successful for the identification of new targets and have, for example, been recently employed to uncover targets involved in the teratogenic effects of thalidomide.^[4] However, sensitivity can be limited, particularly for compounds that exhibit low binding affinity toward their target or for targets expressed at low levels. In these cases, the target protein is lost during the washing steps, or its binding is obscured by the presence of highly abundant (non-specifically binding) proteins.^[5] A systematic, widely applicable, and robust approach is badly needed.

MASPIT (mammalian small molecule protein interaction trap) is a three-hybrid trap variant of the original MAPPIT concept^[6,7] for the detection of small molecule–protein interactions. MASPIT makes use of a signaling-deficient cytokine receptor

[a] Dr. M. D. P. Risseuw, D. J. H. De Clercq, Dr. U. Hillaert, Prof. Dr. S. Van Calenbergh

Laboratory for Medical Chemistry, Faculty of Pharmaceutical Sciences Ghent University, Harelbekestraat 72, 9000 Ghent (Belgium)

E-mail: serge.van.calenbergh@ugent.be

[b] Dr. S. Lievens, Prof. Dr. J. Tavernier

Cytokine Receptor Laboratory, Department of Medical Protein Research, VIB, Ghent and Department of Biochemistry

Ghent University, Albert Swertzlaan 3, 9000 Ghent (Belgium)

[c] Dr. D. Sinnaeve, F. Van den Broeck, Prof. Dr. J. C. Martins, NMR and Structure Analysis Unit, Department of Organic Chemistry Ghent University, Krijgslaan 281 54, 9000 Ghent (Belgium)

[*] These authors contributed equally to this work.

Supporting information for this article is available on the WWW under <http://dx.doi.org/10.1002/cmdc.201200493>.

Re-use of this article is permitted in accordance with the Terms and Conditions set out at <http://chemmedchem.org/lopen>.

Article

Aqueous ZrO₂ and YSZ Colloidal Systems through Microwave Assisted Hydrothermal Synthesis

Kenny Vernieuwe¹, Petra Lommens¹, José C. Martins², Freya Van Den Broeck², Isabel Van Driessche¹ and Klaartje De Buysser^{1,*}

¹ Department of Inorganic and Chemistry, Ghent University, Krijgslaan 281 S3, B-9000 Ghent, Belgium; E-Mails: kenny.vernieuwe@ugent.be (K.V.); petra.lommens@ugent.be (P.L.); isabel.vandriessche@ugent.be (I.V.D.)

² Department of Organic Chemistry, Ghent University, Krijgslaan 281 S4, B-9000 Ghent, Belgium; E-Mails: jose.martins@ugent.be (J.M.); freya.vandenbroeck@ugent.be (F.V.D.B.)

* Author to whom correspondence should be addressed; E-Mail: klaartje.debuysser@ugent.be; Tel.: +32-926-444-41; Fax: +32-926-449-83.

Received: 9 July 2013; in revised form: 4 September 2013 / Accepted: 10 September 2013 /

Published: 16 September 2013

Abstract: In this paper, the formation of ZrO₂ and yttria-stabilised-zirconia (YSZ) aqueous colloidal systems via microwave assisted hydrothermal synthesis is studied. Microwave synthesis allows a fast screening of the influence of different parameters such as time and temperature. The temperature varied from 140 °C up to 180 °C and the used reaction time varied from 5 min up to 1 h. The synthesised zirconia nanoparticles have a particle size of 50 nm confirmed by TEM. A ¹H NMR (nuclear magnetic resonance) study helped to understand the stabilization mechanism of the synthesised particles. By the addition of yttrium ions into the zirconia colloidal solution, YSZ could be formed via an additional thermal treatment. Hereby, the samples are heated up to 400 °C for 1 h. YSZ colloidal solutions are synthesised by making use of complexing agents such as nitrilotriacetic acid, ethylenediaminetetraacetic acid and citric acid to control the hydrolysis and condensation of both ions to avoid non-stoichiometric phases. The ratio of Zr/Y in the particles is quantified by XRF. The amorphous structure of those particles necessitates an additional thermal treatment up to 600 °C during 1 h in order to obtain crystalline YSZ.

Keywords: microwave assisted synthesis; YSZ; zirconia; nanoparticles; NMR

<https://biblio.ugent.be/publication/4190680>

Surface Chemistry of CuInS₂ Colloidal Nanocrystals, Tight Binding of L-Type Ligands

Ruben Dierick,^{†‡} Freya Van den Broeck,^{||} Kim De Nolf,^{†‡} Qiang Zhao,[§] André Vantomme,[§] José C. Martins,^{||} and Zeger Hens^{*,†,‡}

[†]Physics and Chemistry of Nanostructures, Ghent University, Krijgslaan 281-S3, 9000 Ghent, Belgium

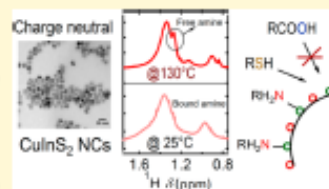
[‡]Center for Nano- and Biophotonics, Ghent University, 9000 Ghent, Belgium

^{||}NMR and Structure Analysis, Ghent University, Krijgslaan 281-S4bis, 9000 Ghent, Belgium

[§]Instituut voor Kern- en Stralingsfysica, KU Leuven, Celestijnenlaan 200 D, 3000 Leuven, Belgium

Supporting Information

ABSTRACT: We analyze the surface chemistry of CuInS₂ nanocrystals synthesized in the presence of amines. Using solution NMR spectroscopy and elemental analysis, we come to the conclusion that as-synthesized CuInS₂ nanocrystals have charge neutral inorganic cores and are stabilized by a layer of tightly bound L-type amines. In situ NMR heating-up experiments show that desorption of amines can be induced by increasing the temperature, which makes the partial exchange of amines for thiols possible. On the other hand, we find that carboxylic acids are unable to bind as L-type ligands to the CuInS₂ surface. In addition, we demonstrate that the use of technical oleylamine in the synthesis of CuInS₂ nanocrystals leads to nonstoichiometric nanocrystals which have, next to oleylamine ligands, also X-type impurities on the surface that can be exchanged for carboxylic acids.



INTRODUCTION

During the past decades, colloidal semiconductor nanocrystals (NCs) have been widely studied as a new material for optoelectronic applications.¹ Especially in the case of Cd and Pb chalcogenides, tremendous progress has been made at the level of nanocrystal synthesis,^{2–8} where control over size and shape and the formation of heterostructures have become common practice along with the development of nanocrystal-based optoelectronic devices.^{9–13} As compared to these NCs, the synthesis, characterization, and application of more environmentally friendly I–III–VI₂ nanocrystals, such as those of the Cu(In,Ga)(S,Se)₂ family (CIGS in short), are still in an early stage of development.¹⁴ CIGS NCs have been successfully synthesized in apolar environments, either by means of heating-up or hot-injection procedures that make use of long chain alkyl amines^{15,25–29} or thiols^{15,30,30,31} or a combination of these. Studies on applications of these NCs can be classified in two main categories. A first, including for example bioimaging,^{15–17} solid-state lighting, and NC solar cells,^{21,22} makes use of the properties of the colloidal NCs themselves—most notably their size-tunable photoluminescence. A second uses dispersions of CIGS NCs as precursor solutions to form dense CIGS layers by solution-based deposition and incorporate these in thin film solar cells.^{20–25} In both cases, the importance of postsynthetic processing of CIGS NCs can hardly be overestimated. Next to the growth of inorganic shells around the as-synthesized NCs, this concerns the tailoring of the CIGS NC surface chemistry, where the long ligands typically used during synthesis are replaced by more

appropriate ligands in view of a particular application. Bioimaging for example requires water-soluble nanocrystals, while for a NC-based solar cell, charge transport between adjacent NCs in a thin film is enhanced when the NC surface is passivated by short chain moieties.^{32,33}

The successful tailoring of the NC surface chemistry starts from an understanding of the binding of ligands to as-synthesized NCs. Detailed studies on metal chalcogenide or pnictide nanocrystals synthesized in apolar media using hot injection or heating up approaches, including CdSe,^{34,35} CdTe,³⁶ PbS,³⁷ PbSe,³⁸ and InP,^{39,40} have shown that the classification of ligands as L-type, X-type, or Z-type depending on the number of electrons the NC–ligand bond takes from the NC (zero, one, and two, respectively) to form a two-electron bond is a convenient approach.^{41–43} In combination with the need to form charge-neutral nanocrystals in apolar environments, this results in two extreme classes. The first describes NCs where the formal charge on the cations and anions is balanced—for binary NCs, this corresponds to the bulk stoichiometry—and which are passivated by L-type ligands (NC-L_n). The second are NCs that have a net formal charge that is balanced by the opposite charge on X-type ligands. Typically, this involves NCs having an excess of metal cations, stabilized by ligands with a formally negative charge—denoted here as NC-(MX_n)[–]—although the opposite situation of an

Received: July 21, 2014

Revised: September 18, 2014

Unravelling the Surface Chemistry of Metal Oxide Nanocrystals, the Role of Acids and Bases

Jonathan De Roo,^{†,‡} Freya Van den Broeck,^{||} Katrien De Keukeleere,[†] José C. Martins,^{||} Isabel Van Driessche,[†] and Zeger Hens^{*,‡,§}

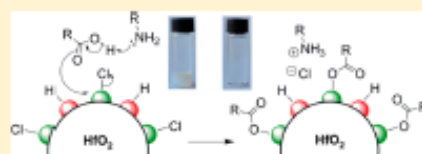
[†]Sol-gel Centre for Research on Inorganic Powders and Thin films Synthesis (SCRIFTS), and [‡]Physics and Chemistry of Nanostructures (PCN), Ghent University, Krijgslaan 281 S3, 9000 Gent, Belgium

[§]Center for Nano and Biophotonics (NB-Photonics), and ^{||}NMR and Structural Analysis Unit, Ghent University, Krijgslaan 281 S4, 9000 Gent, Belgium

Supporting Information

ABSTRACT: We synthesized HfO₂ nanocrystals from HfCl₄ using a surfactant-free solvothermal process in benzyl alcohol and found that the resulting nanocrystals could be transferred to nonpolar media using a mixture of carboxylic acids and amines. Using solution ¹H NMR, FTIR, and elemental analysis, we studied the details of the transfer reaction and the surface chemistry of the resulting sterically stabilized nanocrystals. As-synthesized nanocrystals are charge-stabilized by protons, with chloride acting as the counterion.

Treatment with only carboxylic acids does not lead to any binding of ligands to the HfO₂ surface. On the other hand, we find that the addition of amines provides the basic environment in which carboxylic acids can dissociate and replace chloride. This results in stable, aggregate-free dispersions of HfO₂ nanocrystals, sterically stabilized by carboxylate ligands. Moreover, titrations with deuterated carboxylic acid show that the charge on the carboxylate ligands is balanced by coadsorbed protons. Hence, opposite from the X-type/nonstoichiometric nanocrystals picture prevailing in literature, one should look at HfO₂/carboxylate nanocrystals as systems where carboxylic acids are dissociatively adsorbed to bind to the nanocrystals. Similar results were obtained with ZrO₂ NCs. Since proton accommodation on the surface is most likely due to the high Brønsted basicity of oxygen, our model could be a more general picture for the surface chemistry of metal oxide nanocrystals with important consequences on the chemistry of ligand exchange reactions.



INTRODUCTION

Metal oxide nanocrystals (MONCs) are an important class of nanomaterials regarding their potential in medicine,¹ (photo)catalysis,^{2,3} gas sensing,⁴ magnetic applications,⁵ solar cells,⁶ transparent electrodes,⁷ lithium ion batteries,^{8,9} and light-emitting diodes.¹⁰ Their suitability for a specific application depends on their properties, such as chemical nature, size, shape, size dispersion, crystallinity, colloidal stability, and surface composition, and their eventual industrial implementation requires fast and robust syntheses with a high yield, cheap precursors, and low energy input. Many research activities have therefore been dedicated to the development of various synthetic strategies, where solution-based approaches stand out since they can be applied to prepare a wide range of MONCs with an often exceptional control over size, size dispersion, and shape.

Using solution-based approaches in aqueous media, it proved possible to synthesize monodisperse colloids in short reaction times, but the particles were often very large (>100 nm) and amorphous.^{11,12} The subsequent crystallization step induced undesired agglomeration. In addition, the final properties of the nanoparticles were found to be very sensitive to the precise reaction conditions (e.g., pH, temperature, etc.). In surfactant-assisted nonaqueous methods—typically carried out by hot

injection or heating up—large quantities of ligands are used to control nucleation, (anisotropic) growth, and colloidal stability, often leading to very monodisperse MONCs.^{5,13–16} In general, these syntheses proceed at high temperatures (>300 °C) to quickly decompose the metal precursor and obtain crystalline products. Successful syntheses require a rigorous control of heating rate, precursor addition rate, etc., whereas further complications may result from structural changes of the surfactants at the high temperatures used¹⁷ or from impurities in surfactants, which can be more decisive to the outcome of a synthesis than the surfactant itself.^{18,19} Contrarily, surfactant-free nonaqueous methods are based on chemically robust procedures with high yields.²⁰ The metal precursors—typically cheap metal salts—are simply mixed with a nontoxic solvent such as benzyl alcohol or benzyl amine and heated for several days in an autoclave. The reduced hydrolysis and condensation rates result in crystalline particles even at moderate temperatures of about 200 °C. The slow autoclave process is objectionable, but it was shown that these reactions can be accelerated considerably by using microwave heating, while still retrieving products with excellent crystallinity.^{21,22} With this

Received: April 9, 2014
Published: June 19, 2014

Synthesis of an Apionucleoside Family and Discovery of a Prodrug with Anti-HIV Activity

Kiran S. Toti,[†] Marco Derudas,[‡] Fabrizio Pertusati,[‡] Davy Sinnaeve,[§] Freya Van den Broeck,[§] Lia Margamuljana,^{||} José C. Martins,[§] Piet Herdewijn,^{||} Jan Bazarini,^{||} Christopher McGuigan,[‡] and Serge Van Calenbergh^{*,†}

[†]Laboratory for Medicinal Chemistry, Faculty of Pharmaceutical Sciences, Ghent University, Harelbekestraat 72, B-9000 Ghent, Belgium

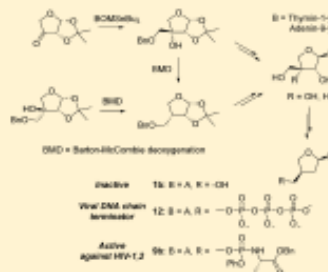
[‡]Cardiff School of Pharmacy and Pharmaceutical Sciences, Cardiff University, Redwood Building, King Edward VII Avenue, Cardiff CF10 3NB, UK

[§]NMR and Structure Analysis Unit, Department of Organic Chemistry, Ghent University, Krijgslaan 281 S4, B-9000 Ghent, Belgium

^{||}Rega Institute for Medical Research, KU Leuven, B-3000 Leuven, Belgium

Supporting Information

ABSTRACT: We report the synthesis of a family of D- and L-furano-D-apionucleosides, their 3'-deoxy, as well as their 2',3'-dideoxy analogues with thymine and adenine nucleobases. Single carbon homologation of 1,2-O-isopropylidene-D-glycero-tetrafuranos-3-ulose (15) and optimized glycosylation conditions involving microwave irradiation were key to the successful synthesis of the target compounds. While all target nucleosides failed to show significant antiviral activity, we demonstrated that the triphosphate of 2',3'-deoxy-D-apio-D-furanoadenosine (1), in contrast to that of its D-apio-L-furanose epimer 2, was readily incorporated into a DNA template by HIV reverse transcriptase to act as a DNA chain terminator. This led us to convert adenine derivative 1 into two phosphoramidate prodrugs. ProTide 9b was found active against HIV-1 and HIV-2 (EC₅₀ = 0.5–1.5 μM), indicating that the lack of activity of the parent nucleoside, and possibly also other members of the D-apio-D-furanose nucleoside family must be sought in the inefficient cellular conversion to the monophosphate.



INTRODUCTION

Although the pharmacological scope of nucleoside analogues is still expanding, they remain most renowned for their utility as antiviral drugs.¹ 2',3'-Dideoxy-β-D-apio-D-furanonucleosides (D-ddANs, 1, Figure 1) were synthesized in the early 1990s as potential antiviral agents, but were found inactive.^{2–4} However, some of us recently discovered that the 3'-O-phosphonomethylated adenine (A) and thymine (T) analogues 7 exhibit promising anti-HIV properties.⁵ Since these phosphonates act as bioisosteres of the phosphorylated species 8, we decided to re-investigate the biological activity of these ddANs. We envisioned a synthetic approach that would also give access to the known apionucleosides 3,^{6,7} their 3'-deoxy counterparts 2,^{8–11} and inadvertently also the D-apio-L-furanose epimers 4–6. Furthermore, we planned to expand the potential of the 2',3'-dideoxyapio nucleosides 1 and 4 as antiviral agents by synthesizing their phosphoramidate prodrugs 9, 10 and 11. These would lead to the intracellular release of the parent nucleosides like 8,^{12,13} thereby bypassing the often problematic first phosphorylation step in the conversion to the active triphosphate species.¹⁴

RESULTS AND DISCUSSION

Chemistry. Compounds 16 and 27 were considered valuable intermediates to access the envisaged family of D-furanoapionucleosides (Scheme 1). They were prepared from 1,2-isopropylidene-α-L-threose (14), which was obtained in six steps from L-ascorbic acid.^{15,16} Interestingly, screening of different oxidation methods^{15,17,18} to convert 14 to ketone 15 indicated that TEMPO-BAIB ([Bis(acetoxy)-iodo]benzene) oxidation, best known for oxidation of primary hydroxyl groups, was the most effective. Conversion of 15 to 16 is feasible by reacting the former with diazomethane to give a spiro-oxirane,¹⁹ which can then be opened with benzylalkoxide to give 16.²⁰ To avoid the use of diazomethane, we explored several variations of the polarity reversal concept to realize the desired carbon homologation. Reaction with benzyltrimethylchloride in the presence of samarium iodide did not yield the desired product, while the corresponding Grignard reaction gave 16 in disappointing yields.²¹ Nucleophilic attack of the ketone with lithiated benzyltrimethyltributyltin afforded 16 in acceptable yield,²² considering the propensity of compound 15

Received: March 21, 2014

Published: May 7, 2014

A modular approach to study protein adsorption on surface modified hydroxyapatite

Vinayaraj Ozhukil Kollath,^{†(a)(b)} Freya Van den Broeck,^(c) Krisztina Fehér,^(c) José C Martins,^(c) Jan Luyten,^{‡(b)} Karl Traina,^{†(a)} Steven Mullens^{*(b)} and Rudi Cloots^{*(a)}

Abstract: Biocompatible inorganic nano and micro carriers can be a suitable candidate for protein delivery. This study demonstrates facile methods of functionalizations using nanoscale linker molecules to change the protein adsorption capacity of hydroxyapatite (HA) powder. Adsorption capacity of bovine serum albumin (BSA) as a model protein is studied with respect to the surface modifications. The selected linker molecules (Lysine, Arginine, Phosphoserine) can influence the adsorption capacity by changing the electrostatic nature of HA surface. Qualitative and quantitative analyses of linker molecule interaction with HA surface was performed using NMR spectroscopy, zeta potential measurements, X-ray photoelectron spectroscopy and thermogravimetric analyses. Additionally, correlations to theoretical isotherm models are calculated with respect to Langmuir and Freundlich Isotherms. Lysine and arginine increased the protein adsorption while phosphoserine reduced the protein adsorption. Results show that the adsorption capacity can be controlled by different functionalization, depending on the protein-carrier selections under consideration. The scientific knowledge acquired from this study can be applied in various biotechnological applications which involve biomolecule-inorganic materials interfaces.

Introduction

Nano and micro carrier based drug delivery systems have attracted research interest for effective delivery of proteins, peptides and other antigens of interest via different routes of administration. It is reported that, proteins or peptides if administered directly, are poorly bio-available^[1]. However the protein when administered along with a microparticulate carrier, antibody-mediated immune response could be enhanced^[2-6]. Different carrier systems such as viral, recombinant protein, inorganic and polymeric carriers have been extensively tested in

the recent past. Inorganic nano and microparticulate carrier materials (e.g.: gold, silica, iron oxide and calcium phosphate)^[7-11] are interesting due to their biocompatibility, higher functionality, easier production and low cost. The material of interest in this study hydroxyapatite [HA, Ca₁₀(PO₄)₆(OH)₂], a crystallographic phase of calcium phosphate (CaP) has the ability to fit into the aforementioned criteria, and is well known for biomaterial applications^[12-14].

However inorganic carriers are still in the pre-clinical stage. Extensive research is needed to assess their potential when compared to the performance of polymeric carriers, certainly with respect to the protein or peptide loading capacity and cellular transfer efficiency^[15]. Protein adsorption on inorganic materials is an important mechanism to be understood for various biomedical applications. This study investigates the adsorption mechanism of bovine serum albumin (BSA; selected as model protein) on HA powder and a method to influence it. It has been reported that the increase in specific surface area (SSA) or certain plasma treatments increases the adsorption capacity of BSA on CaP^[16,17]. Further enhancement of adsorption capacity can be achieved by functionalizing the HA powder with nanoscale linker molecules in order to increase the electrostatic or other kind of interactions with BSA. HA has neutral or slightly negative charge in aqueous suspensions at neutral pH and BSA is a negatively charged protein at the same conditions. Three linker molecules (L-Arginine, L-Lysine and O-Phospho-L-serine) with amino acid units were selected in order to change the BSA loading by altering the electrostatic nature of the surface. As such, the electrostatic interaction between powder and protein was stimulated. In this case, the carboxyl group is expected to have a Coulombic reaction with the Ca²⁺ ions present on the HA^[18] surface which leaves the amino group available for further reactions with BSA. It has also been reported that the amine group can interact with the HA surface through water bridged hydrogen bond^[19], but this is less favorable.

This study reports qualitative and quantitative analyses of the linker molecules adsorbed on to the HA surface. The toolbox used in this study elucidates BSA adsorption mechanism to surface modified HA particles. Bare HA powder was analyzed for the porosity and SSA using the nitrogen adsorption method. BSA adsorption, before and after the functionalization, was evaluated and the subsequent mechanisms underlying the increase in BSA adsorption taking in to account the dissociation constants of ionizable groups in the linker molecules has been elaborated in this study. As amino acid functionalization should potentially modify the electrostatic interaction, the corresponding change in surface charge of the powder was monitored by zeta potential measurements as a function of the pH. Qualitative analyses of functionalized powder was performed using X-ray

(a) Dr. V. Ozhukil Kollath, Dr. K. Traina, Prof. R. Cloots
Department of Chemistry
University of Liège
B6a, Allée de la chimie 3, Liège 4000 (Belgium)
Fax: +32 4366 3413
E-mail: r.cloots@ulg.ac.be

(b) Dr. V. Ozhukil Kollath, Dr. J. Luyten, Dr. S. Mullens
Sustainable Materials Management
Flemish Institute for Technological Research (VITO)
Boeretang 200, Mol 2400
Fax: +32 14 32 11 86

(c) F. Van den Broeck, Dr. K. Fehér, Prof. J. C. Martins
Department of Organic Chemistry
Ghent University
Krijgslaan 281, Ghent 9000
Fax: +32 14 32 11 86

Current address: [†]Department of Physics, UNESP—Univ. Estadual Paulista, 17035-360, Bauri, SP, Brazil; [‡]Department of Metallurgy and Materials Engineering, Katholieke Universiteit Leuven, 3001 Heverlee, Belgium; [§]Galephar MF, 6900 Marche en Famenne, Belgium

Supporting information for this article is available on the WWW under <http://dx.doi.org/10.1002/chem.2015xxxxx>

Carboxylic-Acid-Passivated Metal Oxide Nanocrystals: Ligand Exchange Characteristics of a New Binding Motif[†]

Jonathan De Roo, Yolanda Justo, Katrien De Keukeleere, Freya Van den Broeck, José C. Martins, Isabel Van Driessche, and Zeger Hens*

Abstract: Ligand exchange is central in the processing of inorganic nanocrystals (NCs) and requires understanding of surface chemistry. Studying sterically stabilized HfO_2 and ZrO_2 NCs using ^1H solution NMR and IR spectroscopy as well as elemental analysis, this paper demonstrates the reversible exchange of initial oleic acid ligands for octylamine and self-adsorption of oleic acid at NC surfaces. Both processes are incompatible with an X-type binding motif of carboxylic acids as reported for sulfide and selenide NCs. We argue that this behavior stems from the dissociative adsorption of carboxylic acids at the oxide surface. Both proton and carboxylate moieties must be regarded as X-type ligands yielding a combined X_2 binding motif that allows for self-adsorption and exchange for L-type ligands.

Colloidal nanocrystals (NCs) are hybrid objects in which the properties of core and surface both determine the characteristics of the entire NC. The surface is often capped by (in)organic ligands which determine colloidal stability and the physical and chemical properties.^[1] As a result, NC surface chemistry, i.e., the understanding of and control over the ligand shell, has become one of the central themes in NC research.

The covalent bond classification (CBC)^[2] provides an apt framework to describe NC-ligand binding.^[3,4] Ligands are defined as L-, X-, or Z-type depending on the number of electrons that the neutral ligand contributes to the NC-ligand bond (2, 1, or 0, respectively). This classification is unambiguous^[5] and allows to label distinct NC-ligand model systems (Scheme 1). L-type ligands such as amines and phosphines are neutral donors of a free electron pair. In apolar solvents, they coordinate to surface metal ions of stoichiometric NCs to yield overall charge-neutral objects.^[5] Z-type ligands are neutral electron-pair acceptors (e.g., metal carboxylates) that bind to the surface anions of stoichiometric NCs.^[14] In NC surface chemistry, X-type ligands are presented as negatively



Scheme 1. The covalent bond classification (CBC) considers L-type ligands as Lewis bases, Z-type ligands as Lewis acids, and X-type ligands as radicals.

charged ligands (RCOO^- , OH^- , Cl^-) that bind to excess surface cations of nonstoichiometric NCs.^[14,9] Although this concept is correct, it is a too restrictive description as we argue in this paper. According to the original CBC, ligands must be classified in their neutral form. X-type ligands are thus formally regarded as radicals (Scheme 1).

Obviously, desorption or adsorption of L- and Z-type ligands involves the separation or combination of two neutral, closed-shell moieties. In contrast, self-desorption of X-type ligands implies the formation of either radicals or charged species. The former process is generally unfeasible and the latter is thermodynamically unfavorable in apolar media due to the low dielectric screening. For the same reason, it would be impossible to exchange X-type ligands for L-type ligands. Anionic X-type ligands can only be traded for other anionic X-type ligands by the transfer of a proton or trimethylsilyl group.^[14,6,7]

In contrast to CdSe NCs,^[6] the surface of ZnO, TiO_2 , ZrO_2 , and HfO_2 NCs can adsorb protons.^[8] In case of fatty acid-capped ZrO_2 and HfO_2 NCs, we recently showed that both carboxylate and proton bind to the metal oxide NC surface.^[10] Here, we analyze possible ligand exchange reactions enabled by the presence of this internal proton source, in which we focus on exchange and self-adsorption of oleic acid (HOAc) on HfO_2 and ZrO_2 NCs, benchmarked against oleate-capped CdSe NCs. Our findings indicate that the dissociated carboxylic acid can be described as an X_2 ligand, i.e., a combination of a cationic X-type ligand (H^+) and an anionic X-type ligand (RCOO^-). This new binding motif results in exchange characteristics comparable to those of L-type ligands.

HfO_2 , ZrO_2 , and CdSe NCs were synthesized according to established procedures and HOAc was employed as ligand.^[9] Although HOAc can populate three different states—chemisorbed to the NC, physisorbed in the ligand shell, and free in solution,^[14] the ^1H NMR spectrum of a purified HfO_2 NC dispersion features only the broadened signals of chemisorbed HOAc (Figure 1A), i.e., no free or physisorbed acid is present in the sample. Upon addition of octylamine (Am), the alkene resonance changes and a new signal appears at

[*] J. De Roo, Dr. Y. Justo, K. De Keukeleere, Prof. Dr. I. Van Driessche, Prof. Dr. Z. Hens
Inorganic and Physical Chemistry, Ghent University
Krijgslaan 281-S3, 9000 Gent (Belgium)
E-mail: zeger.hens@ugent.be

F. Van den Broeck, Prof. Dr. J. C. Martins
Organic and Macromolecular Chemistry, Ghent University
Krijgslaan 281-S4, 9000 Gent (Belgium)

[**] This work was financially supported by the Research Foundation Flanders (FWO), the Strategic Initiative Materials (SIM-Flanders), Ghent University, and the Hercules Foundation.

Supporting information for this article is available on the WWW under <http://dx.doi.org/10.1002/anie.201500965>.

The influence of tetraethoxysilane sol preparation on the electrospinning of silica nanofibers

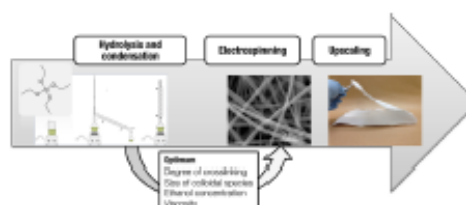
Jozefien Geltmeyer¹ · Jonathan De Roo² · Freya Van den Broeck³ · José C. Martins³ · Klaartje De Buysse² · Karen De Clerck¹

Received: 10 July 2015 / Accepted: 19 September 2015
© Springer Science+Business Media New York 2015

Abstract The critical parameters determining the electrospinning of silica nanofibers starting from tetraethoxysilane sols are reported. By controlling the reaction conditions, the rheological properties of the sol allowed for electrospinning without needing the addition of an organic polymer. This allows the polymer removal step, which is deleterious to the fibers and an economic and ecological inconvenience, to be skipped. The effects on the electrospinning process of the viscosity of the sol, the concentration of ethanol, the degree of crosslinking and the size of the colloidal species were studied in depth with ATR-FTIR, ²⁹Si NMR, ¹H NMR and DLS. Moreover, to separate the contributions of the different parameters three different set-ups for sol preparation were used. An optimum amount of 9 mol L⁻¹ ethanol for electrospinning was determined. In addition, the optimum degree of crosslinking and size of colloidal particles, approximately 3.5–7 nm, were obtained for stable electrospinning and for producing uniform, beadless nanofibers that were stable in time. The optimum viscosity range is in between 100 and 200 mPa s, which is in line with previous work. Using these optimum

conditions, continuous electrospinning was carried out for 3 h, resulting in large flexible silica nanofibrous membranes.

Graphical Abstract



Keywords Electrospinning · Sol-gel · NMR · TEOS · Nanofibers

1 Introduction

The interest in electrospinning of ceramic nanofibers has grown drastically in recent years [1–4]. Due to the small fiber diameters, nanofibrous nonwovens have a very high specific surface area, small pore size and high porosity. Ceramic materials are typically hard and inert and thus well known for their high thermal and chemical resistance. The combination of these unique properties makes these nanofibers advantageous for various applications such as fuel cells [5], solar cells [6], catalysis [7], filtration [8–10] and sensors [11]. Electrospinning is a simple and versatile technique for the production of polymer and ceramic nanofibers [12–16]. Using electrostatic forces, continuous nanofibers can be obtained having controllable compositions and controllable diameters below 500 nm. The

✉ Karen De Clerck
Karen.DeClerck@UGent.be

¹ Fibre and Colouration Technology Research Group, Department of Textiles, Faculty of Engineering and Architecture, Ghent University, Technologiepark 907, 9052 Ghent, Belgium

² Sol-gel Centre for Research on Inorganic Powders and Thin Films Synthesis, Department of Inorganic and Physical Chemistry, Faculty of Sciences, Ghent University, Krijgslaan 281 S3, 9000 Ghent, Belgium

³ NMR and Structure Analysis, Department of Organic and Macromolecular Chemistry, Faculty of Sciences, Ghent University, Krijgslaan 281 S4, 9000 Ghent, Belgium